JAERI-M
91-033

EVALUATION REPORT ON SCTF CORE-II TEST S2-19

(QUANTITATIVE EVALUATION OF RELATION BETWEEN DEGREE OF HEAT TRANSFER ENHANCEMENT DUE TO RADIAL POWER DISTRIBUTION AND AMOUNT OF INCREASE OF UPWARD LIQUID FLOW RATE DURING REFLOOD IN PWR-LOCA)

March 1991

Akira OHNUKI, Hiromichi ADACHI*, Takamichi IWAMURA
Tadashi IGUCHI, Yutaka ABE and Yoshio MURAO

日本原子力研究所
Japan Atomic Energy Research Institute

JAERI-Mレポートは，日本原子力研究所が不定期に公刊している研究報告書です。
入手の問合わせは，日本原子力研究所技術情報部情報資料課（〒319-11茨城県那珂郡東海村）あて，お申しこしください。なお，このほかに財団法人原子力弘済会資料センター（〒319-11 茨城県那珂郡東海村日本原子力研究所内）で複写による実費頒布をおこなっております。

JAERI-M reports are issued irregularly.
Inquiries about availability of the reports should be addressed to Information Division Department of Technical Information, Japan Atomic Energy Research Institute, Tokai-mura, Naka-gun, Ibaraki-ken 319-11, Japan.

編集兼発行　日本原子力研究所
印　　刷　いばらき印刷㈱

JAERI-M 91-033

Evaluation Report on SCTF Core-II Test S2-19 (Quantitative Evaluation of Relation between Degree of Heat Transfer Enhancement due to Radial Power Distribution and Amount of Increase of Upward Liquid Flow Rate during Reflood in PWR-LOCA)

Akira OHNUKI, Hiromichi ADACHI*, Takamichi IWAMURA
Tadashi IGUCHI, Yutaka ABE and Yoshio MURAO

Department of Reactor Engineering
Tokai Research Establishment
Japan Atomic Energy Research Institute
Tokai-mura, Naka-gun, Ibaraki-ken

(Received February 4, 1991)

Experimental studies using Slab Core Test Facility (SCTF) have revealed that the heat transfer enhancement in higher power bundles is mainly governed by the radial power ratio in core duing the reflood in PWR-LOCA. As a physical mechanism for the heat transfer enhancement, it can be considered from the experimental evidence that the increase of upward steam flow rate in a higher power bundle which is caused by the higher steam production rate in the bundle gives the higher upward liquid flow rate in the bundle and the increase of the liquid flow rate gives the heat transfer enhancement. In order to develop a mechanistic model for the heat transfer enhancement based on this idea, the following relations should be identified quantitatively: (1) Relation between the steam production rate and the upward liquid flow rate, (2) Cross flow rate above the quench front and (3) Relation between the degree of heat transfer enhancement due to radial power ratio and the amount of increase of upward liquid flow rate.

In this report, the above relation (3) was investigated experimentally as a step to develop the mechanistic model using the SCTF where

---

* Yamagata University

the relation between the radial power ratio and the heat transfer enhancement has been made clear quantitatively. The degree of increase of heat transfer between two forced feed tests with the different flow rate in LPCI period was compared with the degree of heat transfer enhancement under a radial power ratio in the previous SCTF tests. The two forced feed tests were performed under the condition without any significant two-dimensional hydraulic behavior in core. The ratio of the mass flow rate between the two tests was about double.

The degree of the increase of heat transfer coefficient in the tests of this study was almost correpond to that of the heat transfer enhancement under the radial peak power ratio (PF) of 1.065. In the case that the heat transfer enhancement is attained by the physical mechanism mentioned above, this result indicates that the upward liquid flow rate in the highest power bundle is about twice time higher than that in the lowest one in the tests with PF=1.065.

Keywords: Reactor Safety, PWR-LOCA, Two-Phase Flow, Reflood, SCTF, Cross Flow, Liquid Flow Rate, Heat Transfer, Quench

SCTF第2次炉心試験S 2 － 19評価報告書
(PWR － LOCA時再冠水過程における半径方向出力分布による熱伝達促進の程度と液上昇流量の増加量との関係の定量的評価)

日本原子力研究所東海研究所原子炉工学部
大貫　晃・安達　公道*・岩村　公道・井口　正
阿部　豊・村尾　良夫

(1991年2月4日受理)

平板炉心試験装置（SCTF）を使った今までの実験的研究により，PWR－LOCA時再冠水過程における高出力バンドルでの熱伝達促進の程度は，炉心内半径方向の出力比により主に支配されることが明らかとなった。この熱伝達促進の物理的な機構として，高出力バンドルでの高い蒸気発生率により生ずるバンドル内上昇蒸気流の増加が，共存する液体の上昇流量を増加させ，その結果，熱伝達促進が生ずるという機構が考えられる。この考えに基づく熱伝達促進に対する物理モデルを開発するためには，次に示す関係を定量的に明らかにする必要がある。(1)蒸気発生率と液上昇流量との関係，(2)クエンチフロントより上での横流れ量及び(3)半径方向出力比による熱伝達促進の程度と液上昇流量の増加量との関係。

本報では，上記物理モデルを開発する一環として，半径方向出力比と熱伝達促進の関係が定量的に調べられているSCTFを使い，上の(3)の関係を実験的に調べた。評価方法としては，炉心内の二次的な流動が無視できる半径方向の出力分布が平坦でありLPCI期の流量の異なる二つの試験結果より熱伝達の増加の程度を評価し，以前に行った半径方向出力比の存在による熱伝達促進の程度とを比較する方法をとった。二つの試験の流量の比はほぼ2であった。

本研究で得られた熱伝達率の増加の程度は，半径方向のピーク出力の比（PF）が1.065の場合の熱伝達促進の程度とほぼ同程度であった。このことは，上記の物理的な機構により熱伝達促進が生じるとした場合，PFが1.065の試験では最大出力バンドルと最小出力バンドルでの液上昇流量の違いが約2倍程度であることを示している。

東海研究所：〒319－11　茨城県那珂郡東海村白方字白根2－4
＊　山形大学

Contents

1. Introduction 1
2. Facility and Test Description 3
2.1 Test Facility 3
2.2 Test Conditions and Procedure 3
3. Results and Discussion 5
3.1 Measured Boundary Conditions 5
3.2 Thermal-Hydraulic Behavior in Core 6
3.3 Discussion on Heat Transfer Enhancement 7
4. Conclusion 10
Acknowledgment 11
References 11
Appendix Selected Data of Test S2-19 55

目　　次

1. 序　論 1
2. 試　験 3
2.1 試験装置 3
2.2 試験条件及び試験手順 3
3. 試験結果及び検討 5
3.1 測定された境界条件 5
3.2 炉心内熱水力学的挙動 6
3.3 熱伝達促進に関する検討 7
4. 結　論 10
謝　辞 11
参考文献 11
付録　試験Ｓ２－19のデータ抄 55

List of Tables

Table 2.1.1 Principal dimensions of SCTF core-Ⅱ
Table 2.1.2 Comparison of dimensions between SCTF and the reference PWR
Table 2.2.1 Major specified test conditions

Table 3.1.1 Chronology of major events

List of Figures

Fig.2.1.1 Vertical cross sections of pressure vessel
Fig.2.1.2 Bird's-eye view of SCTF
Fig.2.1.3 Comparison of dimensions between SCTF and the reference PWR
Fig.2.1.4 Arrangement of rod bundles
Fig.2.1.5 Dimension, configuration and axial power distribution of heater rods
Fig.2.1.6 Horizontal cross sections in upper head and in upper plenum

Fig.3.1.1 Comparison of ECC mass flow rate
Fig.3.1.2 Comparison of ECC fluid temperature
Fig.3.1.3 Comparison of pressure at containment tank-Ⅱ
Fig.3.1.4 Comparison of power at bundles 2, 4, 6 and 8
Fig.3.1.5(1) Comparison of core inlet mass flow rate
Fig.3.1.5(2) Comparison of core inlet flooding velocity
Fig.3.1.6 Comparison of integrated core inlet mass flow
Fig.3.1.7 Comparison of core inlet fluid temperature
Fig.3.1.8 Comparison of core inlet subcooling
Fig.3.1.9 Comparison of pressure at upper plenum
Fig.3.1.10 Comparison of pressure at lower plenum and at core center
Fig.3.1.11(1) Comparison of liquid level in upper plenum above bundle 1
Fig.3.1.11(2) Comparison of liquid level in upper plenum above bundle 3
Fig.3.1.11(3) Comparison of liquid level in upper plenum above bundle 5
Fig.3.1.11(4) Comparison of liquid level in upper plenum above bundle 8
Fig.3.1.12 Comparison of radial difference of liquid level in upper plenum between above bundles 8 and 1

Fig.3.2.1 Comparison of differential pressure of core full height at bundle 4
Fig.3.2.2(1) Comparison of differential pressure of core lower half at bundle 4
Fig.3.2.2(2) Comparison of differential pressure of core upper half at bundle 4
Fig.3.2.3(1) Comparison of sectional void fraction in bundle 4 at 0.085-0.7m and 0.7-1.365m
Fig.3.2.3(2) Comparison of sectional void fraction in bundle 4 at 1.365-1.905m and 2.03-2.57m
Fig.3.2.3(3) Comparison of sectional void fraction in bundle 4 at 2.695-3.235m and 3.36-3.685m
Fig.3.2.4(1) Radial comparison of sectional void fraction at 0.085-0.7m in reference test
Fig.3.2.4(2) Radial comparison of sectional void fraction at 0.085-0.7m in high LPCI test
Fig.3.2.4(3) Radial comparison of sectional void fraction at 0.7-1.365m in reference test
Fig.3.2.4(4) Radial comparison of sectional void fraction at 0.7-1.365m in high LPCI test
Fig.3.2.4(5) Radial comparison of sectional void fraction at 1.365-1.905m in reference test
Fig.3.2.4(6) Radial comparison of sectional void fraction at 1.365-1.905m in high LPCI test
Fig.3.2.4(7) Radial comparison of sectional void fraction at 2.03-2.57m in reference test
Fig.3.2.4(8) Radial comparison of sectional void fraction at 2.03-2.57m in high LPCI test
Fig.3.2.4(9) Radial comparison of sectional void fraction at 2.695-3.235m in reference test
Fig.3.2.4(10) Radial comparison of sectional void fraction at 2.695-3.235m in high LPCI test
Fig.3.2.5(1) Comparison of radial differential pressure at 1.905m between bundles 1 and 4
Fig.3.2.5(2) Comparison of radial differential pressure at 1.905m between bundles 4 and 8

Fig.3.2.6(1) Comparison of clad temperature at 0.52m and 1.38m in bundle 4
Fig.3.2.6(2) Comparison of clad temperature at 1.905m and 2.33m in bundle 4
Fig.3.2.6(3) Comparison of clad temperature at 2.76m and 3.19m in bundle 4
Fig.3.2.7 Comparison of quench time in bundle 4
Fig.3.2.8(1) Comparison of heat transfer coefficient in bundle 4 at 0.52m and 1.38m
Fig.3.2.8(2) Comparison of heat transfer coefficient in bundle 4 at 1.905m and 2.33m
Fig.3.2.8(3) Comparison of heat transfer coefficient in bundle 4 at 2.76m and 3.19m
Fig.3.2.9(1) Radial comparison of heat transfer coefficient at 1.38m
Fig.3.2.9(2) Radial comparison of heat transfer coefficient at 1.905m
Fig.3.2.9(3) Radial comparison of heat transfer coefficient at 2.33m
Fig.3.2.10 Comparison of quench time in bundles 2, 4 and 8

Fig.3.3.1(1) Comparison of heat transfer coefficient in bundle 4 at 1.735m
Fig.3.3.1(2) Comparison of heat transfer coefficient in bundle 4 at 1.905m
Fig.3.3.1(3) Comparison of heat transfer coefficient in bundle 4 at 2.33m
Fig.3.3.1(4) Comparison of heat transfer coefficient in bundle 4 at 3.19m
Fig.3.3.2(1) Radial comparison of heat transfer coefficient at 1.735m under peak power ratio of 1.065
Fig.3.3.2(2) Radial comparison of heat transfer coefficient at 1.905m under peak power ratio of 1.065
Fig.3.3.2(3) Radial comparison of heat transfer coefficient at 2.33m under peak power ratio of 1.065
Fig.3.3.3(1) Radial comparison of heat transfer coefficient at 1.735m under peak power ratio of 1.2
Fig.3.3.3(2) Radial comparison of heat transfer coefficient at 1.905m under peak power ratio of 1.2
Fig.3.3.3(3) Radial comparison of heat transfer coefficient at 2.33m under peak power ratio of 1.2
Fig.3.3.4 Comparison of difference of heat transfer coefficient
Fig.3.3.5 Comparison of horizontal differential pressure at 1.905m in tests with a radial power profile

1. Introduction

The test program of Slab Core Test Facility (SCTF) is a part of the large scale reflood test program in which the test program of Cylindrical Core Test Facility (CCTF) is also conducted. The principal purposes of both test programs are to clarify thermal-hydraulic behaviors in the primary coolant system of a pressurized water reactor (PWR) during a reflood phase of a large break loss-of-coolant accident (LOCA) and to demonstrate and quantify the safety margin of the emergency core coolant system (ECCS) against the accident. In the CCTF test program, major objective is to study system behaviors. On the other hand, major objective of the SCTF test is to study two-dimensional thermal-hydraulic behaviors in pressure vessel which has a core of electrically heated rod bundles with a full height, full radial width and single bundle along the azimuthal direction.

Many small scale reflood experiments have been performed in the past.[1] However, the two-dimensional behaviors have not been clarified because the flow area of core was much smaller than that in an actual reactor. Therefore, effects of various test parameters on the two-dimensional reflooding phenomena have been studied in the SCTF test series[2]-[6] and the radial power ratio of core was revealed to be the dominant parameter for heat transfer enhancement in higher power bundles[7]. It was also reported in reference (7) that the shape of radial power distribution within the maximum power ratio of 1.36 and the scale of core radius from 1/4.6 to 1/1 had little effect on the two-dimensional heat transfer behavior.

The results in reference (7) indicate that the degree of heat transfer enhancement does not depend on the two-dimensional flow pattern in pressure vessel affected by the shape of radial power distribution and the core radius but is determined by the degree of steam production rate in bundle. As a physical mechanism for the heat transfer enhancement, it can be considered from the experimental evidence that the increase of upward steam flow rate in a higher power bundle which is caused by the higher steam production rate in the bundle gives the higher upward liquid flow rate in the bundle and the two-dimensional hydraulic behavior such as the cross flow among bundles is then determined to compensate the increase of the upward flow rate. The increase of the liquid flow rate can give the heat transfer enhancement because the film boiling heat transfer is increased with the liquid flow rate[8]. In order to develop a mechanistic model for the heat

transfer enhancement based on this idea, the following relations should be identified quantitatively: (1) Relation between the steam production rate and the upward liquid flow rate, (2) Cross flow rate above the quench front and (3) Relation between the degree of heat transfer enhancement due to radial power ratio and the amount of increase of upward liquid flow rate.

In this report, the above relation (3) is investigated as a step in order to develop the mechanistic model mentioned above using the SCTF where the relation between the radial power ratio and the heat transfer enhancement has been made clear quantitatively. The degree of increase of heat transfer between two forced feed tests with the different flow rate in LPCI period will be compared with the degree of heat transfer enhancement under a radial power ratio in the previous SCTF tests. The two forced feed tests are carried out under the condition without any significant cross flow in the core. Namely, the radial power profile for both tests is flat and the radial distribution of liquid levels in the upper plenum is intended to be flat by extracting water from the upper plenum. By this method, the increase of ECC water mass flow rate injected into the lower plenum can be considered to simulate the increase of the liquid flow rate in bundle.

Tests investigated in this report are Tests S2-14 (Run number 619, Reference test) and S2-19 (624, High LPCI test) in the SCTF Core-Ⅱ tests. The selected data obtained in Test S2-19 are presented in Appendix.

2. Facility and Test Description

2.1 Test Facility

The SCTF was designed to properly simulate the two-dimensional thermal-hydraulic behaviors in pressure vessel during refill-reflood phase. The pressure vessel is slab geometry as shown in Fig. 2.1.1. Full scale radial and axial section of a reference PWR is provided using a simulated core with single bundle depth. The reference reactor is the Trojan reactor in the United States which is a four loop 3300MWt PWR. The simulated core consists of 8 bundles arranged in a row. On the other hand, simplified primary coolant loops are provided. Bird's-eye view of the pressure vessel and the coolant loop is shown in Fig. 2.1.2. The scaling of flow area and fluid volume of each component is in accordance with the core flow area scaling. The principal dimensions of the facility is shown in Table 2.1.1, and the comparison of dimensions between the SCTF and the referred PWR is shown in Table 2.1.2 and in Fig. 2.1.3.

Each bundle has 234 electrically heated rods and 22 non-heated rods. The arrangement of rod bundles is shown in Fig. 2.1.4. The dimensions of the heater rods are based on a 15×15 type fuel bundle and the heated length and the outer diameter of each heater rod are 3.66m and 10.7mm, respectively. The dimension, configuration and axial power distribution of each heater rod are shown in Fig. 2.1.5. The axial peaking factor is 1.4. The heater rods and non-heated rods are fixed at the top of the core allowing the rods to move downward when the thermal expansion occurs. For better simulation for flow resistance in the lower plenum the simulated rods do not penetrate through the bottom plate of the lower plenum.

The design of upper plenum internals is based on that of the new Westinghouse 17×17 array fuel assemblies. The internals consist of control rod guide tubes, support columns, orifice plates and open holes as shown in Fig. 2.1.6. The radius of each component is scaled down by factor 8/15 from that of an actual reactor.

More detailed information on the SCTF is available in reference (9).

2.2 Test Conditions and Procedure

ECC water was injected directly into the lower plenum in the tests examined in this report. The downcomer had been isolated from the lower

plenum by inserting a blocking plate. This test method is called as forced feed reflooding method.

The results in two force feed tests were used in this study to meet the objective in Introduction, those are Tests S2-14 (Reference test) and S2-19 (High LPCI test). The test conditions except for the ECC water mass flow rate in LPCI period were intended to be the same for the two tests. These two tests were performed under the flat radial power distribution. Water extraction from the upper plenum was performed for both tests to maintain the flat distribution of collapsed liquid level because the non-uniform distribution of liquid level in upper plenum was found to affect the two-dimensional core thermal-hydraulic behaviors as described in reference (5). Therefore, data from these two tests are considered to give informations under the condition without inducing two-dimensional thermal-hydraulic behaviors due to test conditions. Major specified test conditions are listed in Table 2.2.1.

The test procedure for these two tests is as follows: After setting the initial conditions (pressure and saturation condition, etc.), core heating was initiated. When four thermocouple signals at the surface of cladding exceeded 910K, the accumulator (Acc) injection into the lower plenum was initiated. The initial water level in the lower plenum was about 0.14m below the bottom of heated part. The maximum cladding temperature at the reflood initiation was intended to be 922K. At the time of the Acc injection start, the core power decay simulation was started from the value at 40s after shutdown of an actual reactor. The decay curve was based on the "1.02×(ANS standard + actinides)".

3. Results and Discussion

3.1 Measured Boundary Conditions

Figures 3.1.1 and 3.1.2 show the comparison of ECC mass flow rate and ECC water temperature. In these figures, L.P. means the port at lower plenum. ECC mass flow rate in ACC injection period is almost the same for these two tests. ECC water temperature in high LPCI test is slightly lower than that in reference test after about 100s.

Figure 3.1.3 shows the comparison of pressure at containment tank-Ⅱ. Pressure overshoot is recognized in the period between reflood initiation time and about 100s for both tests. In the other period, the pressure is kept at about 0.2 MPa. No significant difference is observed on the pressure between the two tests.

Figure 3.1.4 shows the comparison of heating power supplied to each bundle. Initial set value and the shape of transient are the same between the two tests. As shown in this figure, the radial power profile is flat during whole transients.

Figures 3.1.5(1), 3.1.5(2) and 3.1.6 show the comparison of core inlet mass flow rate and integrated mass into the core. These values were obtained by mass balance in the SCTF pressure vessel. Basic equation for the mass balance is as follows:

Mass flow rate at the core inlet =

ECC mass flow rate - Accumulated mass flow rate in the lower plenum and in the core baffle region.

Flooding velocity shown in Fig.3.1.5(2) was calculated based on the core flow area of $0.35m^2$. Since this flow area is the maximum area as described in Table 2.1.1, effective flooding velocity might be higher than the value shown in Fig. 3.1.5(2). It is found from these figures that the difference of the mass flow rate is negligible small between the two tests in the ACC injection period and the mass flow rate in high LPCI test is about double against that in reference test after about 100s.

Figures 3.1.7 and 3.1.8 show the comparison of core inlet fluid temperature and core inlet subcooling between the two tests. The temperature and the subcooling are almost the same until about 200s. The difference of the subcooling of about 10K is observed after about 300s.

Figures 3.1.9 and 3.1.10 show the comparison of pressure at each region in the pressure vessel. The pressures are almost the same for both tests.

Figures 3.1.11(1) through 3.1.11(4) show the comparison of liquid level in the upper plenum above each bundle. Since the water in the upper plenum was extracted to keep the constant liquid level, these liquid levels are almost constant and no significant difference is observed between the two tests. The radial difference of the liquid level (Liquid level above bundle 8 - Liquid level above bundle 1) is slightly observed as shown in Fig. 3.1.12 and however the degree of the radial distribution is almost the same for the two tests.

As shown in the comparison plots until here in this section, the main difference for the core inlet and outlet conditions between the two tests was the mass flow rate at the core inlet in the LPCI period although the difference of the core inlet subcooling of about 10K was observed after about 300s. Since the core is almost quenched until about 300s as will be shown in the next section, the difference of the subcooling does not affect the objective in this study described in Introduction.

Chronology of major events is summarized in Table 3.1.1.

3.2 Thermal-Hydraulic Behavior in Core

In this section, water accumulation and heat transfer behaviors in the core including two-dimensional behaviors are presented using the data in bundles 2, 4 and 8.

Figures 3.2.1 through 3.2.2(2) show the comparison of vertical differential pressures in bundle 4. The differential pressure for each region is larger in high LPCI test than that in reference test after about 50s. Figures 3.2.3(1) through 3.2.3(3) show the comparison of sectional void fractions in bundle 4. Each void fraction was calculated from sectional differential pressure measurement by neglecting the effects of frictional and accelerational pressure drops. These comparisons indicate that the amount of water accumulation in the core is larger in high LPCI test after about 50s in the region from 0.7m measured from the bottom of core to the upper part of core.

Figures 3.2.4(1) through 3.2.4(10) show the comparison of the radial difference of sectional void fractions in the core. No significant difference is observed on the radial difference between the two tests and almost flat distribution is observed. Figures 3.2.5(1) and 3.2.5(2) show the comparison of horizontal differential pressures at 1.905m elevation (almost

middle part of the core). Plus sign of these differential pressures indicates that the pressure in bundles 1 or 4 is higher than that in bundles 4 or 8, respectively. The pressure in each bundle is found to be almost the same for the two tests.

Figures 3.2.6(1) through 3.2.6(3) show the comparison of clad surface temperatures along center rod in bundle 4. The degree of heat transfer is higher in high LPCI test except for the lower part of the core. Quench envelope in bundle 4 is compared in Fig. 3.2.7. Quench velocity becomes faster with propagating the quench front after about 100s in high LPCI test. These characteristics of better core cooling in high LPCI test are also recognized in the comparison of heat transfer coefficients shown in Figs. 3.2.8(1) through 3.2.8(3).

Figures 3.2.9(1) through 3.2.9(3) show the radial comparison of heat transfer coefficients at 1.38m, 1.905m and 2.33m elevations in each test. No significant difference is observed for the two tests. Radial comparison of quench envelopes is shown in Fig. 3.2.10. Although the slight difference of quench time among bundles is observed at the top part of the core for the two tests, no significant radial difference of quench velocity along each bundle is observed in almost the entire core for the two tests.

It is found from the results on the two-dimensional thermal-hydraulic behaviors described in this section that the relation between the liquid flow rate and the heat transfer coefficient in SCTF can be examined quantitatively by using the data of these two tests because no significant two-dimensional behaviors are observed for the two tests.

3.3 Discussion on Heat Transfer Enhancement

In this section, the increase of heat transfer coefficient due to the increase of liquid flow rate obtained in this study is quantitatively compared with the radial difference of heat transfer coefficient in the tests with a non-uniform radial power distribution.

Figures 3.3.1(1) through 3.3.1(4) show the comparison of heat transfer coefficient at a same distance from the quench front in bundle 4 for the two tests in this study. The heat transfer coefficient in high LPCI test is higher than that in reference test even at a same distance from the quench front. Figures 3.3.2(1) through 3.3.2(3) and Figs. 3.3.3(1) through 3.3.3(3) show the radial difference of heat transfer coefficient on the same

plane in Fig. 3.3.1 under radial peak power ratio (PF) of 1.065 and 1.2, respectively. These results were obtained in Tests S2-02 and S2-16, respectively. As shown in these figures, the steeper radial power distribution gives the larger radial difference of heat transfer coefficient. In these figures, the power in bundle 4 (B4) is the highest and that in bundle 8 (B8) is the lowest.

Figure 3.3.4 shows the comparison between the difference of heat transfer coefficient obtained in this study and the radial difference (heat transfer coefficient in B4 - that in B8) in the tests with a radial power profile. The difference obtained in this study is almost correspond to that under PF=1.065 although the peak recognized in the tests with a radial power profile is not clearly observed for the data in this study. In the case that the heat transfer enhancement under a radial power distribution is attained by the difference of upward liquid flow rate among different power bundles mentioned in Introduction, the above result indicates that the liquid upward flow rate in the highest power bundle is about twice time higher than that in the lowest one in the test with PF=1.065.

The radial difference of heat transfer coefficient in the tests with a radial power profile is characterized as two broad peaks at a certain distance from the quench front. The first peak in the region more than 1m is correspond to the period of ACC injection. The second one is in the LPCI period. On the other hand, no significant peaks are recognized for the data in this study. The reason of no peak in the Acc period is because the core inlet mass flow rate is almost the same in the period in the tests of this study. The difference of heat transfer coefficient in this study tends to become larger with approaching the quench front although the radial difference in the tests with a radial power profile has a peak and becomes smaller near the quench front. The different tendency in the LPCI period is not clear at present and however the relation between the amount of liquid flow rate and the distance from quench front in the tests with a radial power profile might be different from that in this study.

Figure 3.3.5 shows the comparison of the horizontal differential pressure between the highest power bundle, bundle 4, and the lowest power bundle, bundle 8, at 1.905m elevation for the tests with a radial power profile. The larger differential pressure under the steeper radial power profile (PF=1.2) is observed. If it can be assumed that the horizontal differential pressure indicates the degree of the cross flow rate which was

considered in this study to be governed by the upward liquid flow rate mentioned in Introduction, this result indicates that the radial difference of liquid upward flow rate under PF=1.2 is larger than the difference of liquid flow rate in the tests of this study.

4. Conclusion

The present study on SCTF Core-Ⅱ tests was performed to investigate the quantitative relation between the degree of heat transfer enhancement due to radial power ratio and the amount of increase of upward liquid flow rate in a bundle as a step to develop the mechanistic model for the heat transfer enhancement mentioned in Introduction.

The degree of the increase of heat transfer coefficient in the tests of this study was almost correspond to that of the heat transfer enhancement under PF=1.065. In the case that the heat transfer enhancement is attained by the physical mechanism mentioned in Introduction, this result indicates that the upward liquid flow rate in the highest power bundle is about twice time higher than that in the lowest one in the tests with PF=1.065. Under the steeper profile condition the difference of upward liquid flow rate between in the highest power bundle and in the lowest one was supposed to be larger than the difference of liquid flow rate in the tests of this study (about double).

Acknowledgment

The authors would like to express their appreciation to Dr. M.Sobajima in Department of Fuel Safety Research of JAERI and to Messrs. T.Iguchi, T.Okubo, Drs. J.Sugimoto and H.Akimoto of CCTF analysis group in Department of Reactor Engineering of JAERI for their useful discussions.

References

(1) For instance, L.E. Hochreiter, FLECHT SEASET Program Final Report, NUREG/CR-4167, (1985).

(2) H. Adachi, et al., System Pressure Effects on Reflooding Phenomena observed in the SCTF Core-I Forced Flooding Tests, JAERI-M 83-079, (1982).

(3) Y. Sudo, et al., Effect of Upper Plenum Water Accumulation on Reflooding Phenomena under Forced Flooding in SCTF Core-I Test, JAERI-M 83-114, (1983).

(4) T. Iwamura, et al., Effects of Core Inlet Water Subcooling on Reflooding Phenomena - SCTF Core-I Forced Feed Flooding Test -, JAERI-M 83-122, (1983).

(5) T. Iwamura, et al., Effects of Radial Core Power Profile on Core Thermo-Hydraulic Behavior during Reflood Phase in PWR-LOCA, J. Nucl. Sci. Tech., 20[9], 743-751, (1983).

(6) T. Iwamura, et al., Two-Dimensional Thermal-Hydraulic Behavior In Core In SCTF Core-II Cold Leg Injection Tests (Radial Power Profile Test Results), JAERI-M 85-106, (1985).

(7) T. Iwamura, et al., Quantitative Evaluation of Heat Transfer Enhancement due to Radial Power Distribution during Reflood Phase of PWR-LOCA, J. Nucl. Sci. Tech., 26[4], 428-440, (1989).

(8) A. Ohnuki, et al., Effect of Liquid Flow Rate on Film Boiling Heat Transfer during Reflood in Rod Bundle, J. Nucl. Sci. Tech., 27[6], 535-546, (1990).

(9) H. Adachi, et al., Design of Slab Core Test Facility (SCTF) in Large Scale Reflood Test Program, Part I : Core-I, JAERI-M 83-080, (1983).

Acknowledgment

The authors would like to express their appreciation to Dr. M.Sobajima in Department of Fuel Safety Research of JAERI and to Messrs. T.Iguchi, T.Okubo, Drs. J.Sugimoto and H.Akimoto of CCTF analysis group in Department of Reactor Engineering of JAERI for their useful discussions.

References

(1) For instance, L.E. Hochreiter, FLECHT SEASET Program Final Report, NUREG/CR-4167, (1985).

(2) H. Adachi, et al., System Pressure Effects on Reflooding Phenomena observed in the SCTF Core-I Forced Flooding Tests, JAERI-M 83-079, (1982).

(3) Y. Sudo, et al., Effect of Upper Plenum Water Accumulation on Reflooding Phenomena under Forced Flooding in SCTF Core-I Test, JAERI-M 83-114, (1983).

(4) T. Iwamura, et al., Effects of Core Inlet Water Subcooling on Reflooding Phenomena - SCTF Core-I Forced Feed Flooding Test -, JAERI-M 83-122, (1983).

(5) T. Iwamura, et al., Effects of Radial Core Power Profile on Core Thermo-Hydraulic Behavior during Reflood Phase in PWR-LOCA, J. Nucl. Sci. Tech., 20[9], 743-751, (1983).

(6) T. Iwamura, et al., Two-Dimensional Thermal-Hydraulic Behavior In Core In SCTF Core-II Cold Leg Injection Tests (Radial Power Profile Test Results), JAERI-M 85-106, (1985).

(7) T. Iwamura, et al., Quantitative Evaluation of Heat Transfer Enhancement due to Radial Power Distribution during Reflood Phase of PWR-LOCA, J. Nucl. Sci. Tech., 26[4], 428-440, (1989).

(8) A. Ohnuki, et al., Effect of Liquid Flow Rate on Film Boiling Heat Transfer during Reflood in Rod Bundle, J. Nucl. Sci. Tech., 27[6], 535-546, (1990).

(9) H. Adachi, et al., Design of Slab Core Test Facility (SCTF) in Large Scale Reflood Test Program, Part I : Core-I, JAERI-M 83-080, (1983).

Table 2.1.1 Principal dimensions of SCTF core-Ⅱ

1.	Core Dimension	
(1)	Quantity of Bundle	8 Bundles
(2)	Bundle Array	1 × 8
(3)	Bundle Pitch	230 mm
(4)	Rod Array in a Bundle	16 × 16
(5)	Rod Pitch in a Bundle	14.3 mm
(6)	Quantity of Heater Rod in a Bundle	234 rods
(7)	Quantity of Non-Heated Rod in a Bundle	22 rods
(8)	Total Quantity of Heater Rods	234×8=1872 rods
(9)	Total Quantity of Non-Heated Rods	22×8=176 rods
(10)	Effective Heated Length of Heater Rod	3660 mm
(11)	Diameter of Heater Rod	10.7 mm
(12)	Diameter of Non-Heated Rod	13.8 mm
2.	Flow Area & Fluid Volume	
(1)	Core Flow Area	0.259 m^2
(2)	Core Fluid Volume	0.92 m^3
(3)	Baffle Region Flow Area	0.10 m^2
(4)	Baffle Region Fluid Volume (nominal)	0.36 m^3
(5)	Effective Core Area Based on the Measured Level-Volume Relationship Including Gap between Core Barrel and Pressure Vessel Wall and Various Penetration Holes	0.35 m^2
(6)	Downcomer Flow Area	0.121 m^2
(7)	Upper Annulus Flow Area	0.158 m^2
(8)	Upper Plenum Horizontal Flow Area	0.525 m^2
(9)	Upper Plenum Fluid Volume	1.16 m^3
(10)	Upper Head Fluid Volume	0.86 m^3
(11)	Lower Plenum Fluid Volume	1.305 m^3
(12)	Steam Generator Inlet Plenum Simulator Flow Area	0.626 m^2
(13)	Steam Generator Inlet Plenum Simulator Fluid Volume	0.931 m^3

Table 2.1.1 (Continued)

(14) Steam Water Separator Fluid Volume	5.3	m^3
(15) Flow Area at the Top Plate of Steam Generator Inlet Plenum Simulator	0.195	m^3
(16) Hot Leg Flow Area	0.0826	m^2
(17) Intact Cold Leg Flow Area (Diameter = 297.9 mm)	0.0697	m^2
(18) Broken Cold Leg Flow Area (Diameter = 151.0 mm)	0.0179	m^2
(19) Containment Tank-Ⅰ Fluid Volume	30	m^3
(20) Containment Tank-Ⅱ Fluid Volume	50	m^3
3. Elevation & Height		
(1) Top Surface of Upper Core Support Plate (UCSP)	0	mm
(2) Bottom Surface of UCSP	- 76	mm
(3) Top of the Effective Heated Length of Heater Rod	- 393	mm
(4) Bottom of the Skirt in the Lower Plenum	-5270	mm
(5) Bottom of Intact Cold Leg	+ 724	mm
(6) Bottom of Hot Leg	+1050	mm
(7) Top of Upper Plenum	+2200	mm
(8) Bottom of Steam Generator Inlet Plenum Simulator	+1933	mm
(9) Centerline of Loop Seal Bottom	-2281	mm
(10) Bottom Surface of End Box	-185.1	mm
(11) Top of Upper Annulus of Downcomer	+2234	mm
(12) Height of Steam Generator Inlet Plenum Simulator	1595	mm
(13) Height of Loop Seal	3140	mm
(14) Inner Height of Hot Leg Pipe	737	mm
(15) Bottom of Lower Plenum	-5770	mm
(16) Top of Upper Head	+2887	mm

Table 2.1.2 Comparison of dimensions between SCTF and the reference PWR

Item	SCTF	PWR	Ratio
Quantity of Bundle	8	193	1/24.1
Number of Heater Rod	1872	39372	1/21.0
Number of Rods	2048	43425	1/21.2
Effective Length of Heater Rod (mm)	3660	3660	1/1
Rod Pitch (mm)	14.30	14.30	1/1
Diameter of Heater Rod (mm)	10.70	10.70	1/1
Diameter of Unheated Rod (mm)	13.80	13.87	1/1
Flow Area between Core Walls (m^2)	0.259	4.76	1/17.7
Effective Core Area Based on the Measured Level-Volume Relationship (m^2)	0.35	4.76	1/13.6
Fluid Volume of Core Enveloped by Honeycomb Insulators*	0.92	17.95	1/19.5
Fluid Volume of Lower Plenum (m^3)	1.305	29.62	1/22.7
Fluid Volume of Upper Head (m^3)	0.86	19.8	1/23.0
Baffle Region Flow Area (m^2)	0.10	1.76	1/17.6
Upper Plenum Fluid Volume (m^3)	1.16	23.8	1/20.5
Downcomer Flow Area (m^2)	0.121	2.47	1/20.4
UCSP Thickness (m)	76	76	1/1
Steam Generator Inlet Plenum Simulator Volume (m^3)	0.931	4.25×4	1/18.3
Height of Steam Generator Inlet Plenum Simulator (m)	1.595	1.595	1/1
Flow Area at the Top Plate of Steam Generator Inlet Plenum Simulator (m^2)	0.19	4.0	1/21.2
Major Axis Length of Hot Leg Cross Section (mm)	737	736.6	1/1
Flow Area of Hot Leg (m^2) (4 Loops)	0.0826	1.704	1/20.6
Flow Area of Intact Loop (m^2) (3 Loops)	0.0696	1.149	1/16.5
Flow Area of Broken Cold Leg (m^2)	0.0179	0.383	1/21.4
* Fluid Volume of Core Including Gaps between Core Barrel and Pressure Vessel Wall (m^3)	1.74		

Table 2.2.1 Major specified test conditions

	High LPCI Test (S2-19)	Reference Test (S2-14)
Initial system pressure (MPa)	0.2	0.2
Acc injection mass flow rate (kg/s)	26.2	26.1
LPCI injection mass flow rate (kg/s)	9.6	4.8
Acc and LPCI injection port	Lower plenum (Forced feed)	Lower plenum (Forced feed)
Acc water temperature (K)	363	368
LPCI water temperature (K)	365 ～ 393	393
Initial total core power (MW)	7.12	7.12
Power decay curve	(ANS + Actinides) × 1.02 from 40s after scram	
Radial power profile	Flat	Flat
Maximum core temp. at reflood initiation (K)	922	922
Set value of maximum liquid level above UCSP (m)	0.13	0.13

Table 3.1.1 Chronology of major events

	High LPCI Test (S2-19)	Reference Test (S2-14)
	Time after flood (s)	
Core power "ON"	-113.0	-114.0
ECC injection initiation	-2.5	-3.0
Core power decay initiation	-2.0	-3.0
Reflood initiation	0	0
Maximum core temperature	10.0 (957.8K)	10.0 (965K)
Maximum containment tank II pressure	23.0 (0.223MPa)	23.0 (0.22MPa)
Maximum core pressure	29.0 (0.27MPa)	28.0 (0.266MPa)
Initiation time for controlling the liquid level above UCSP	77.5	77.0
Whole core quenched	314.5	368.0
Stop time for controlling the liquid level above UCSP	377.5	377.0

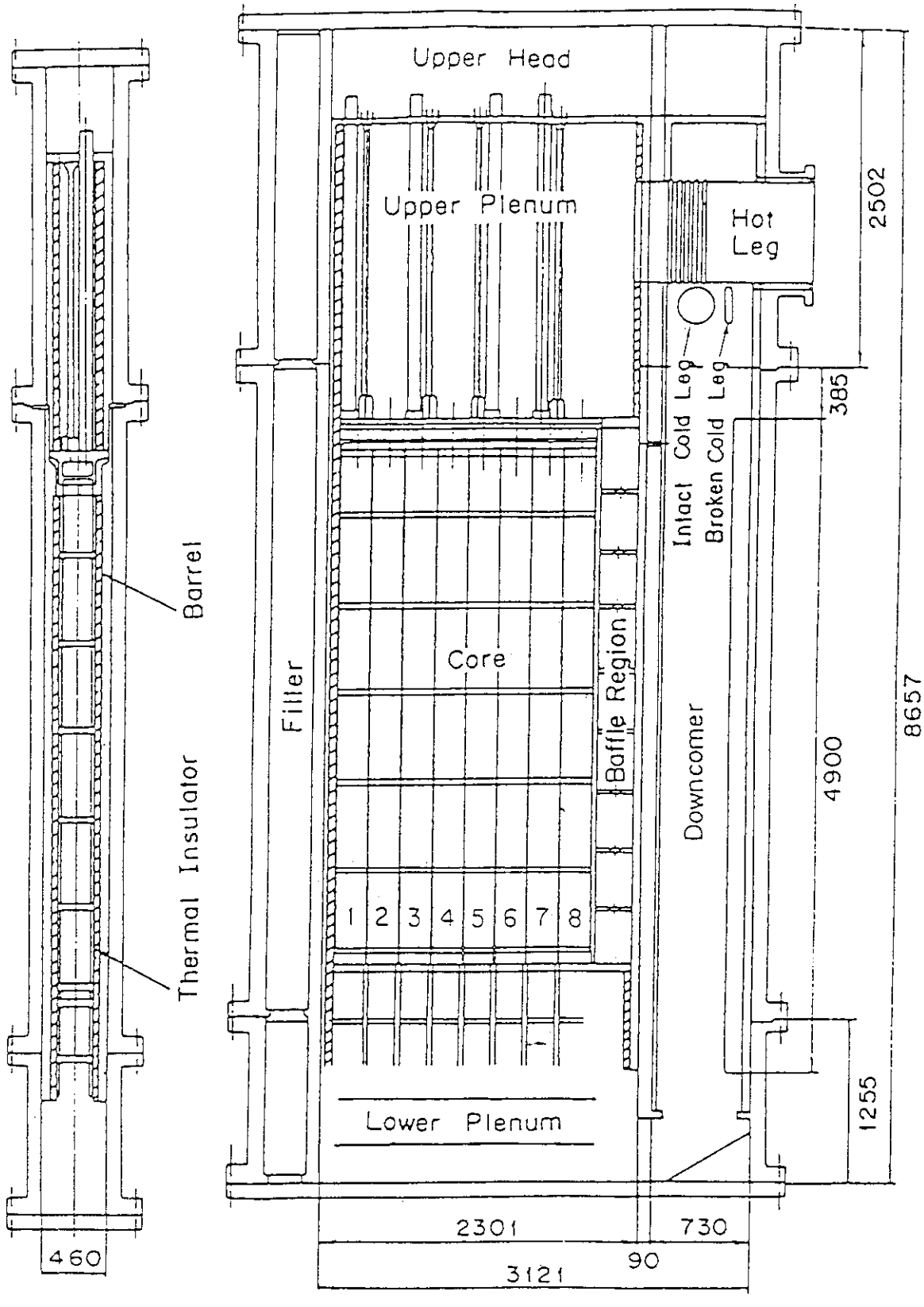

Fig.2.1.1 Vertical cross sections of pressure vessel

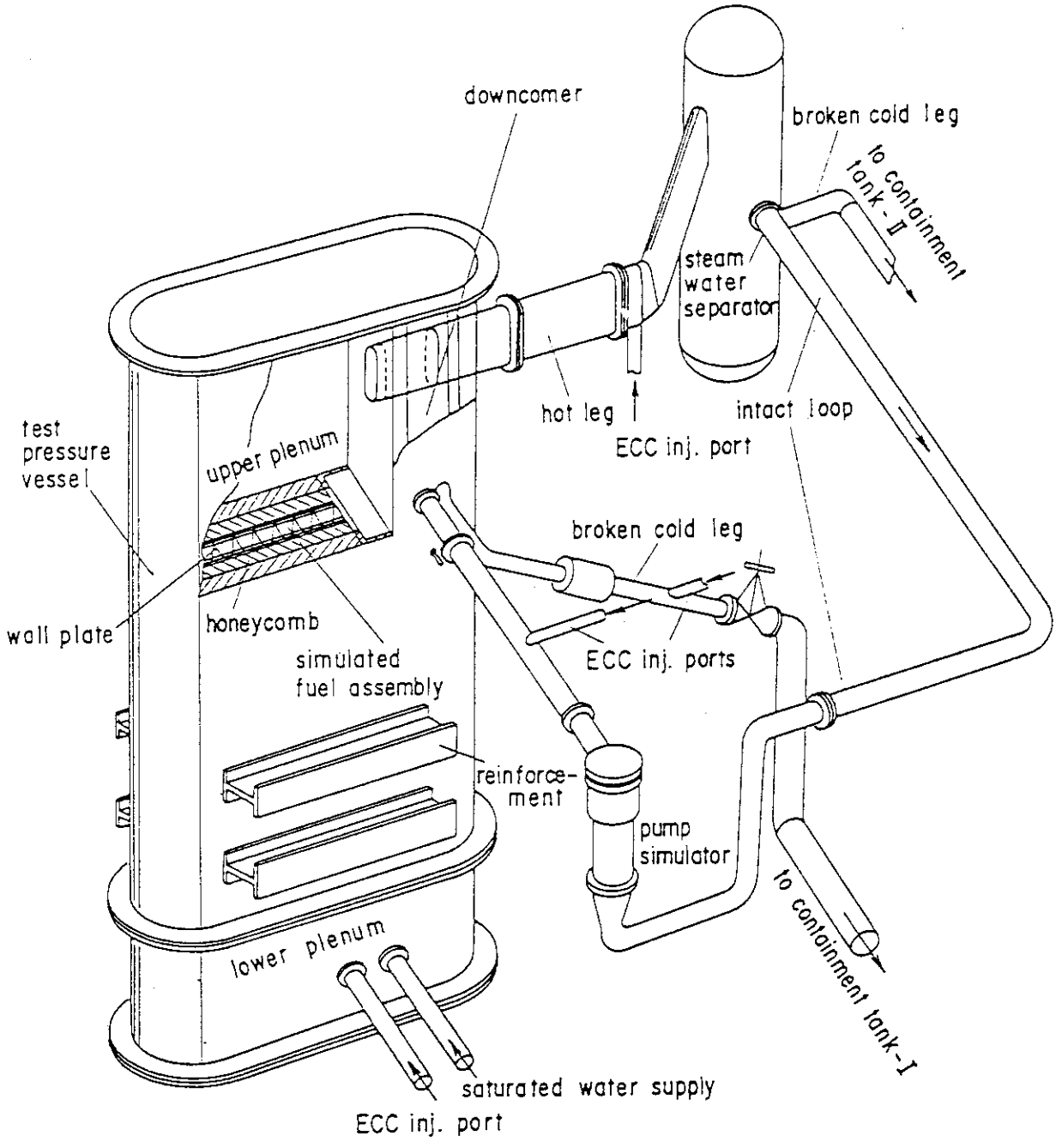

Fig.2.1.2 Bird's-eye view of SCTF

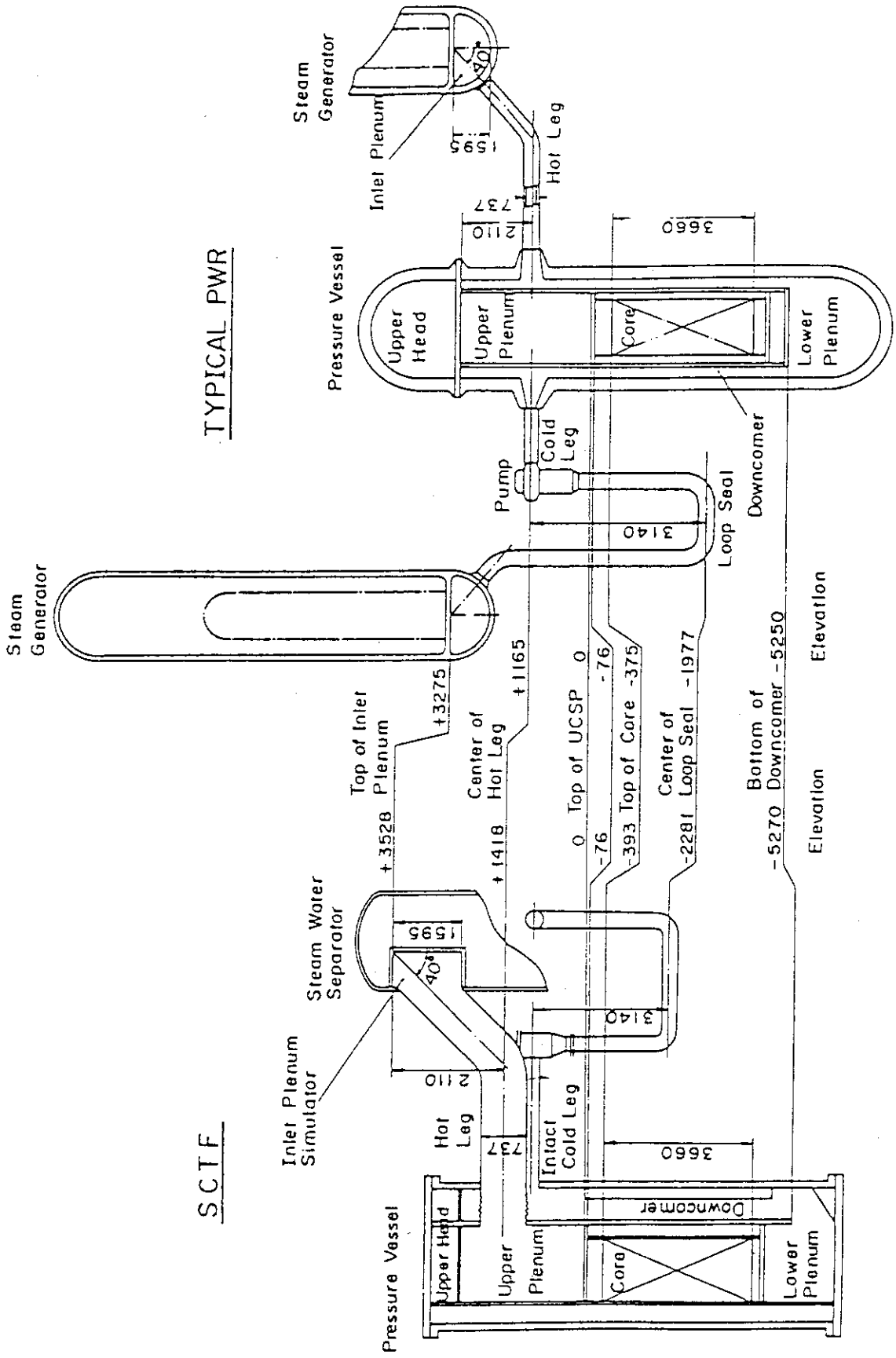

Fig.2.1.3 Comparison of dimensions between SCTF and the reference PWR

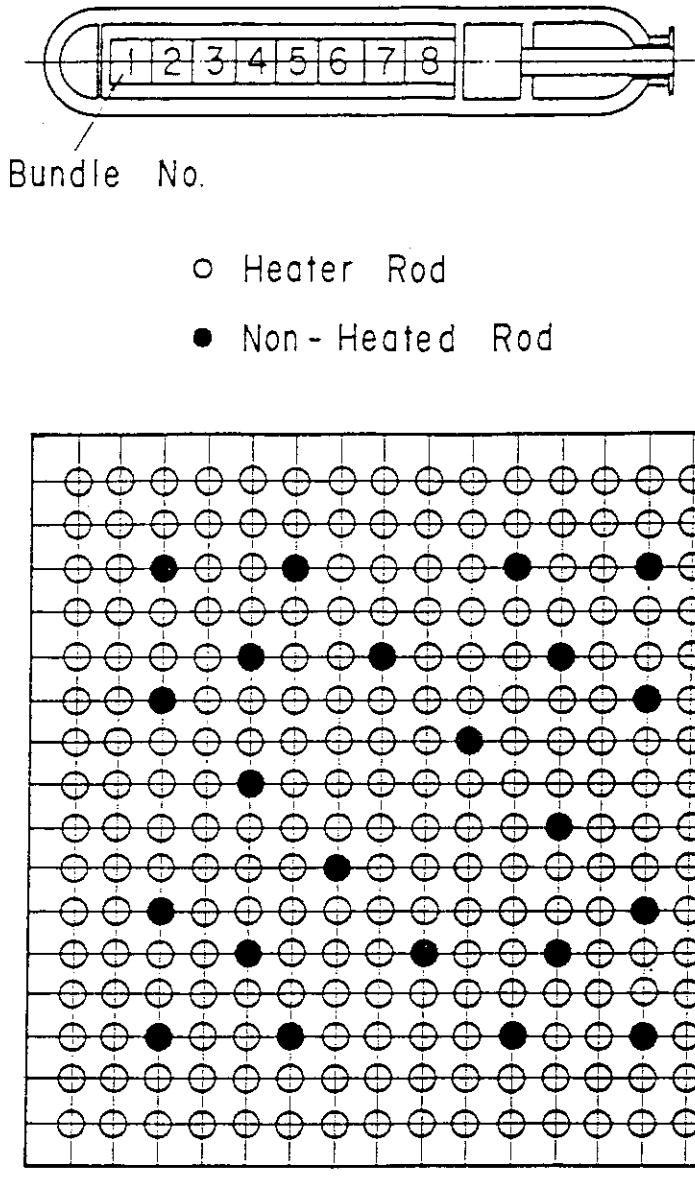

Fig.2.1.4 Arrangement of rod bundles

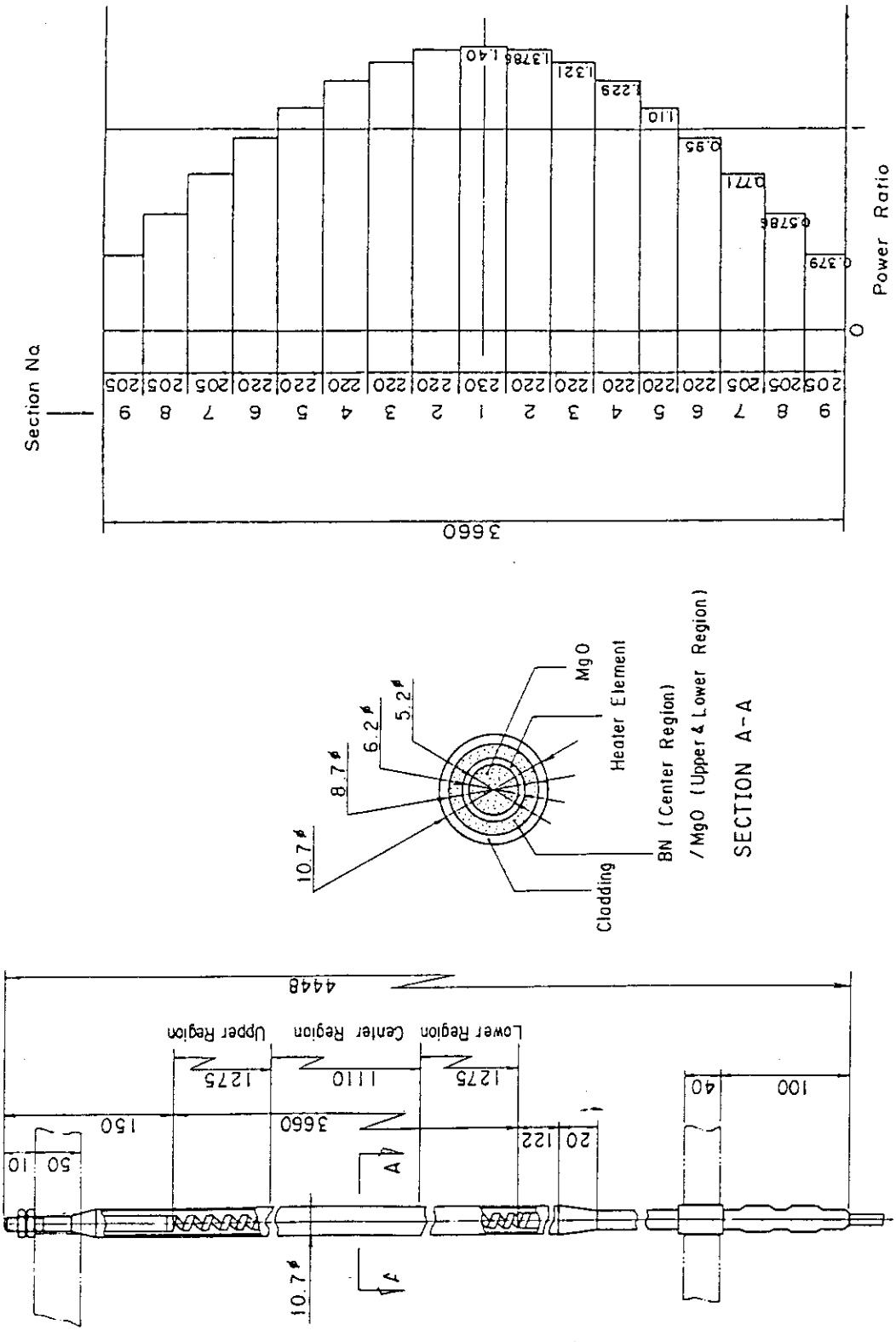

Heater Rod

Fig.2.1.5 Dimension, configuration and axial power distribution of heater rods

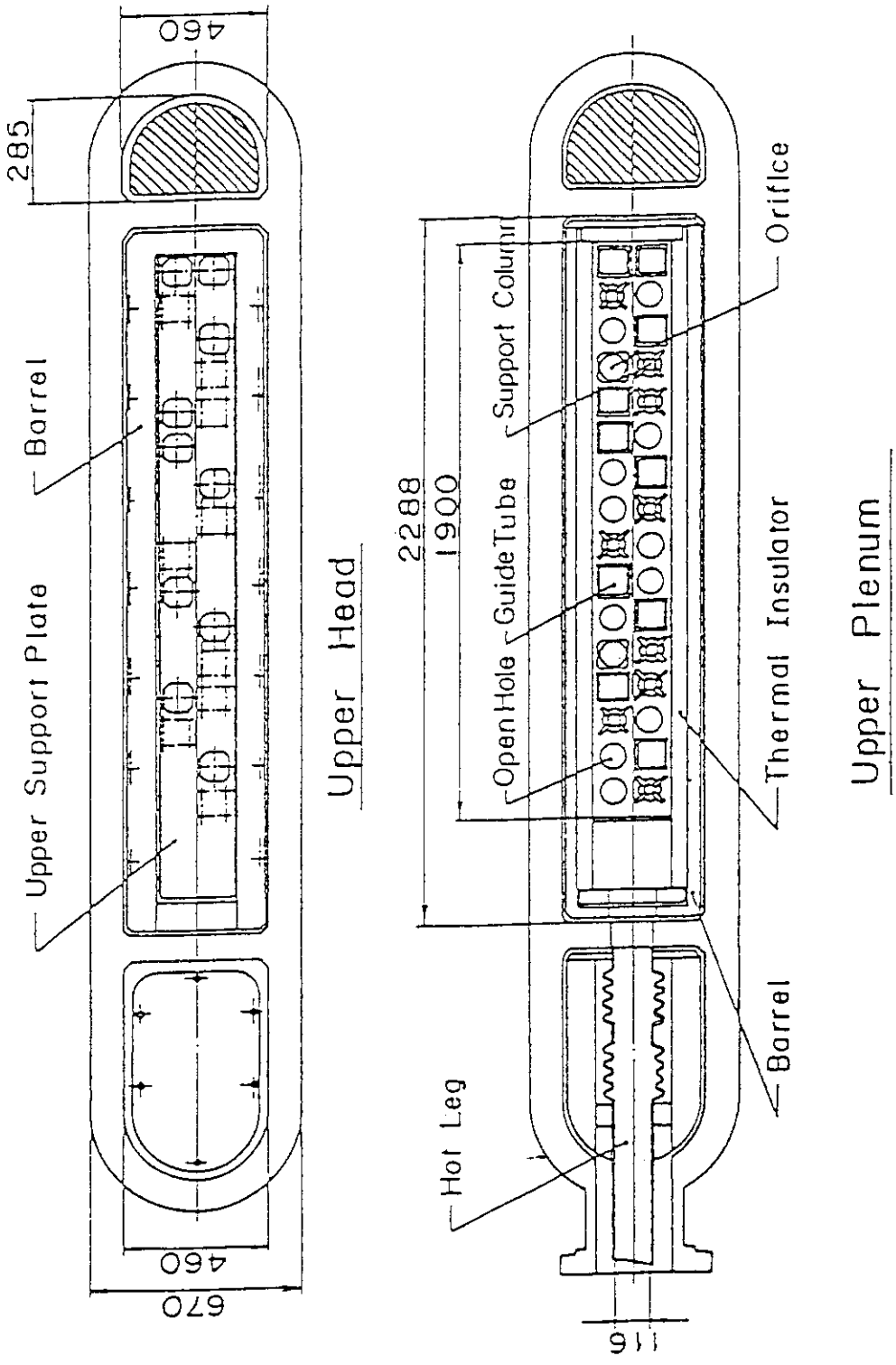

Fig.2.1.6 Horizontal cross sections in upper head and in upper plenum

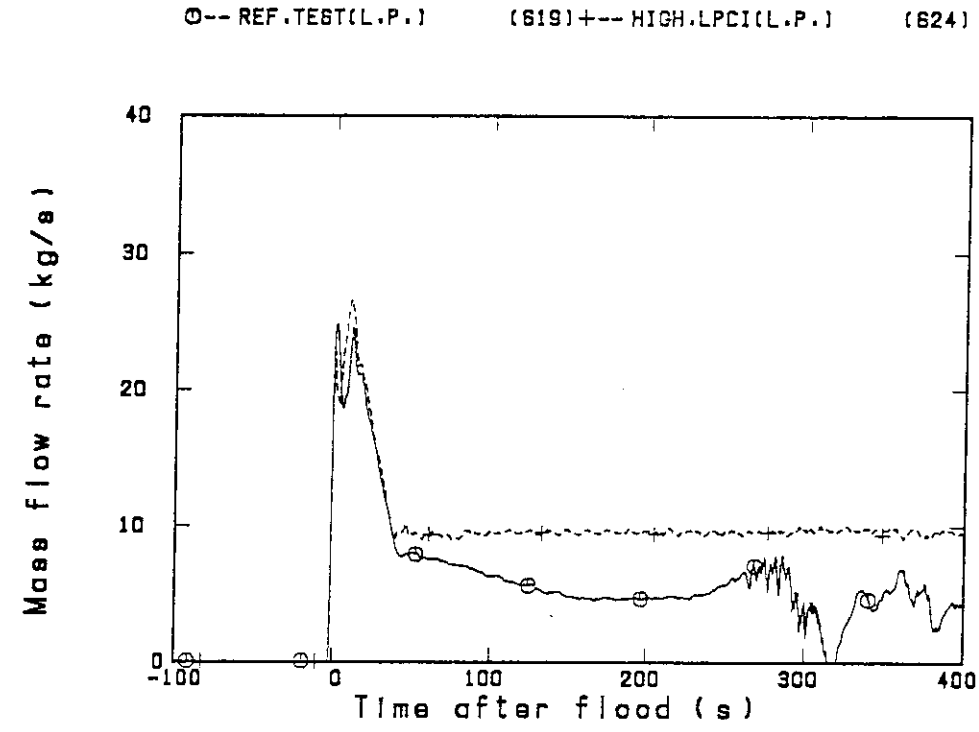

Fig.3.1.1 Comparison of ECC mass flow rate

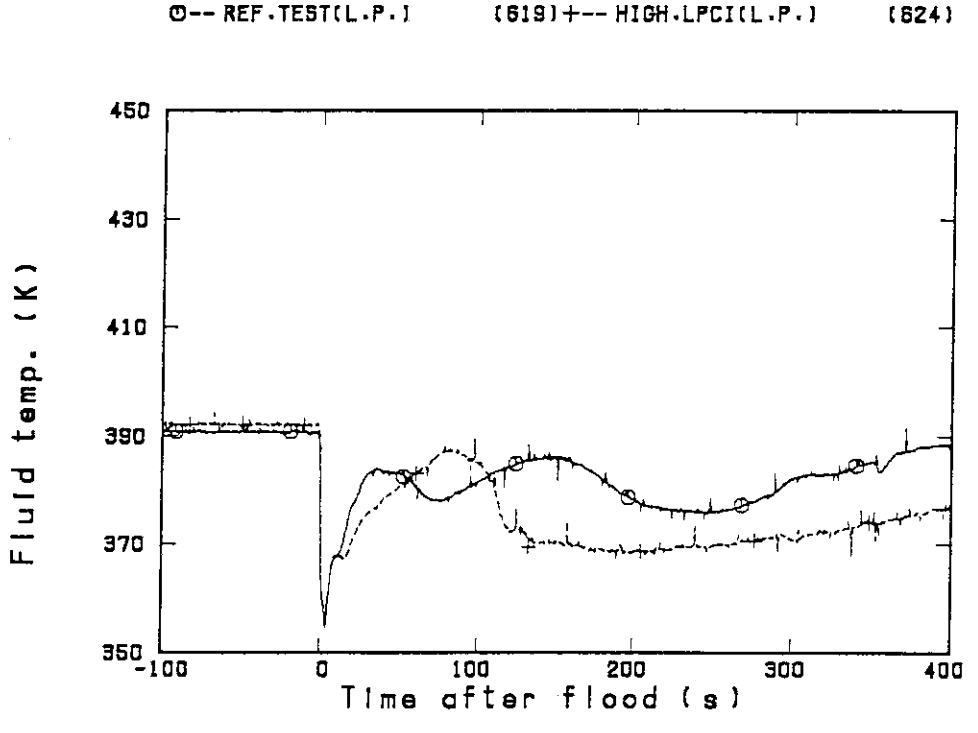

Fig.3.1.2 Comparison of ECC fluid temperature

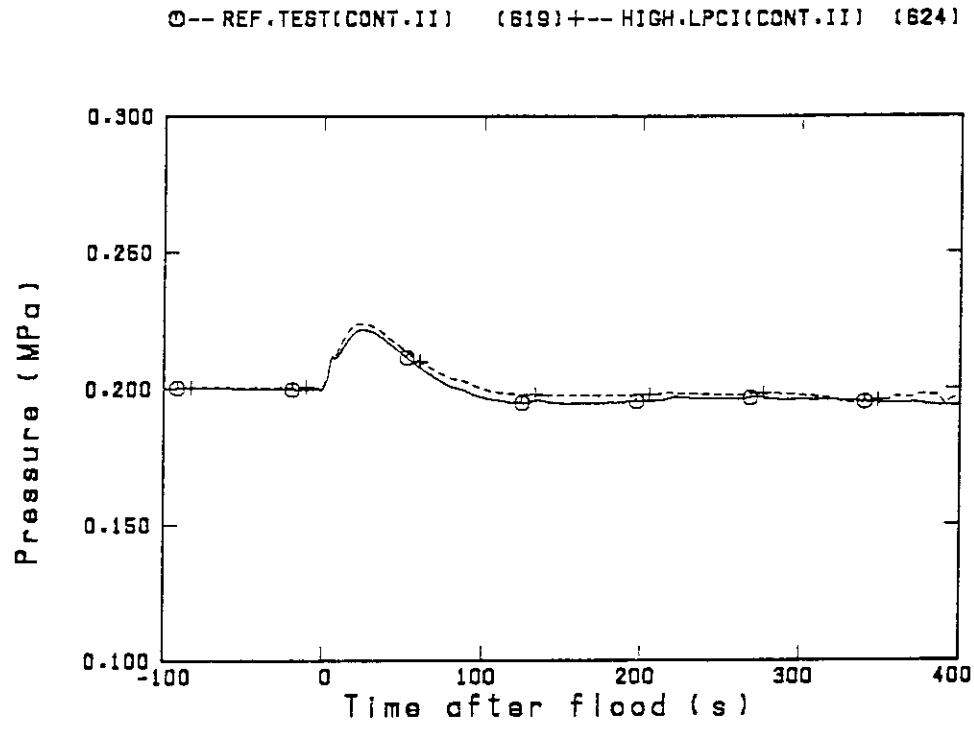

Fig.3.1.3 Comparison of pressure at containment tank-II

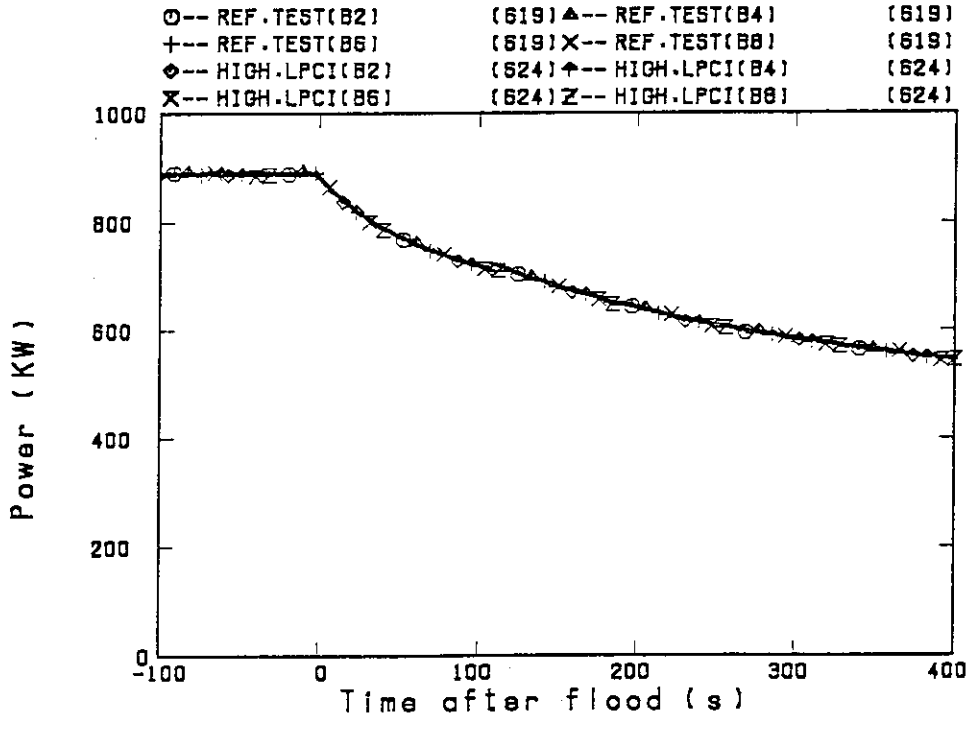

Fig.3.1.4 Comparison of power at bundles 2, 4, 6 and 8

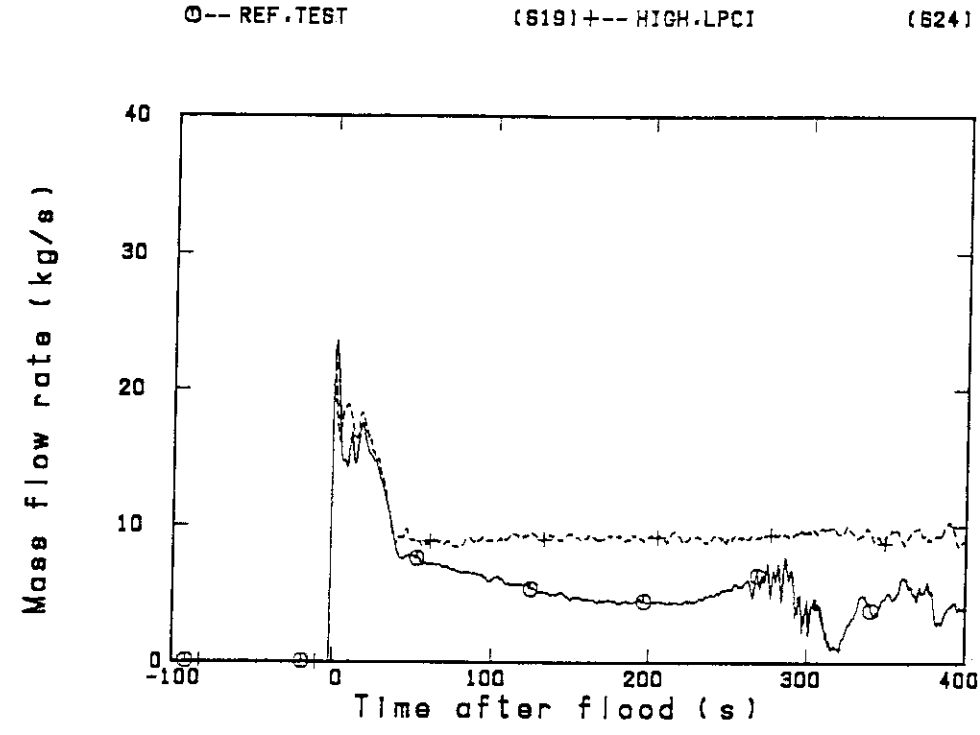

Fig.3.1.5(1)　Comparison of core inlet mass flow rate

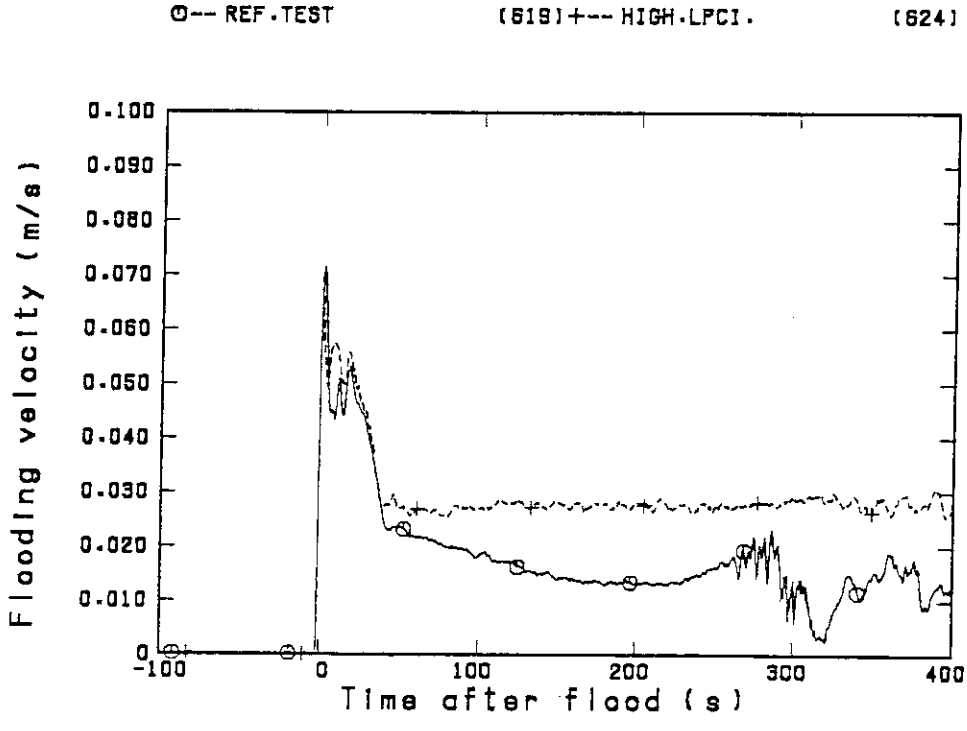

Fig.3.1.5(2)　Comparison of core inlet flooding velocity

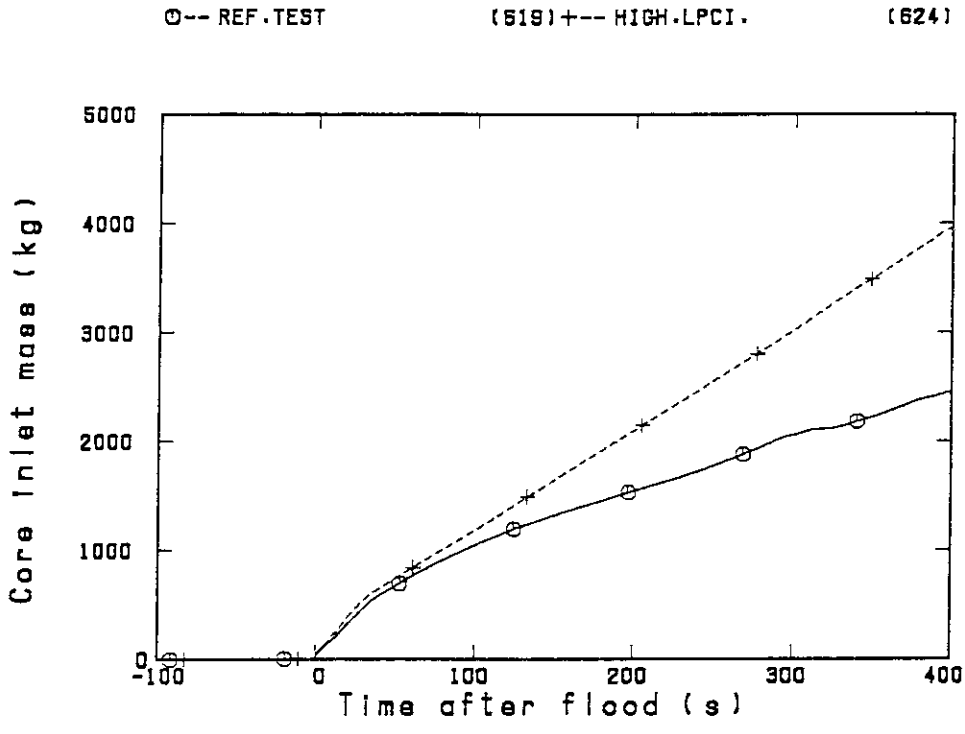

Fig.3.1.6 Comparison of integrated core inlet mass flow

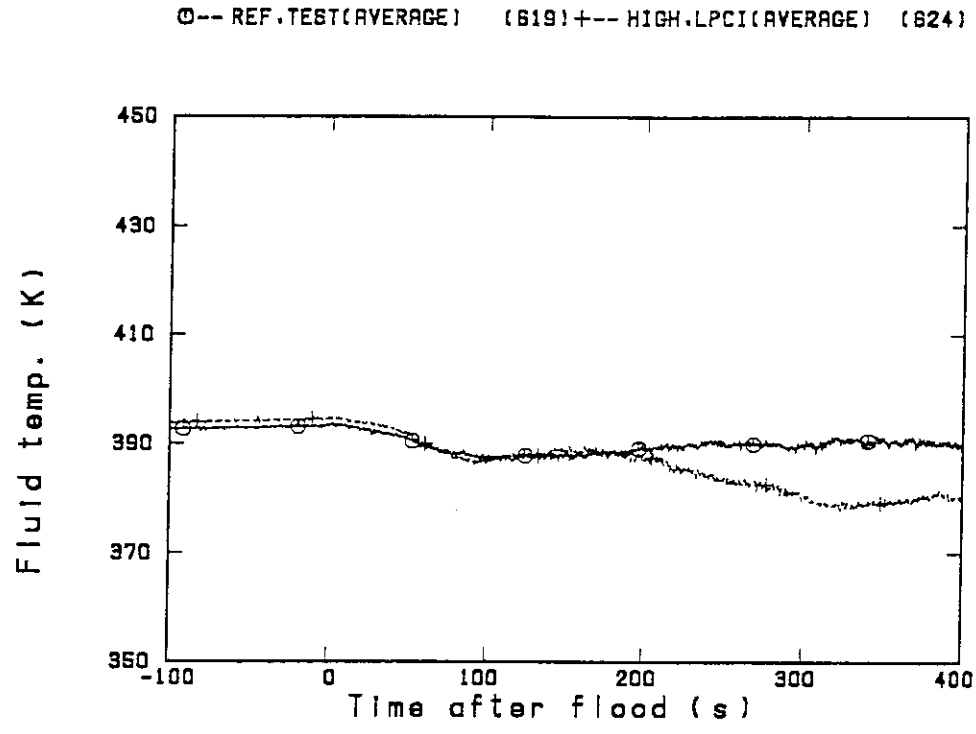

Fig.3.1.7　　Comparison of core inlet fluid temperature

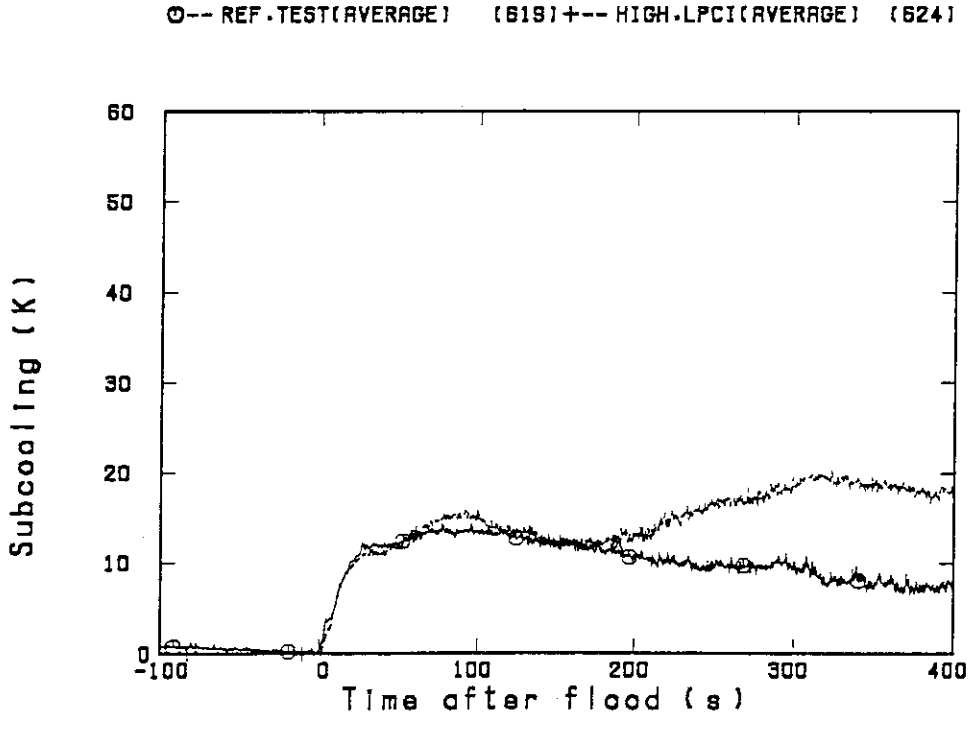

Fig.3.1.8　　Comparison of core inlet subcooling

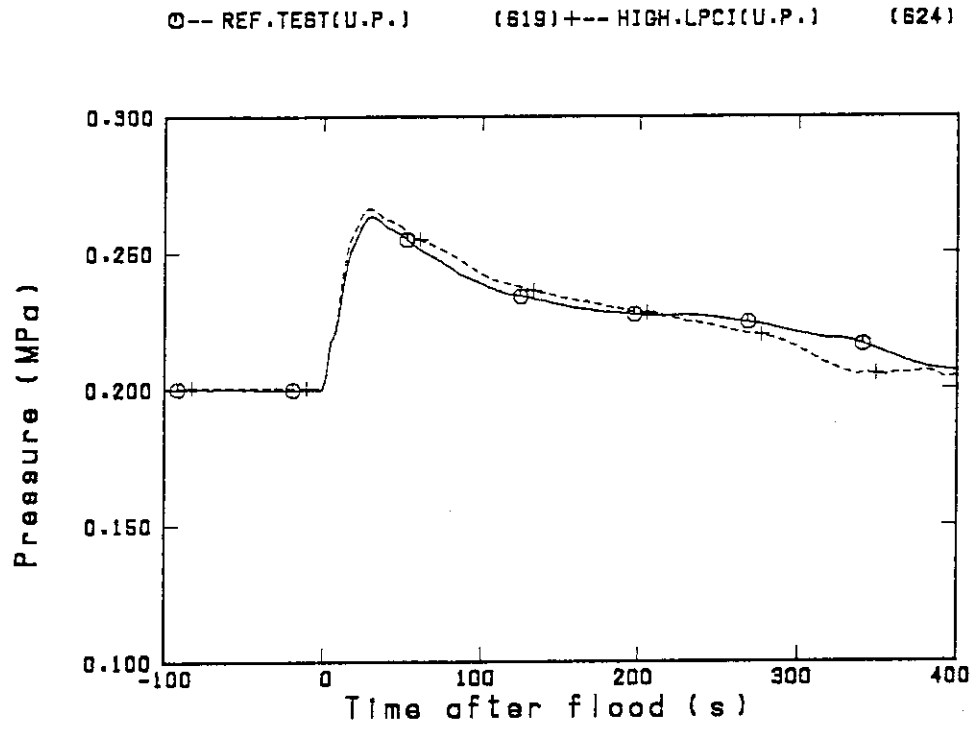

Fig.3.1.9 Comparison of pressure at upper plenum

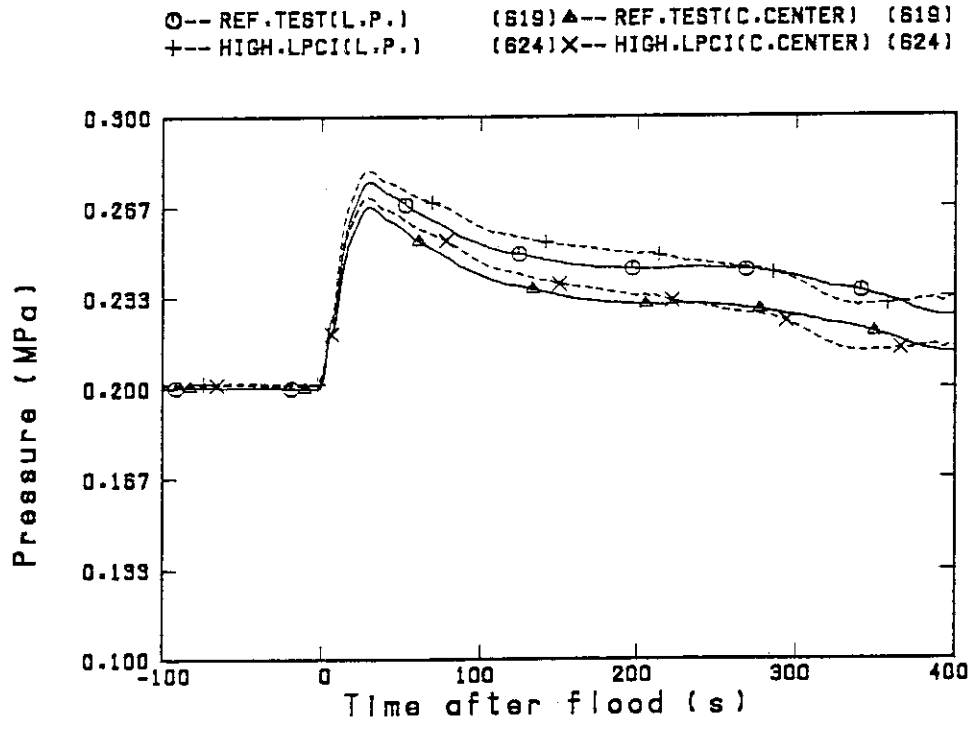

Fig.3.1.10 Comparison of pressure at lower plenum and at core center

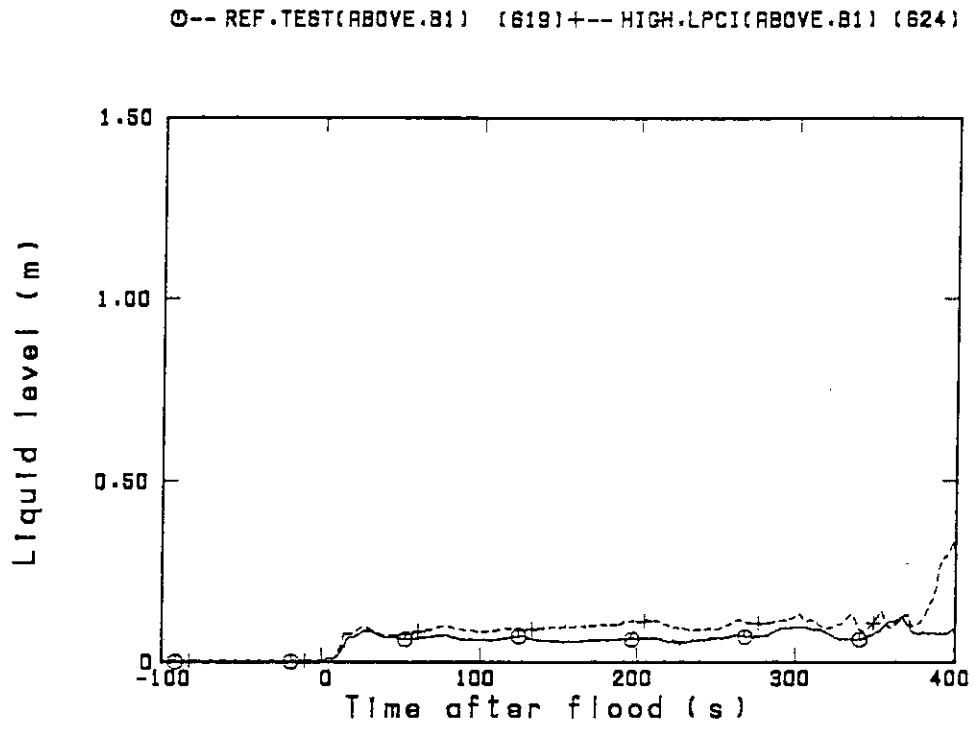

Fig.3.1.11(1) Comparison of liquid level in upper plenum above bundle 1

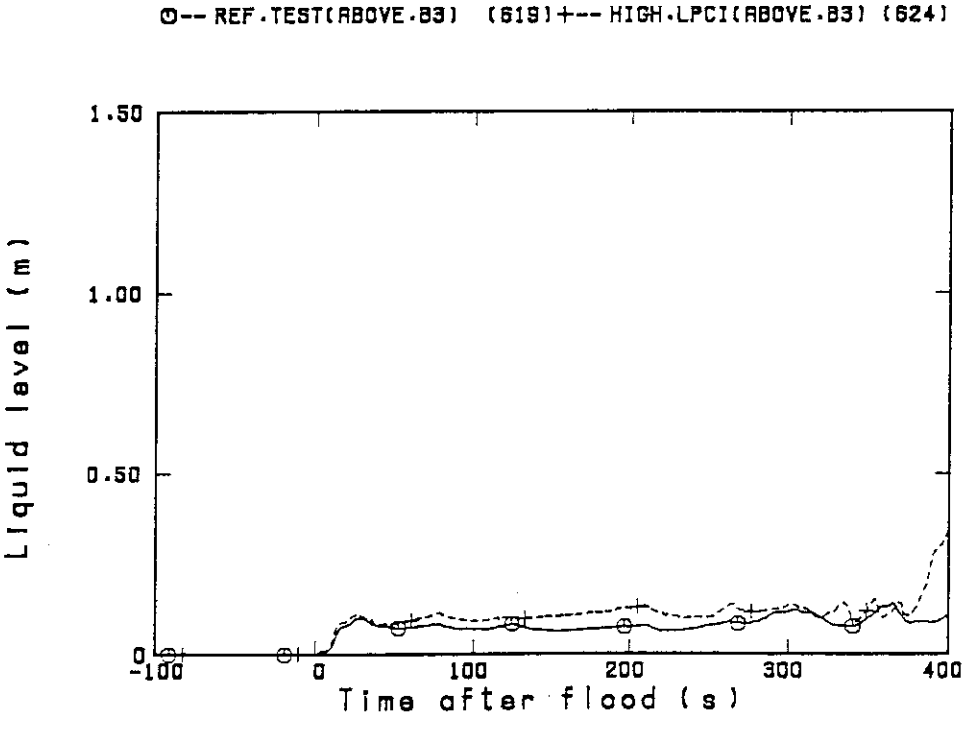

Fig.3.1.11(2) Comparison of liquid level in upper plenum above bundle 3

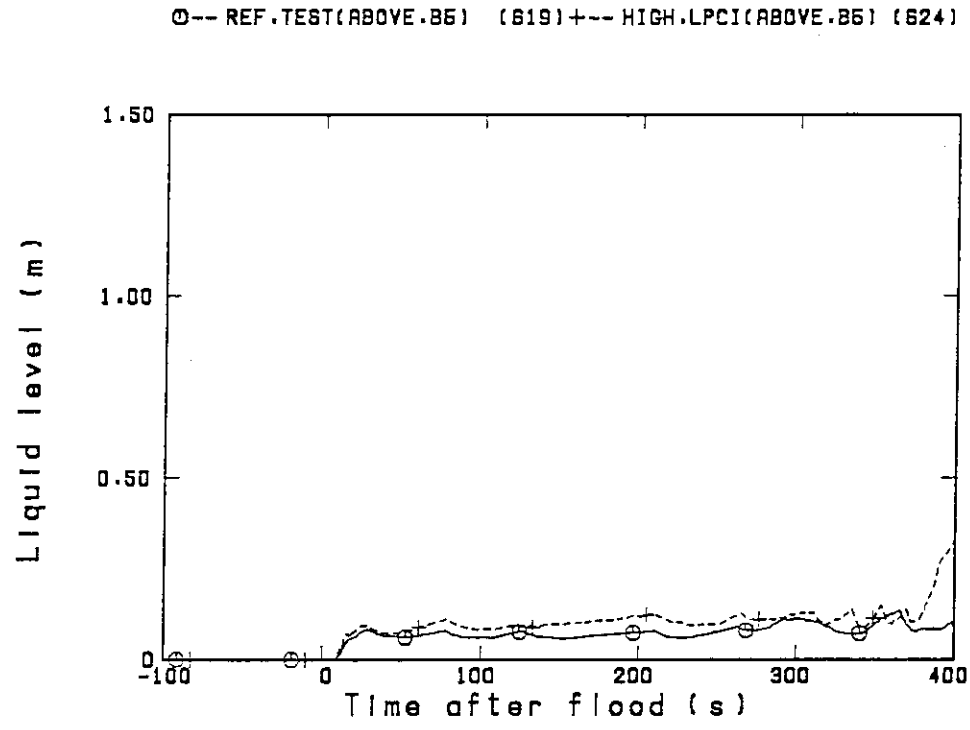

Fig.3.1.11(3) Comparison of liquid level in upper plenum above bundle 5

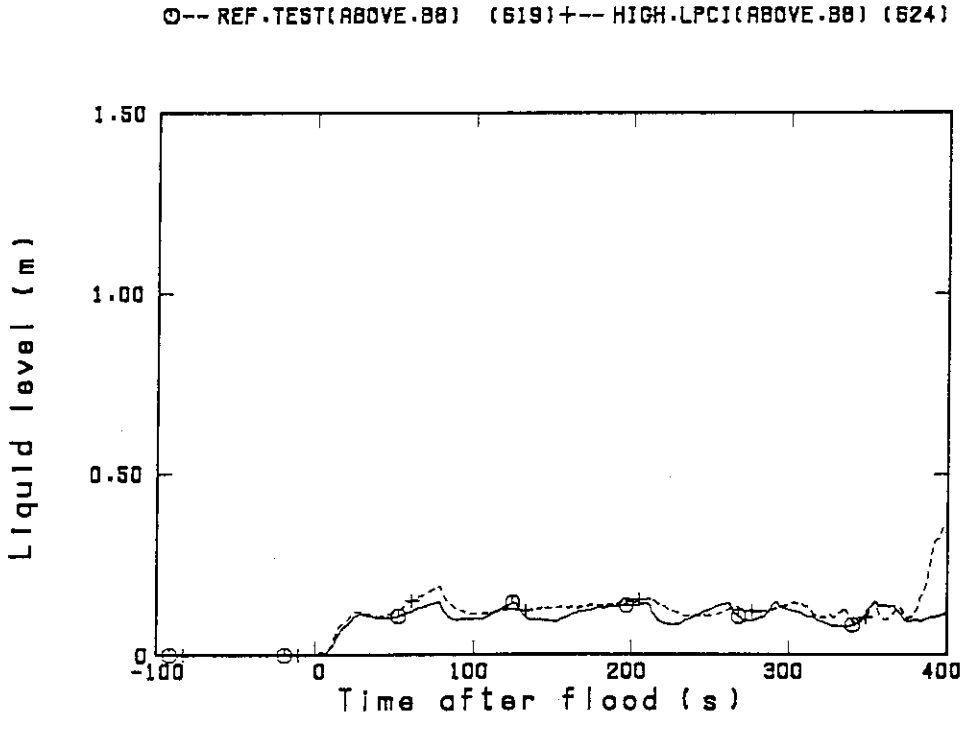

Fig.3.1.11(4) Comparison of liquid level in upper plenum above bundle 8

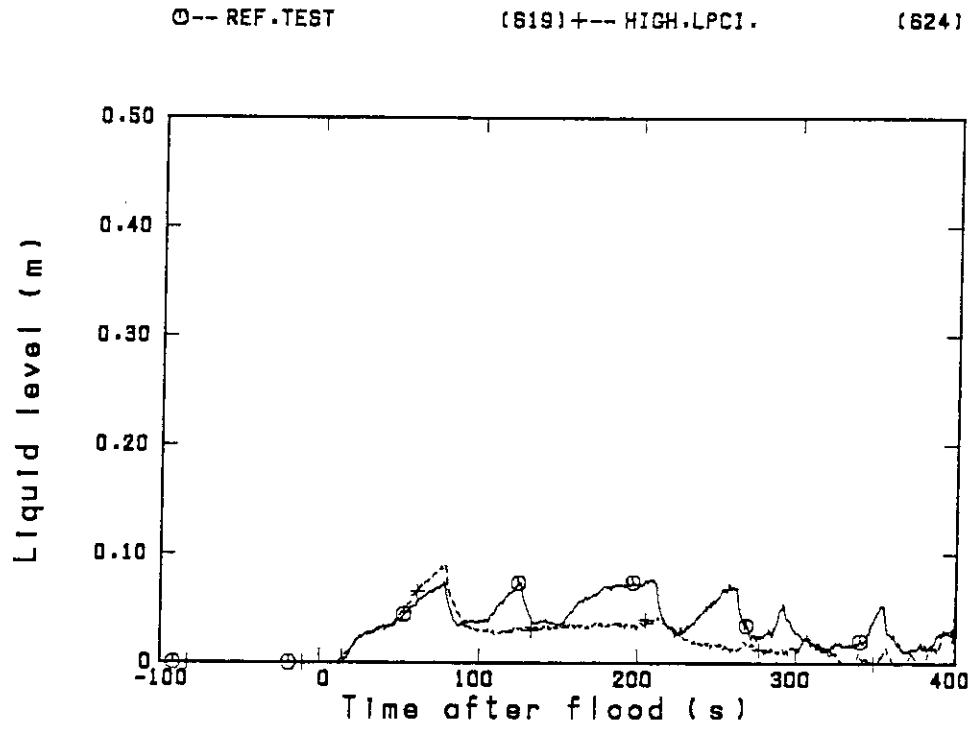

Fig.3.1.12 Comparison of radial difference of liquid level in upper plenum between above bundles 8 and 1

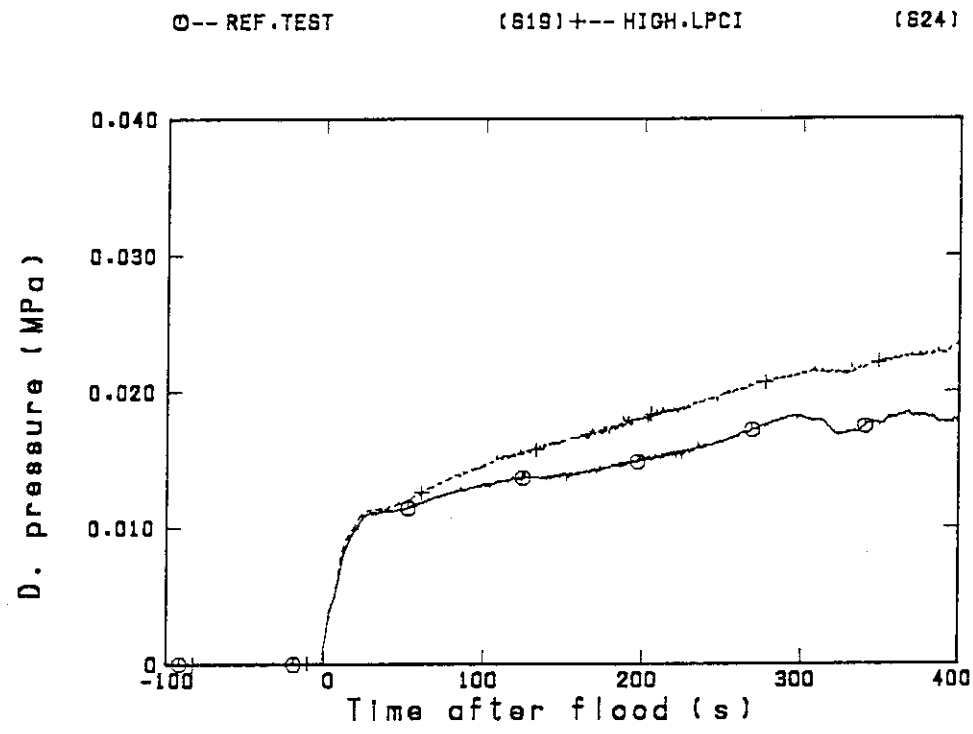

Fig.3.2.1 Comparison of differential pressure of core full height at bundle 4

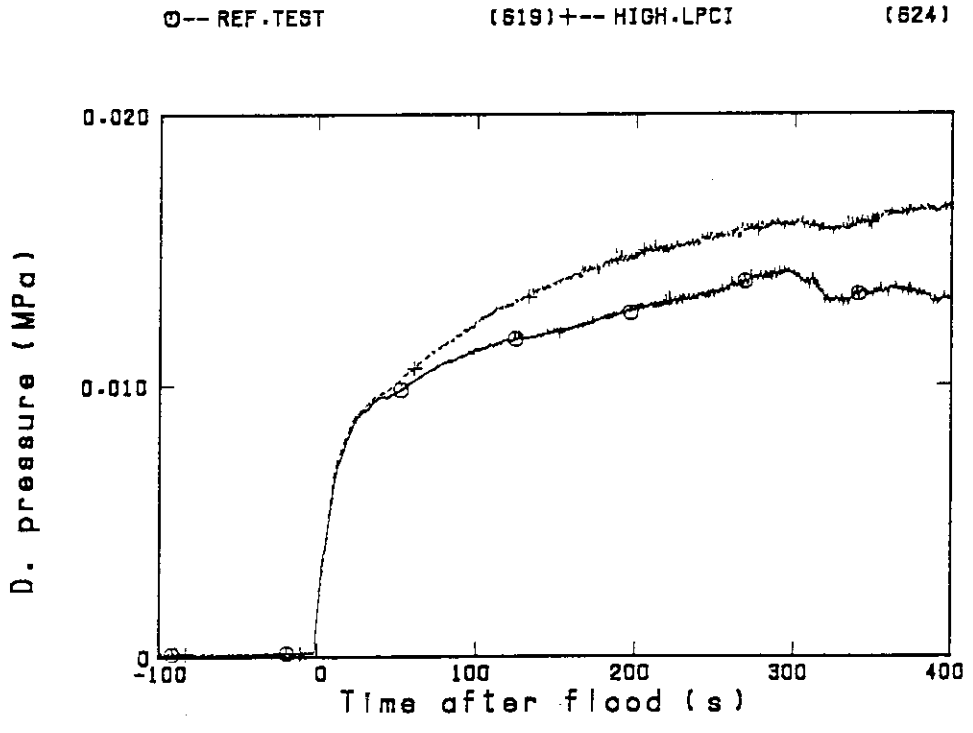

Fig.3.2.2(1) Comparison of differential pressure of core lower half at bundle 4

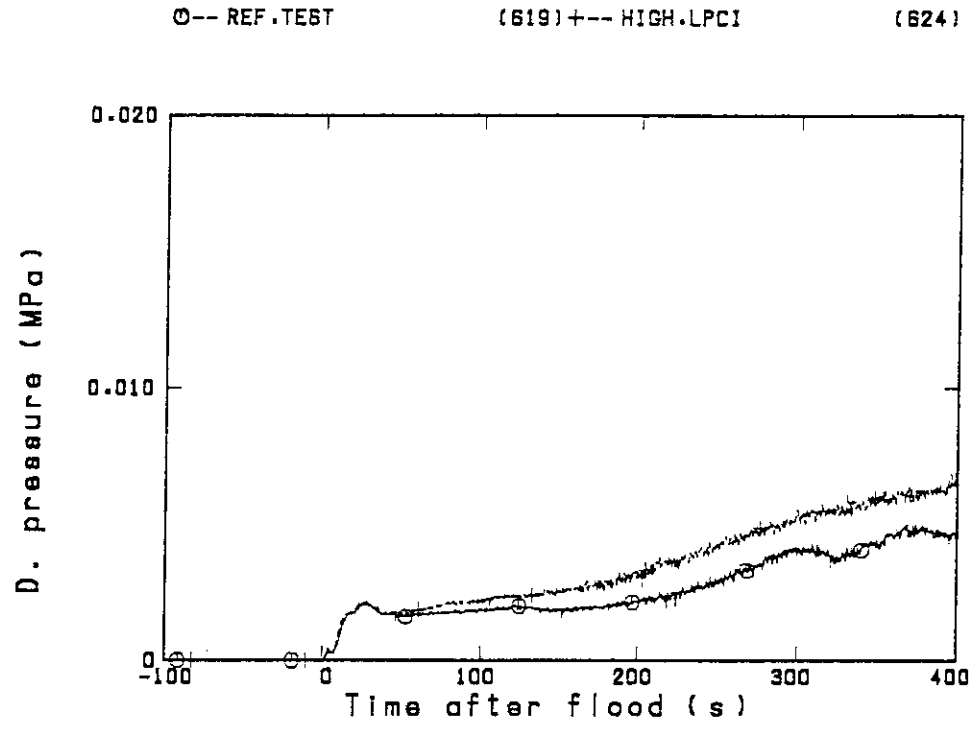

Fig.3.2.2(2) Comparison of differential pressure of core upper half at bundle 4

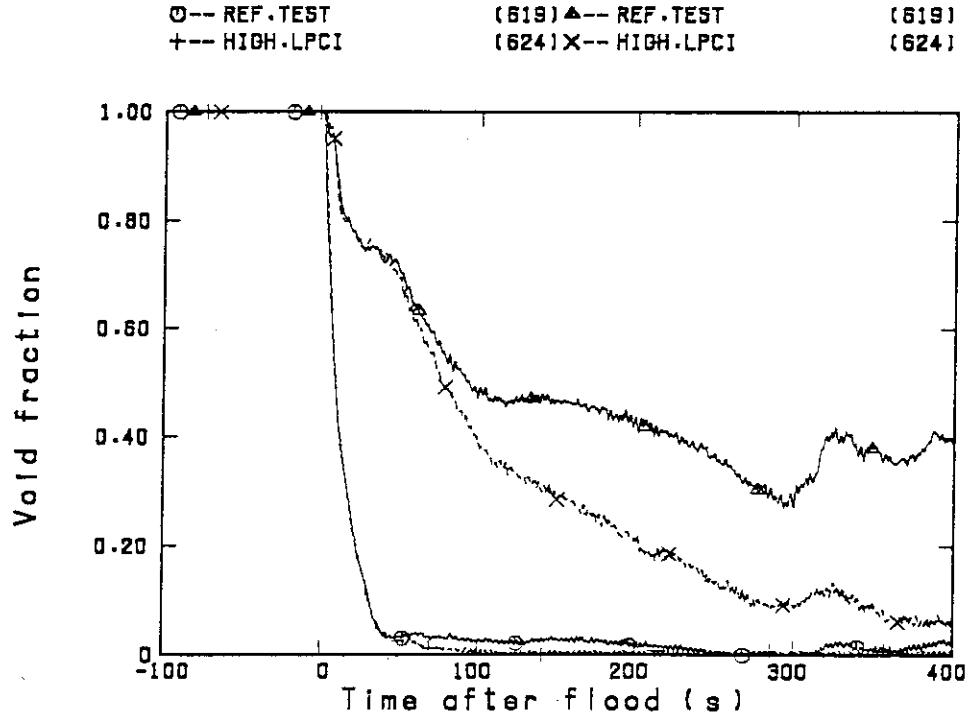

Fig.3.2.3(1) Comparison of sectional void fraction in bundle 4 at 0.085 -0.7m and 0.7-1.365m

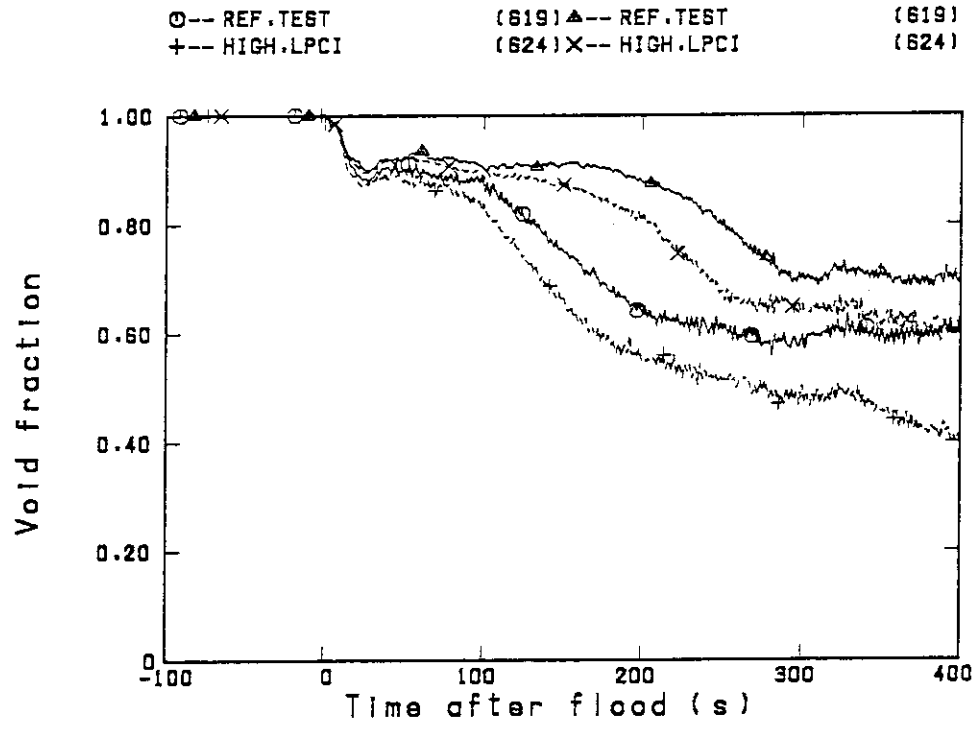

Fig.3.2.3(2) Comparison of sectional void fraction in bundle 4 at 1.365 -1.905m and 2.03-2.57m

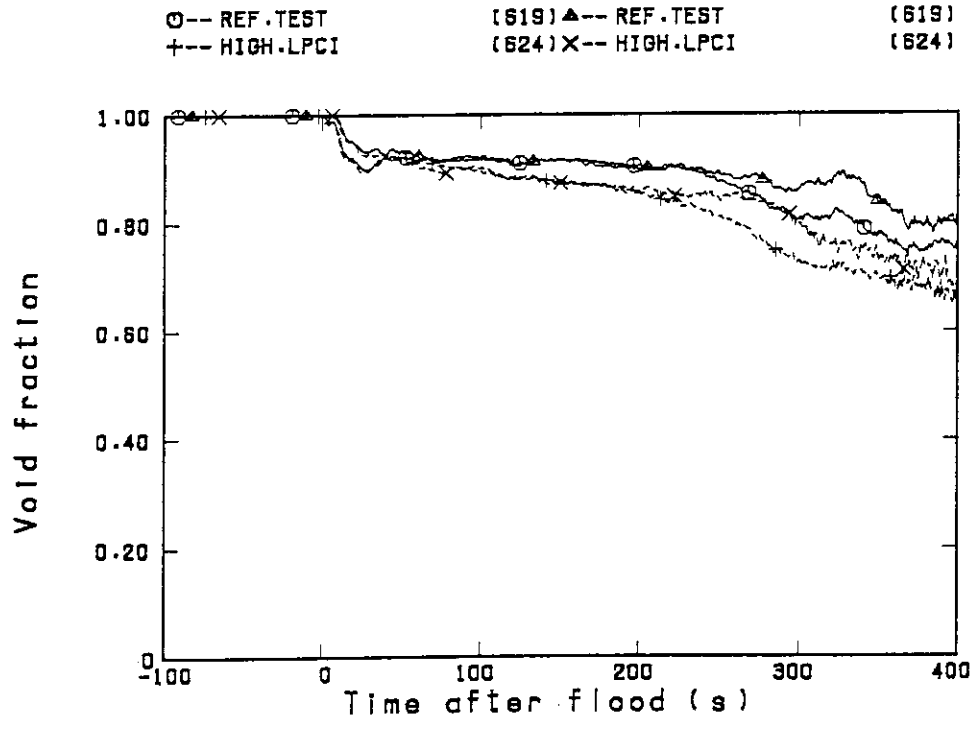

Fig.3.2.3(3) Comparison of sectional void fraction in bundle 4 at 2.695 -3.235m and 3.36-3.685m

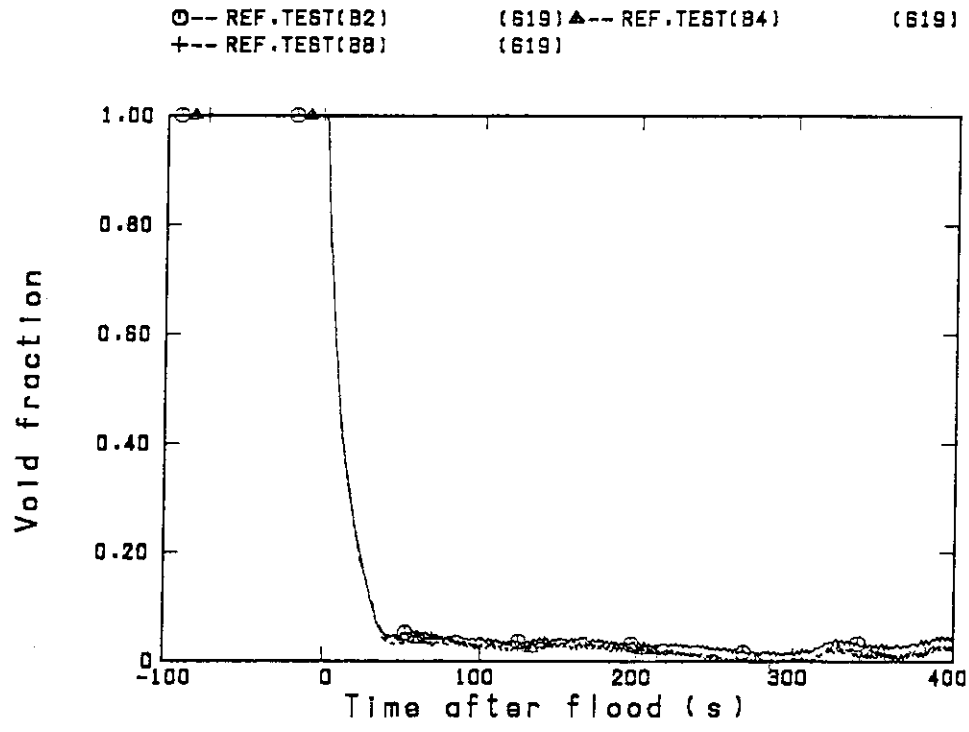

Fig.3.2.4(1) Radial comparison of sectional void fraction at 0.085-0.7m in reference test

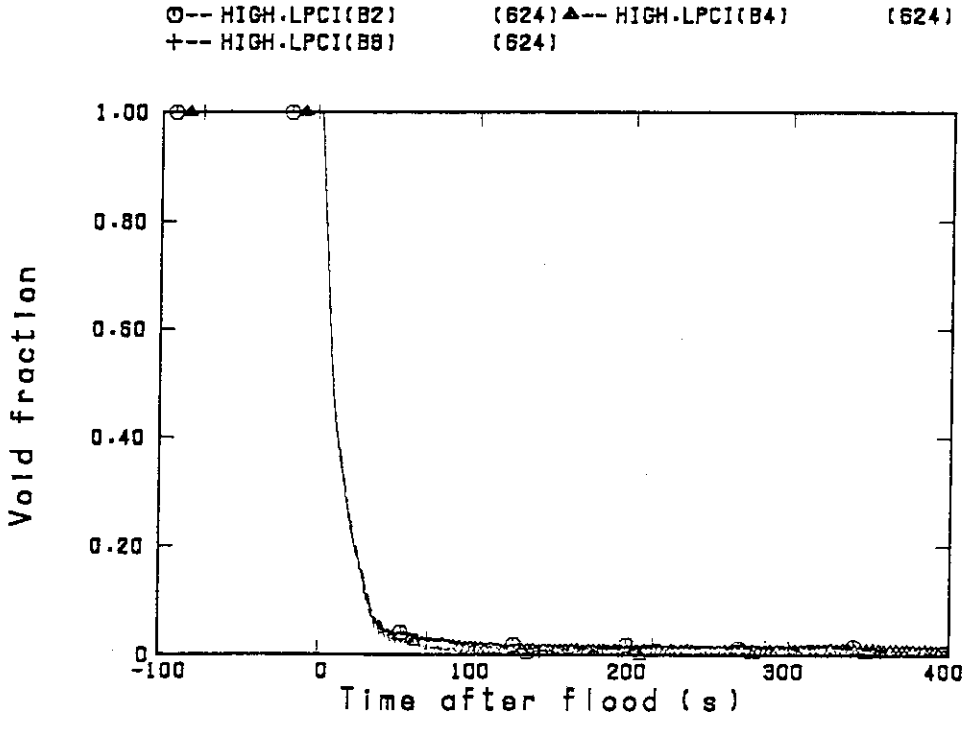

Fig.3.2.4(2) Radial comparison of sectional void fraction at 0.085-0.7m in high LPCI test

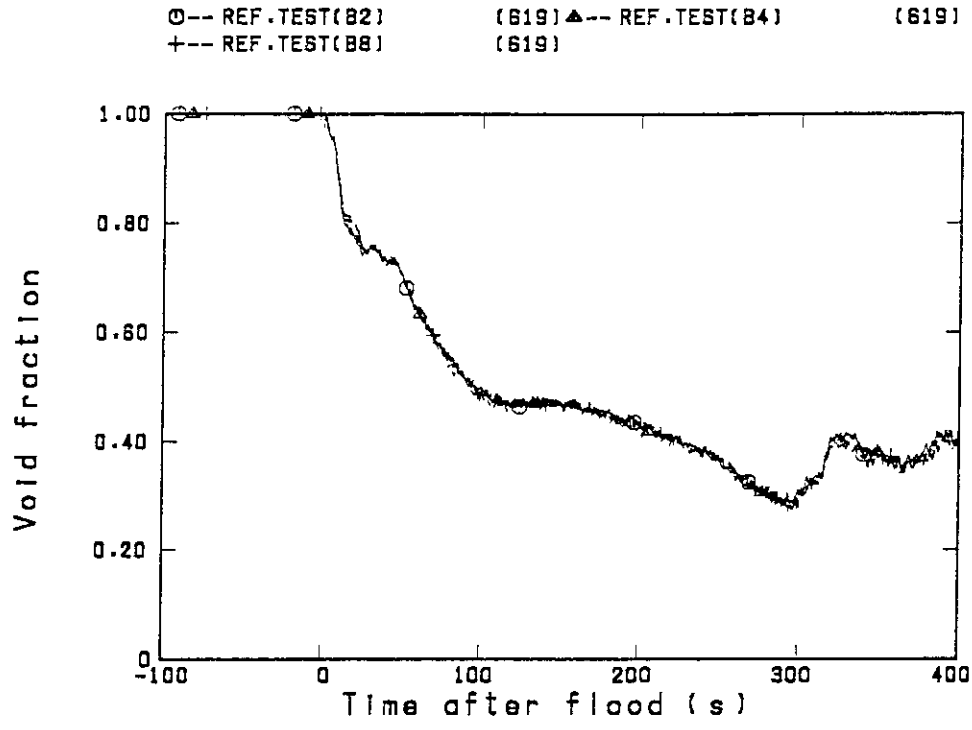

Fig.3.2.4(3) Radial comparison of sectional void fraction at 0.7-1.365m in reference test

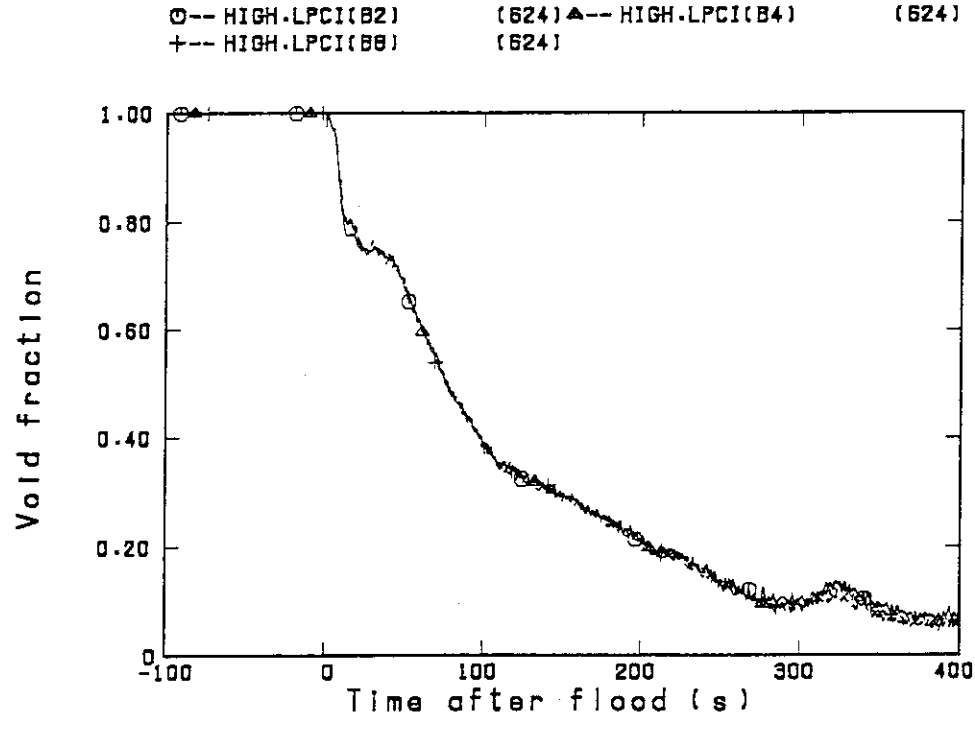

Fig.3.2.4(4) Radial comparison of sectional void fraction at 0.7-1.365m in high LPCI test

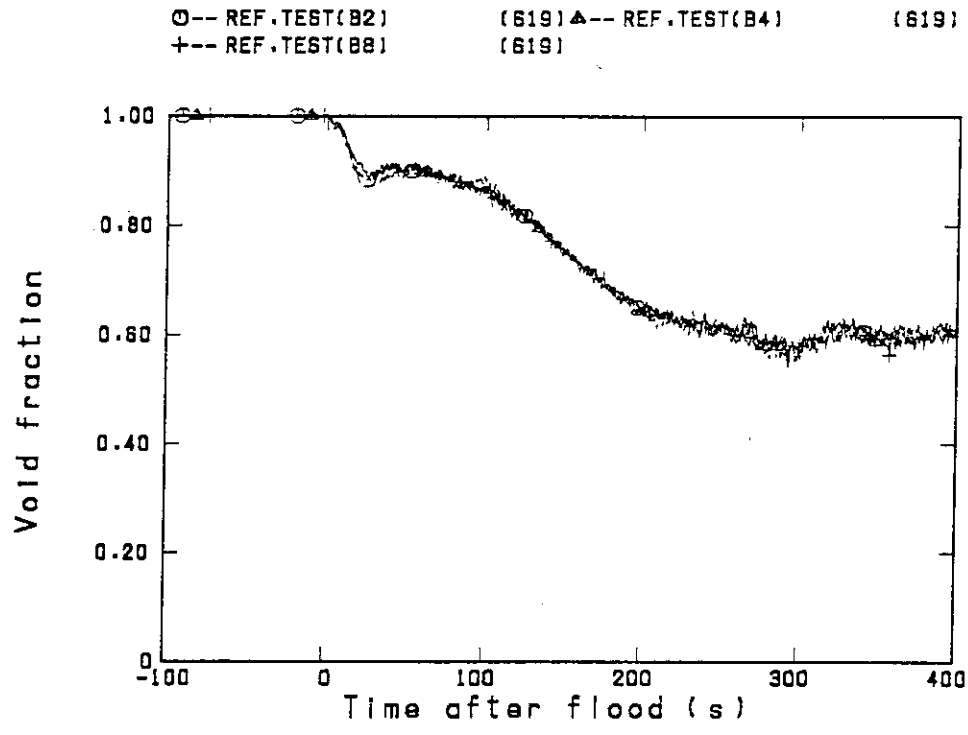

Fig.3.2.4(5) Radial comparison of sectional void fraction at 1.365-1.905m in reference test

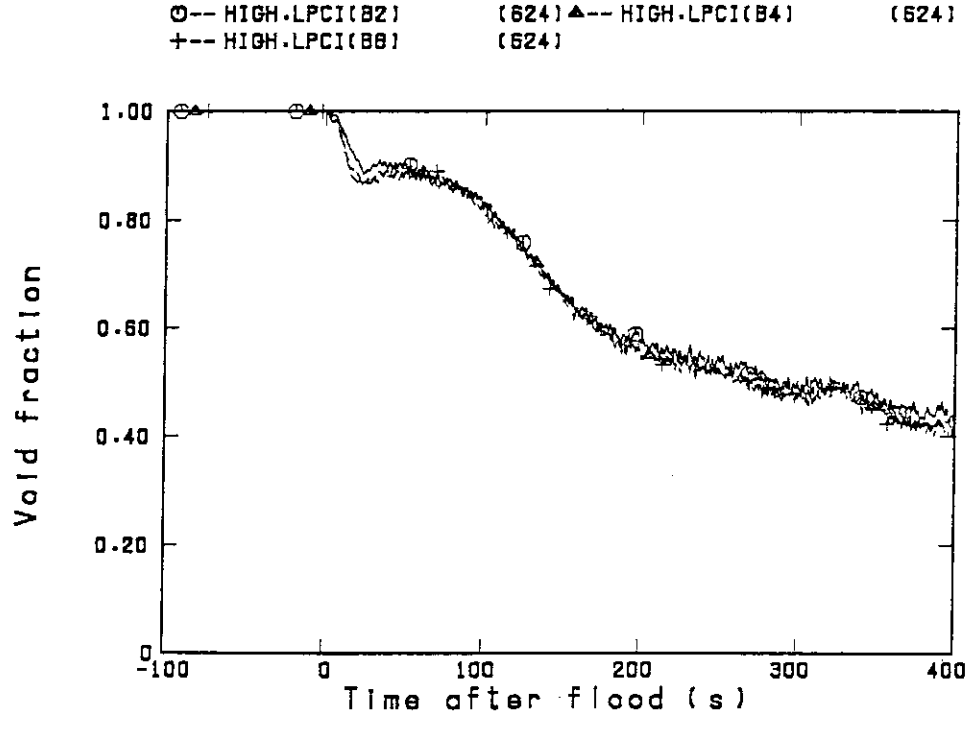

Fig.3.2.4(6) Radial comparison of sectional void fraction at 1.365-1.905m in high LPCI test

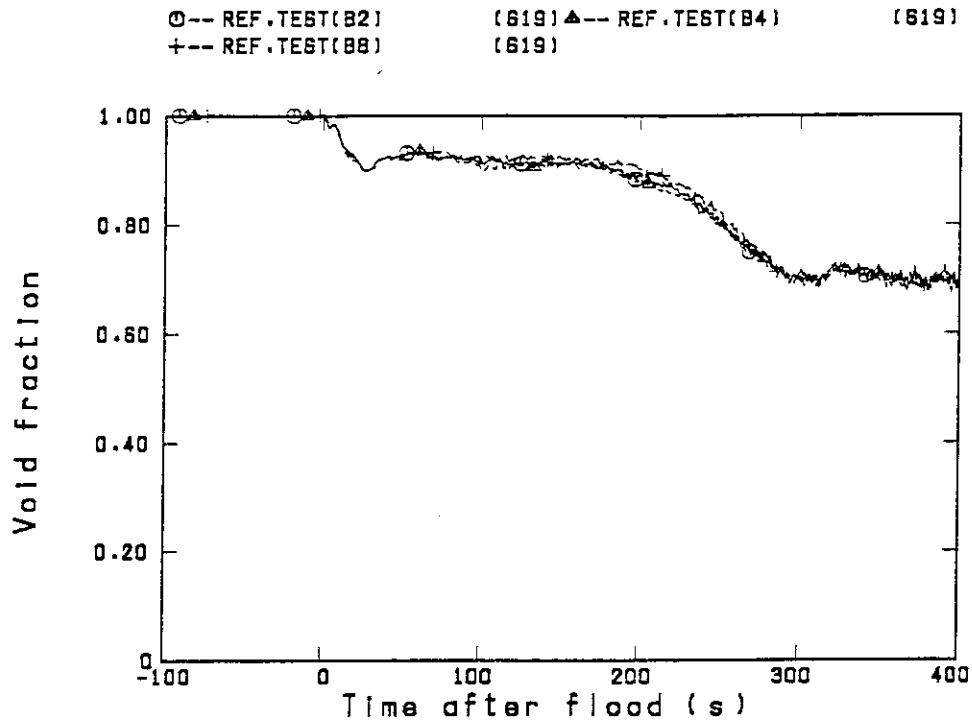

Fig.3.2.4(7) Radial comparison of sectional void fraction at 2.03-2.57m in reference test

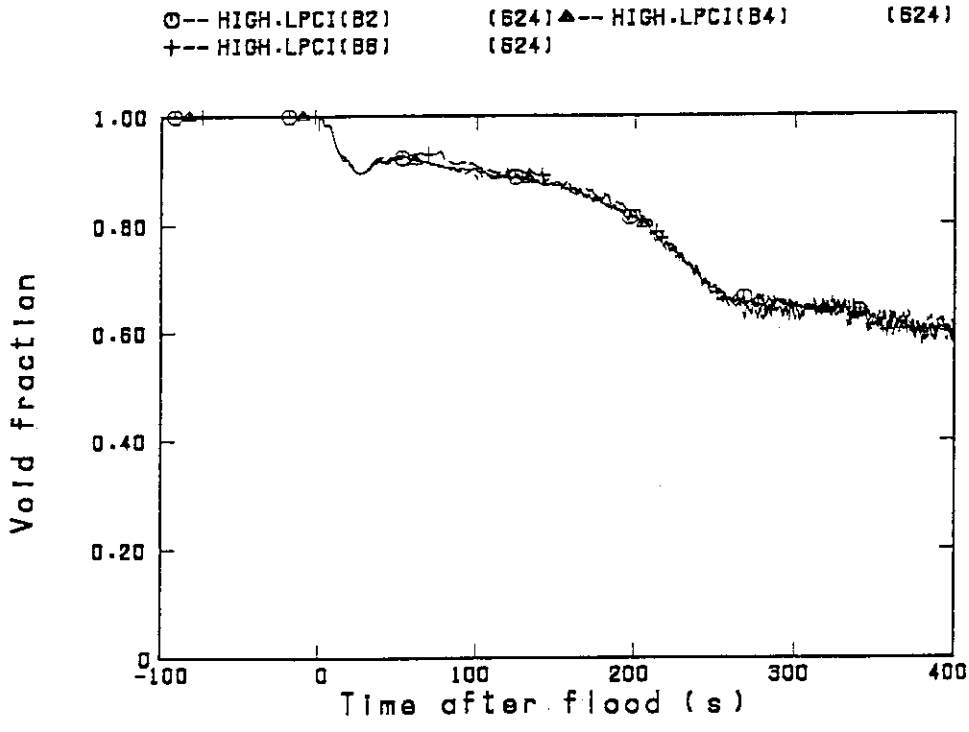

Fig.3.2.4(8) Radial comparison of sectional void fraction at 2.03-2.57m in high LPCI test

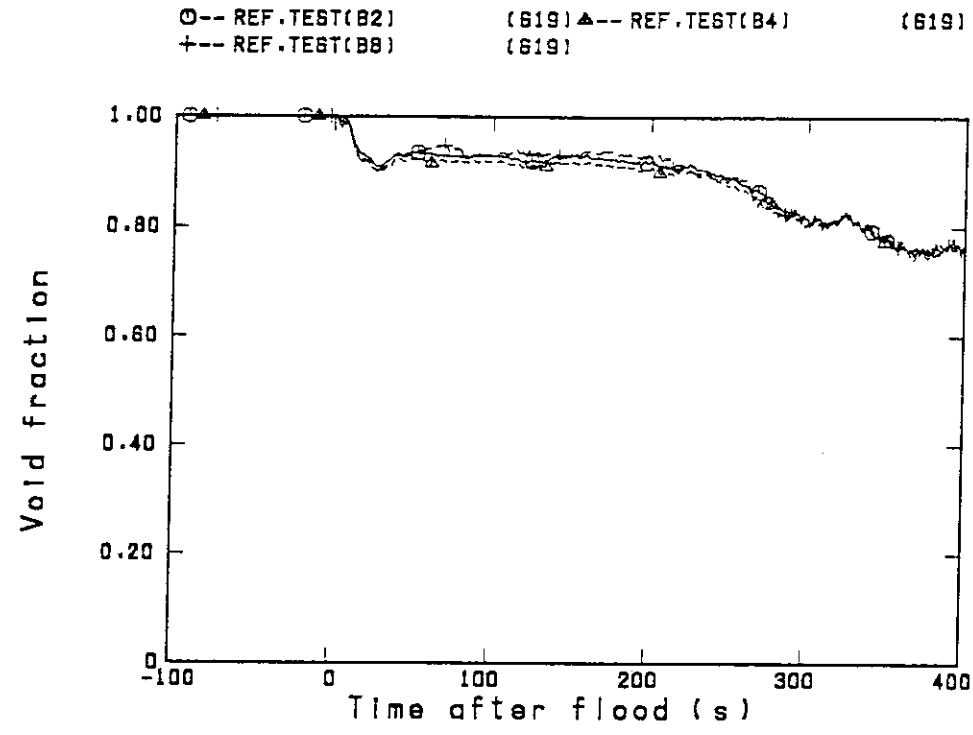

Fig.3.2.4(9) Radial comparison of sectional void fraction at 2.695-3.235m in reference test

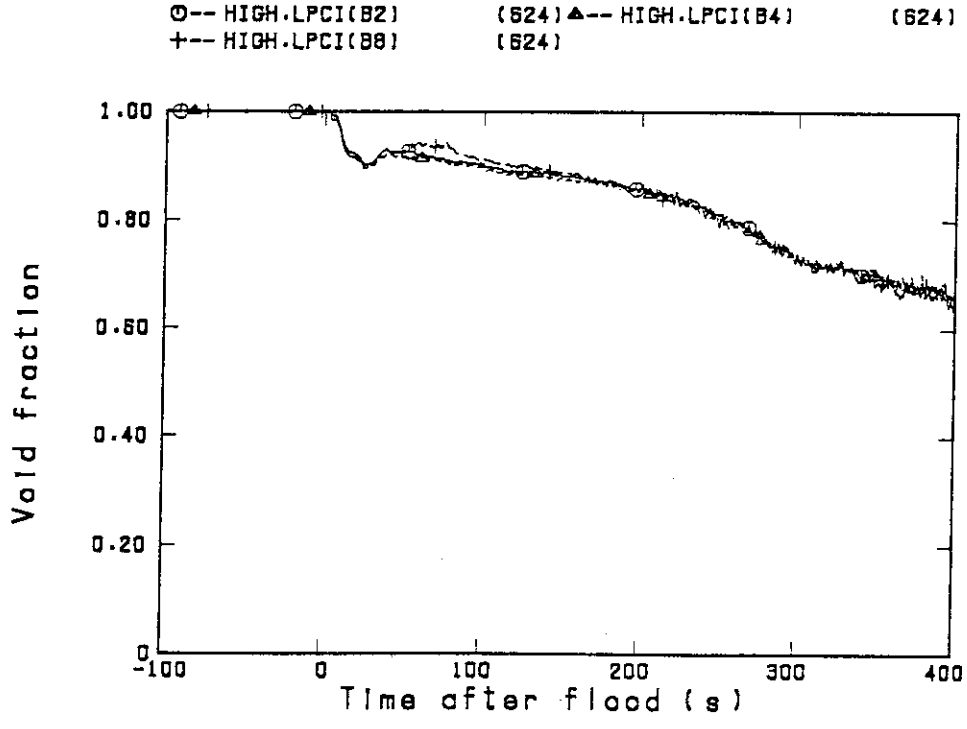

Fig.3.2.4(10) Radial comparison of sectional void fraction at 2.695-3.235m in high LPCI test

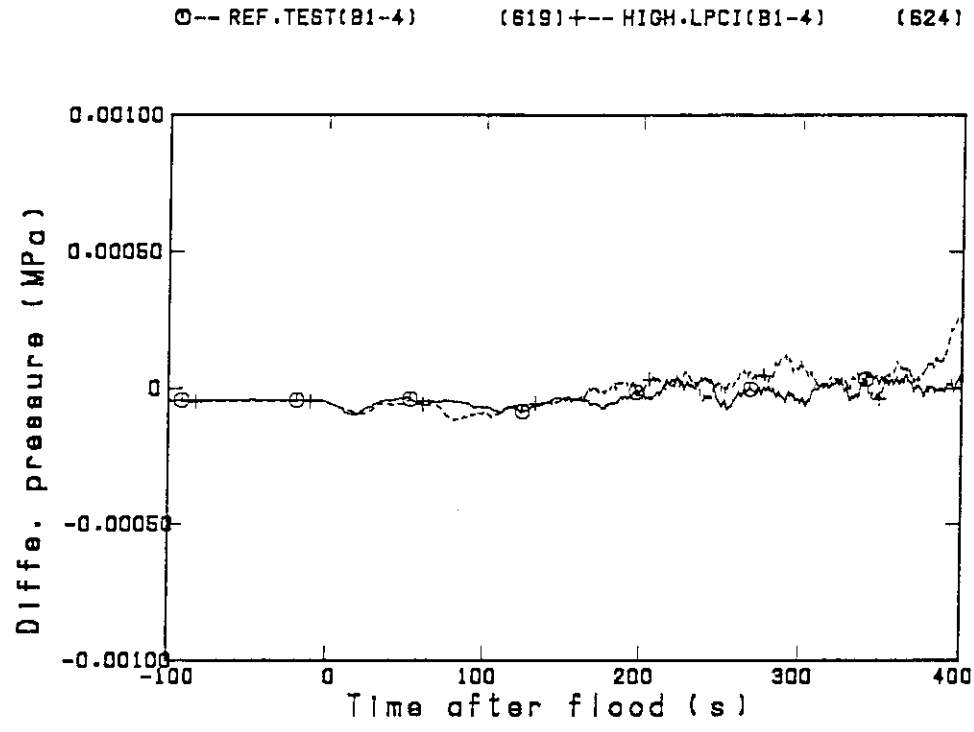

Fig.3.2.5(1) Comparison of radial differential pressure at 1.905m between bundles 1 and 4

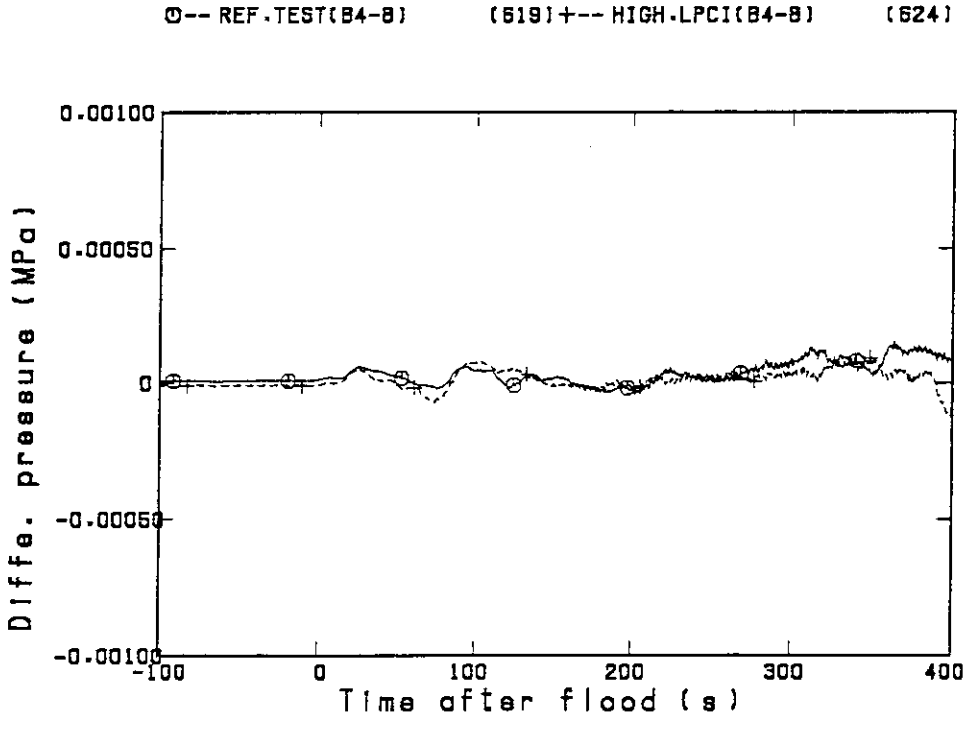

Fig.3.2.5(2) Comparison of radial differential pressure at 1.905m between bundles 4 and 8

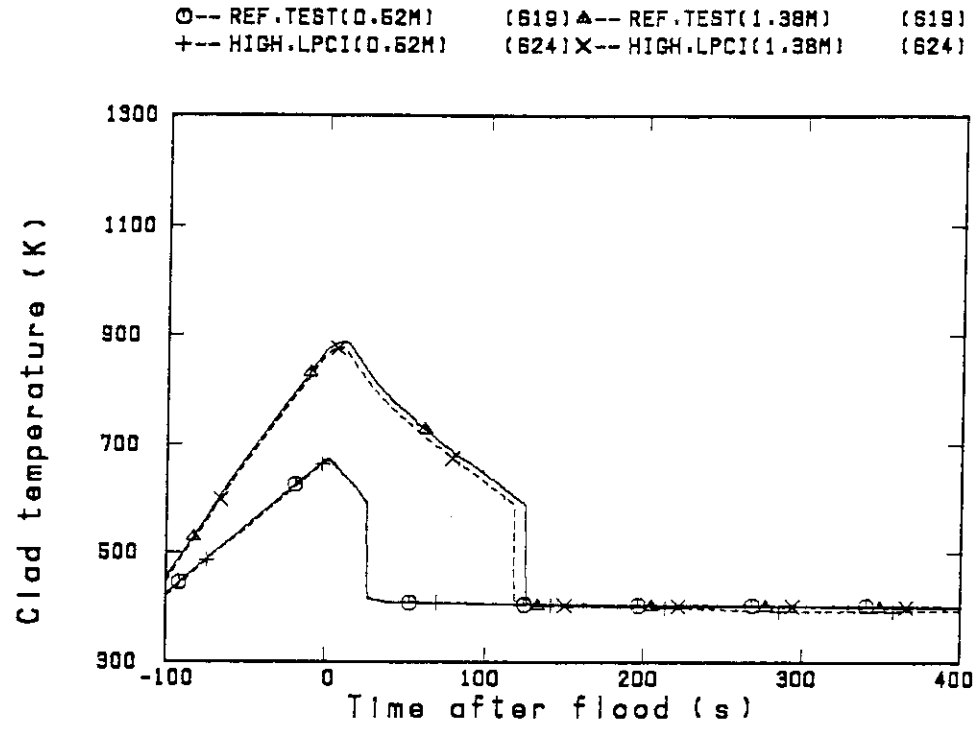

Fig.3.2.6(1) Comparison of clad temperature at 0.52m and 1.38m in bundle 4

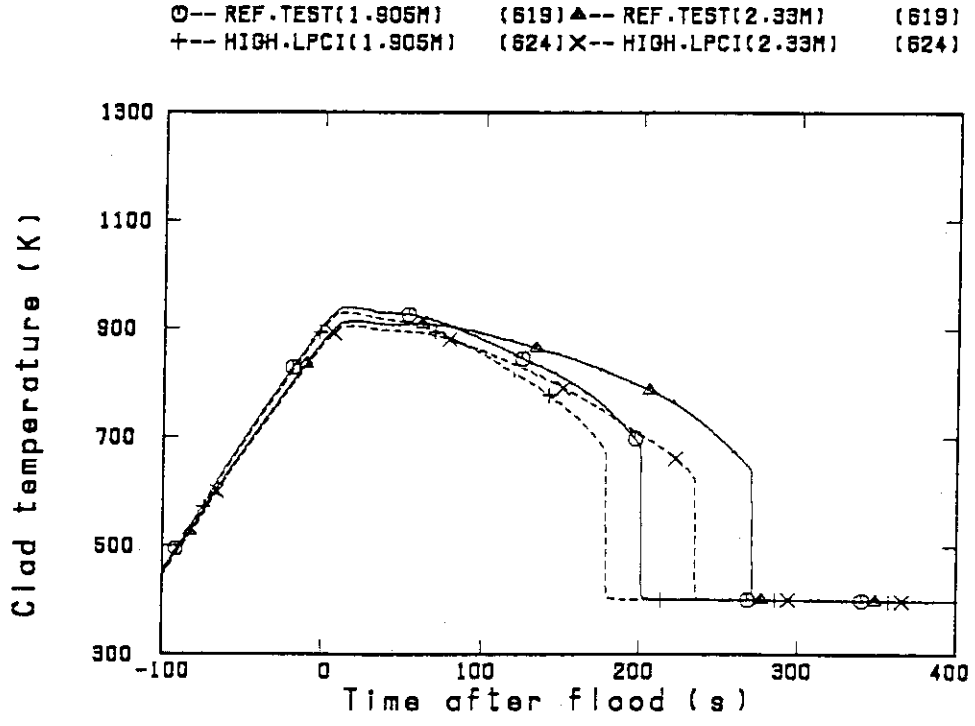

Fig.3.2.6(2) Comparison of clad temperature at 1.905m and 2.33m in bundle 4

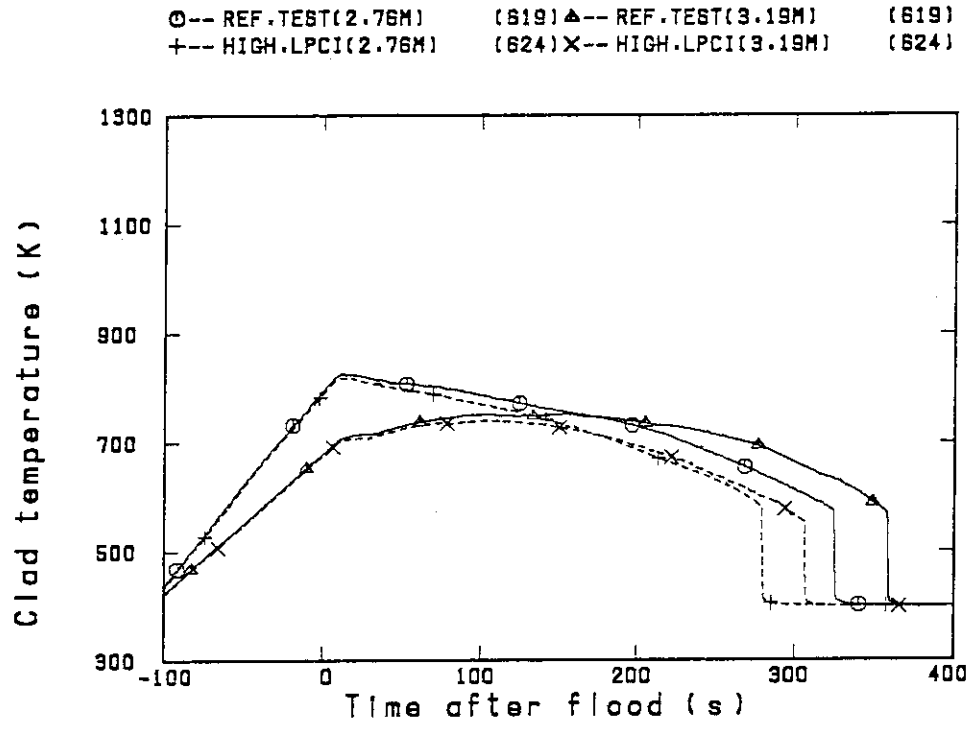

Fig.3.2.6(3) Comparison of clad temperature at 2.76m and 3.19m in bundle 4

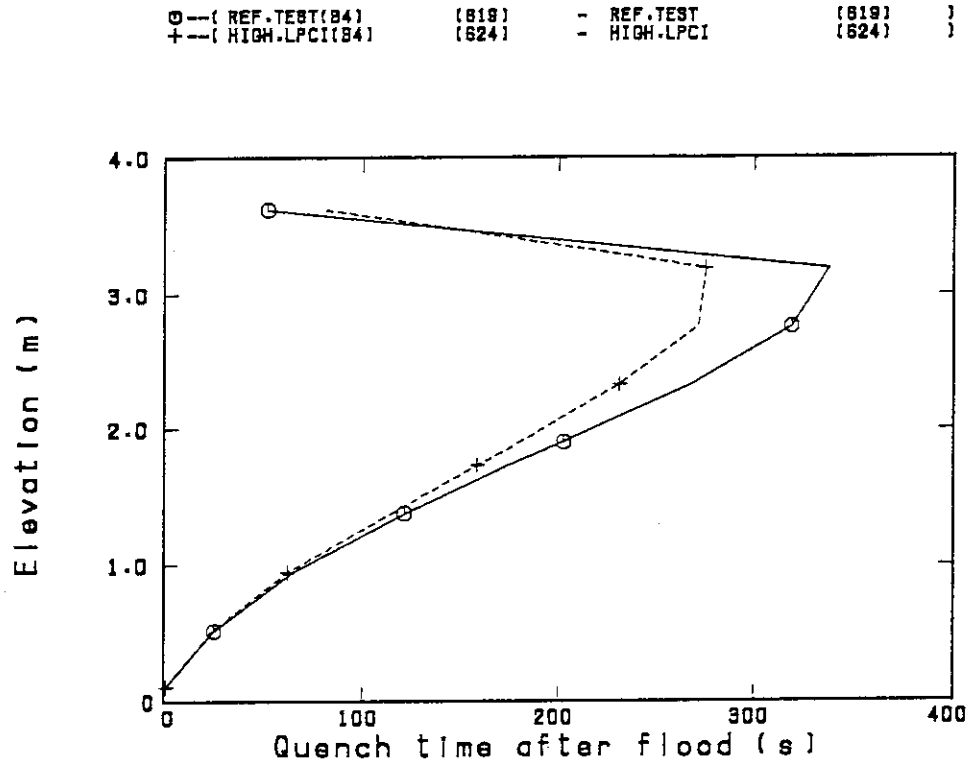

Fig.3.2.7 Comparison of quench time in bundle 4

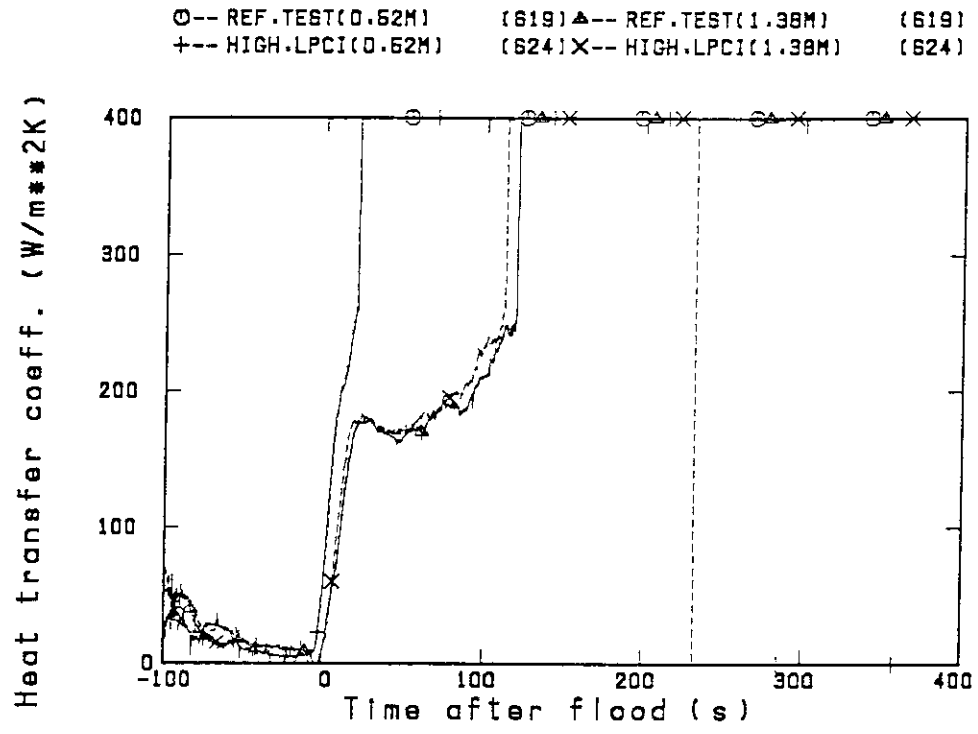

Fig.3.2.8(1) Comparison of heat transfer coefficient in bundle 4 at 0.52m and 1.38m

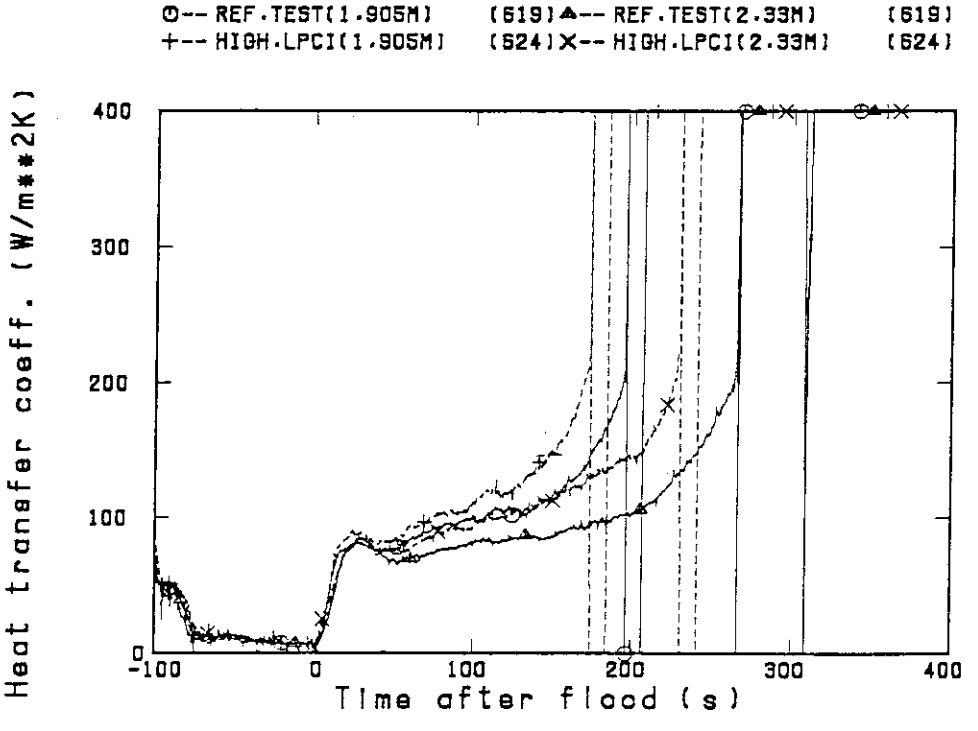

Fig.3.2.8(2) Comparison of heat transfer coefficient in bundle 4 at 1.905m and 2.33m

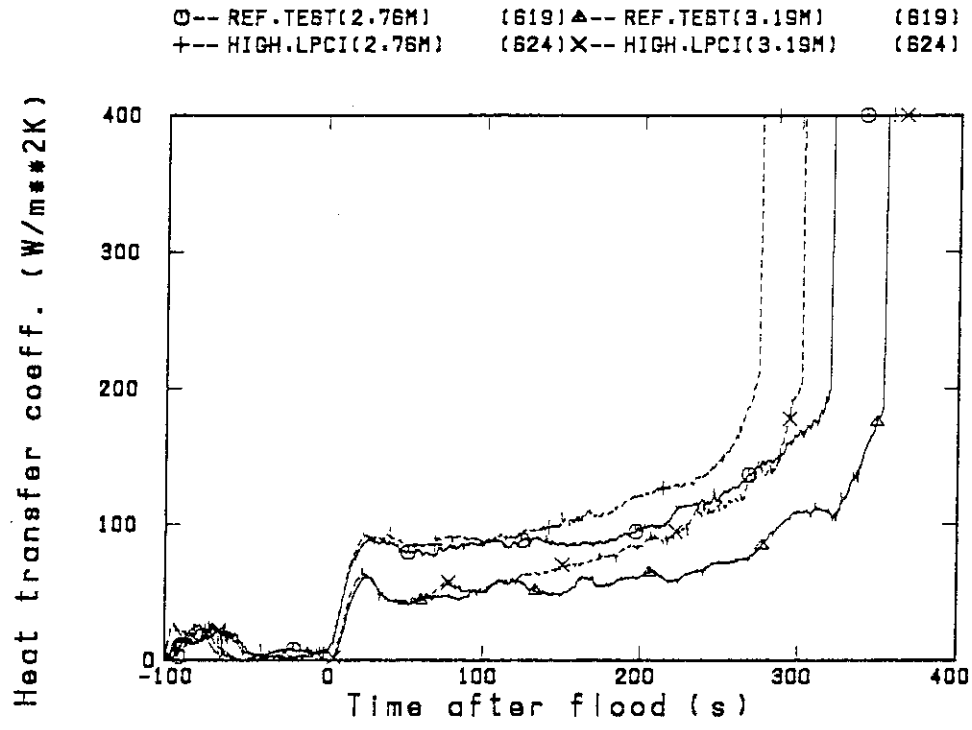

Fig.3.2.8(3) Comparison of heat transfer coefficient in bundle 4 at 2.76m and 3.19m

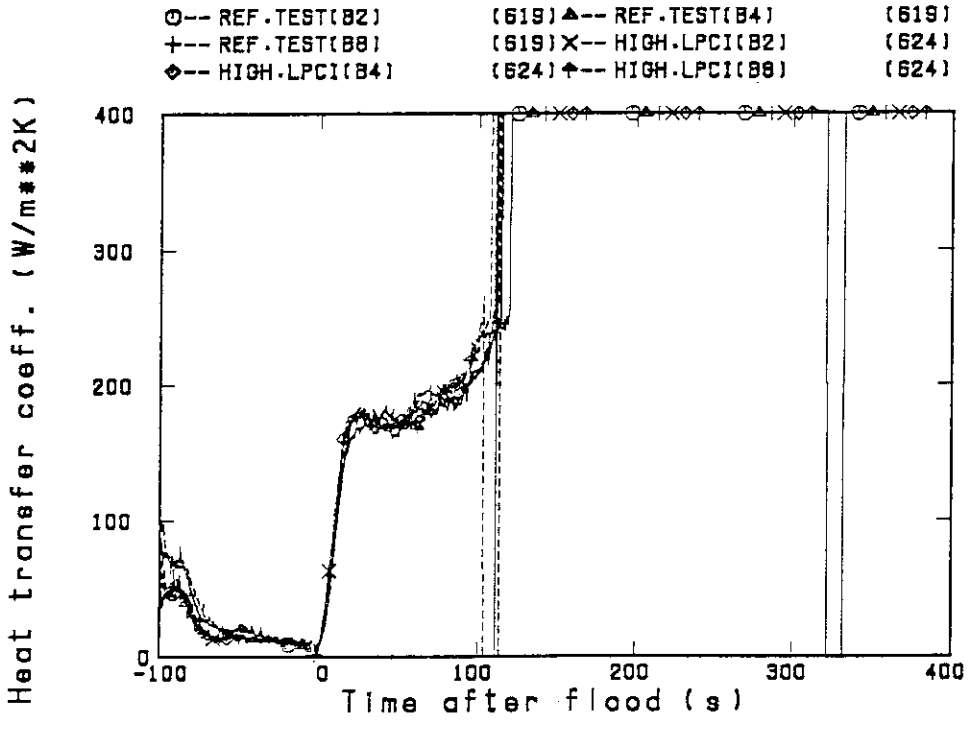

Fig.3.2.9(1) Radial comparison of heat transfer coefficient at 1.38m

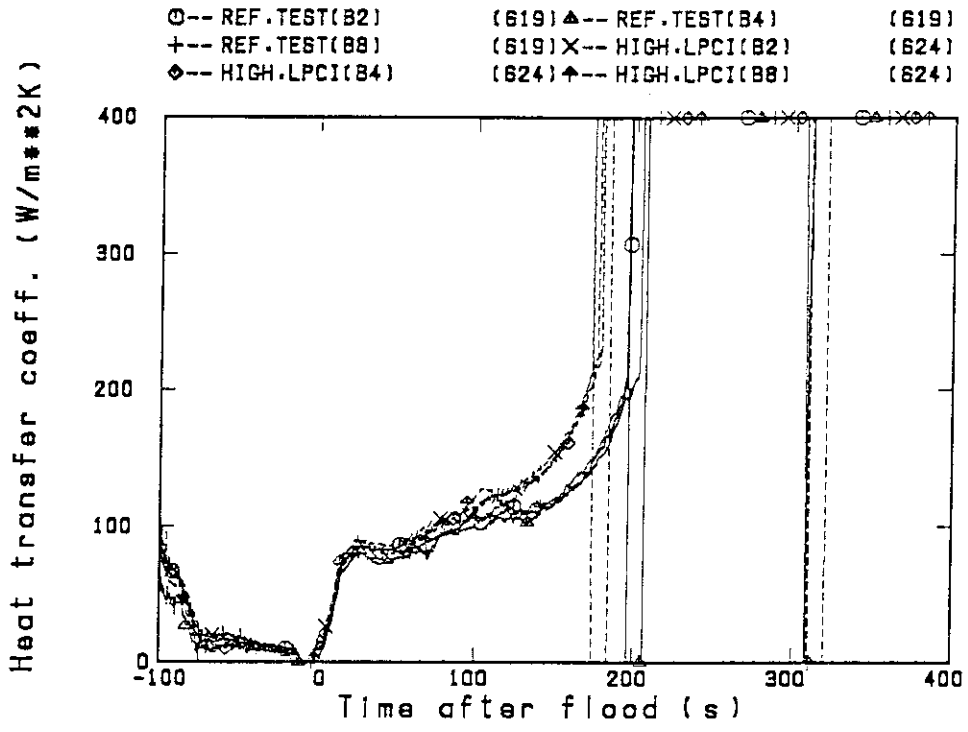

Fig.3.2.9(2) Radial comparison of heat transfer coefficient at 1.905m

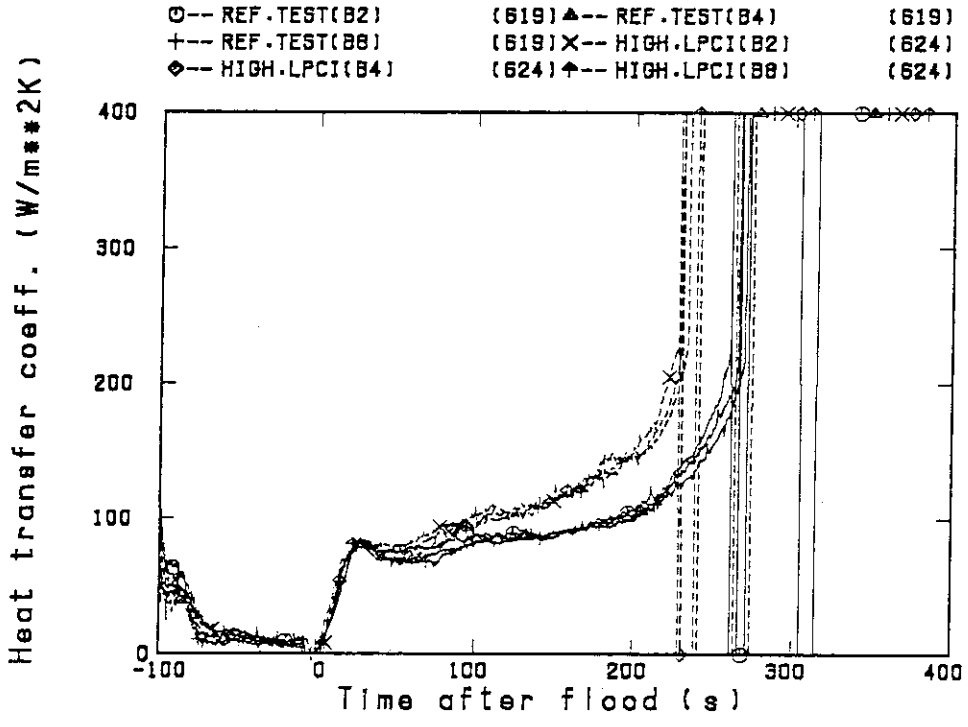

Fig.3.2.9(3) Radial comparison of heat transfer coefficient at 2.33m

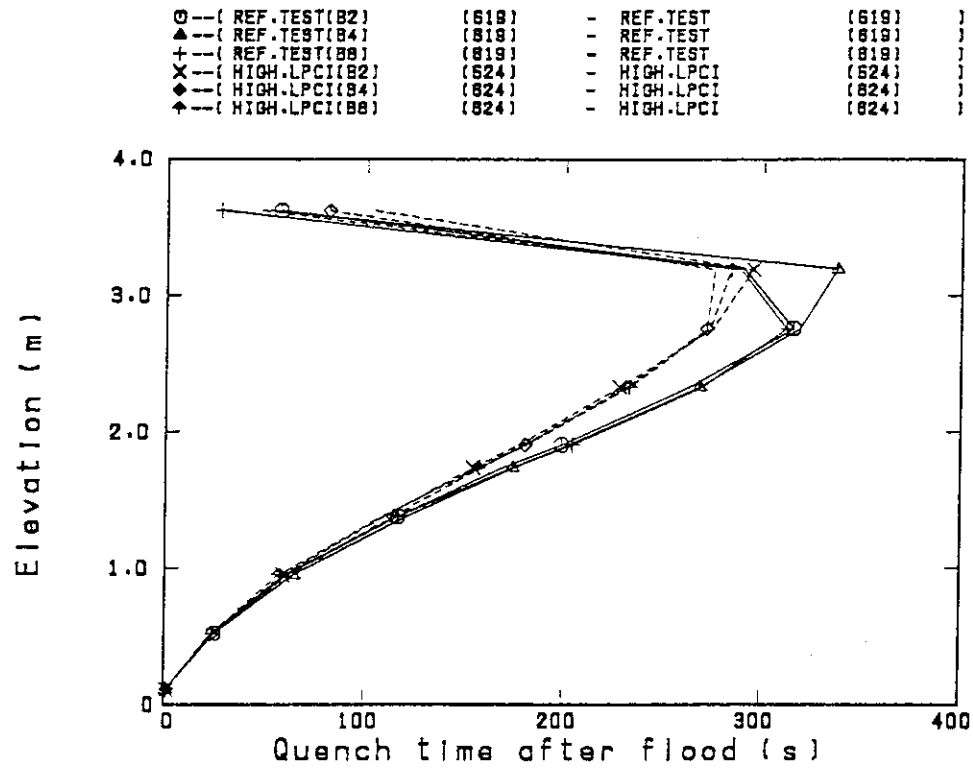

Fig.3.2.10 Comparison of quench time in bundles 2, 4 and 8

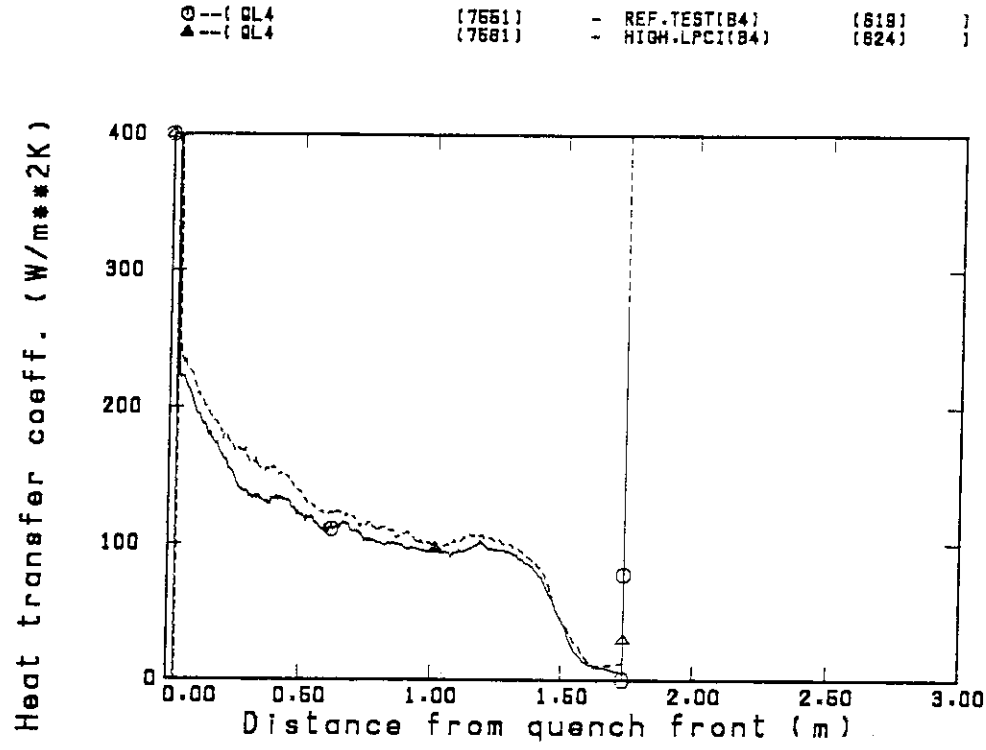

Fig.3.3.1(1)　Comparison of heat transfer coefficient in bundle 4 at 1.735m

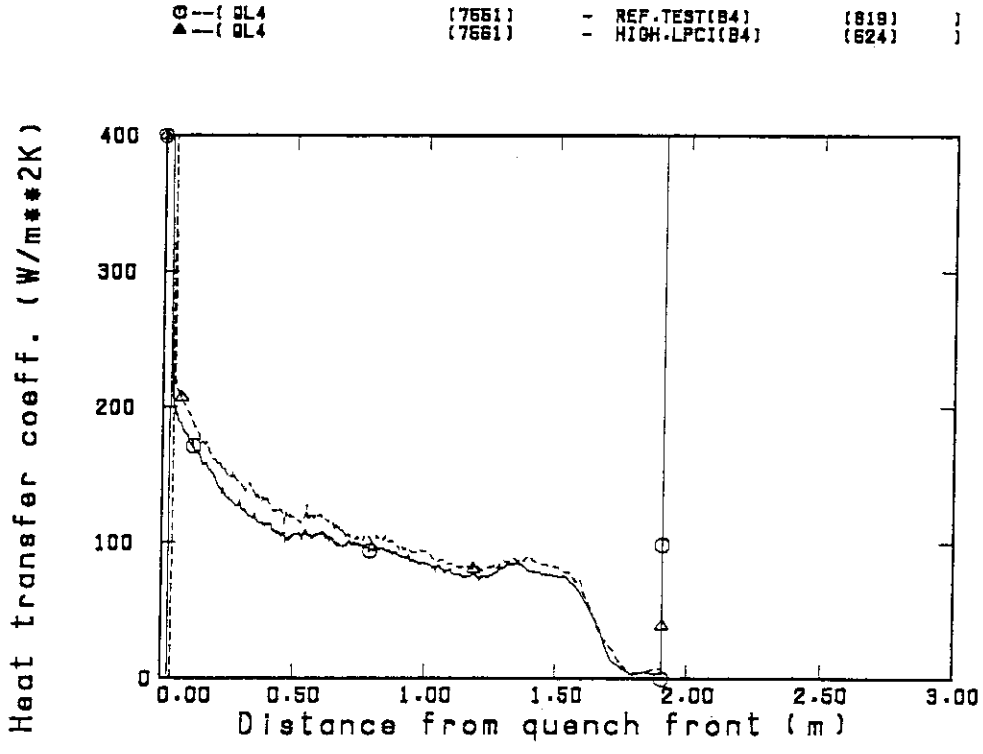

Fig.3.3.1(2)　Comparison of heat transfer coefficient in bundle 4 at 1.905m

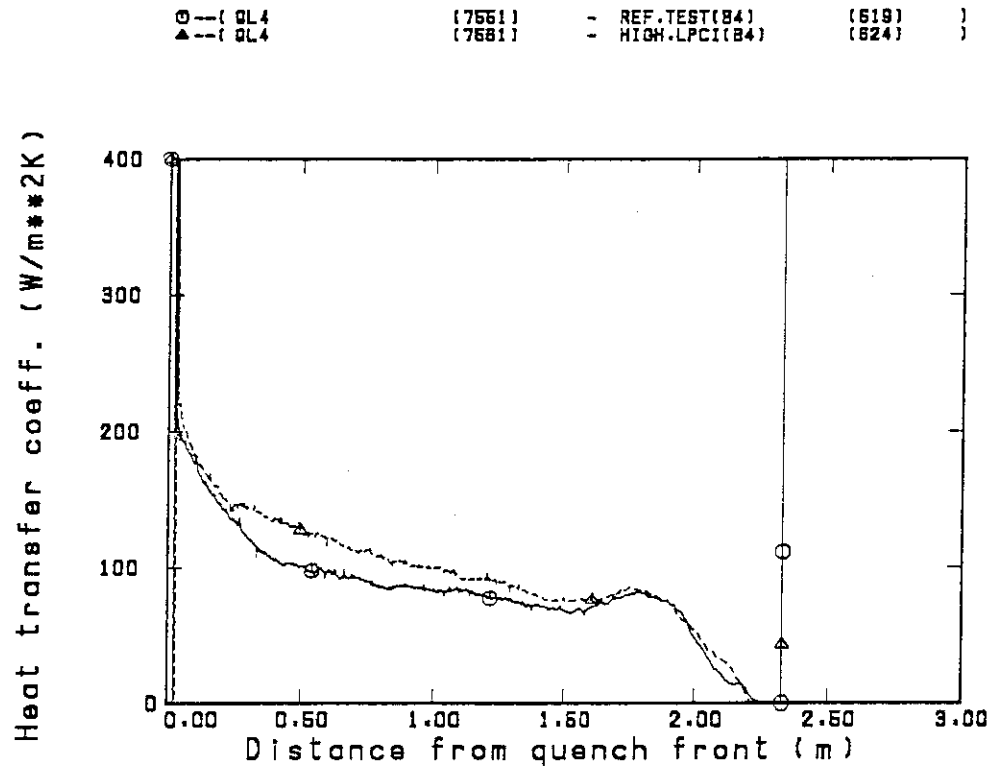

Fig.3.3.1(3) Comparison of heat transfer coefficient in bundle 4 at 2.33m

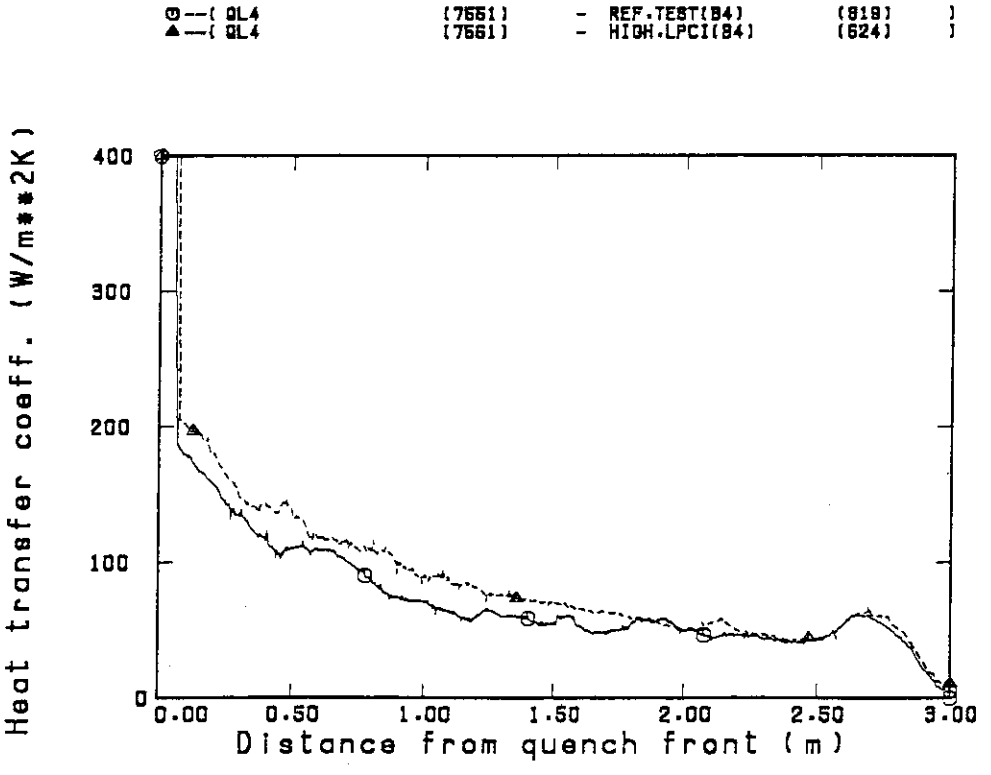

Fig.3.3.1(4) Comparison of heat transfer coefficient in bundle 4 at 3.19m

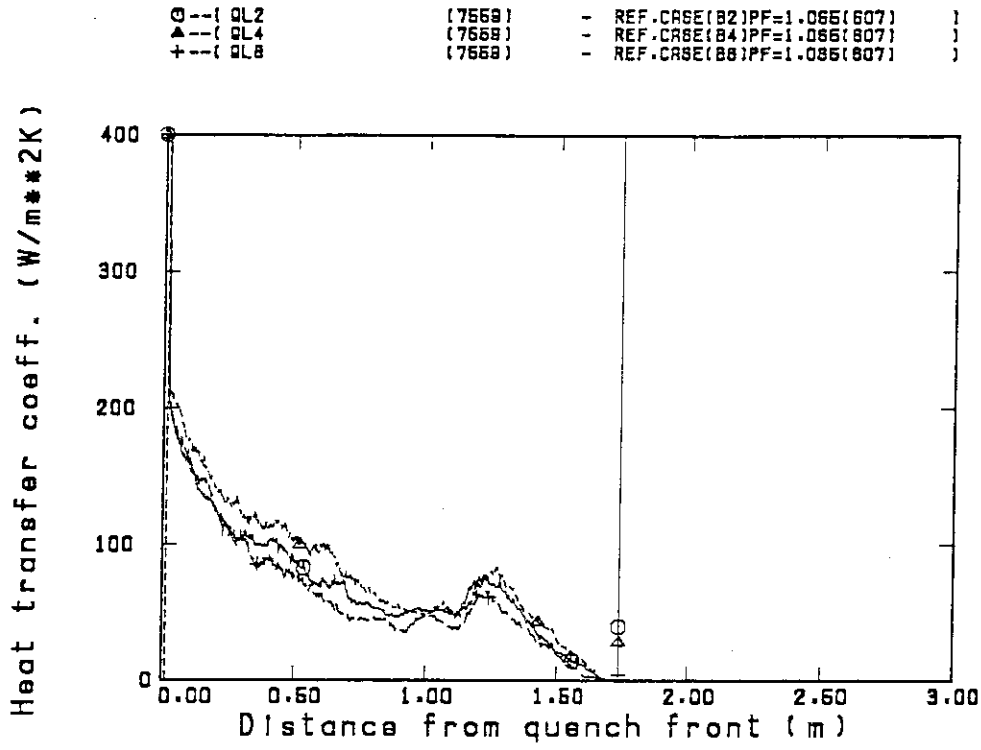

Fig.3.3.2(1) Radial comparison of heat transfer coefficient at 1.735m under peak power ratio of 1.065

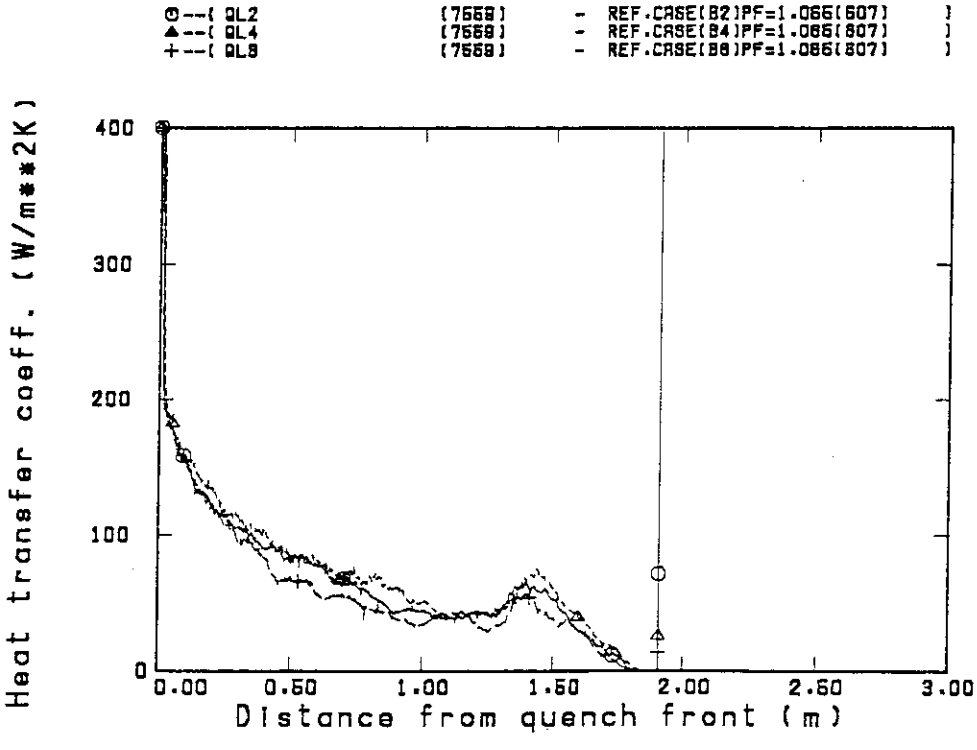

Fig.3.3.2(2) Radial comparison of heat transfer coefficient at 1.905m under peak power ratio of 1.065

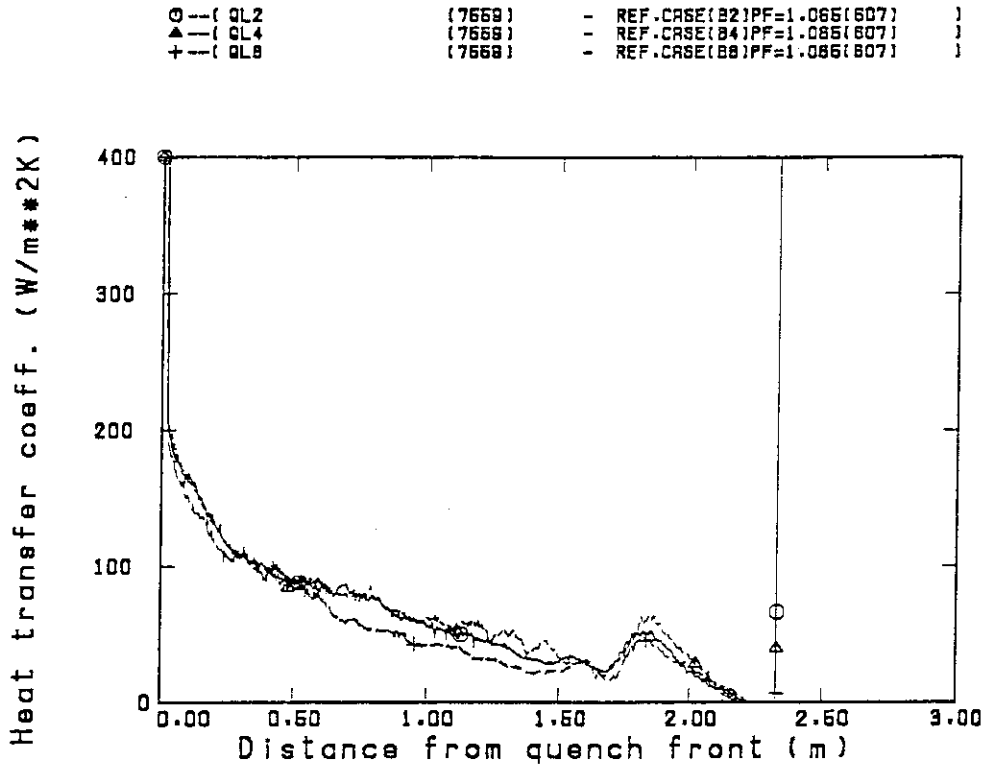

Fig.3.3.2(3) Radial comparison of heat transfer coefficient at 2.33m under peak power ratio of 1.065

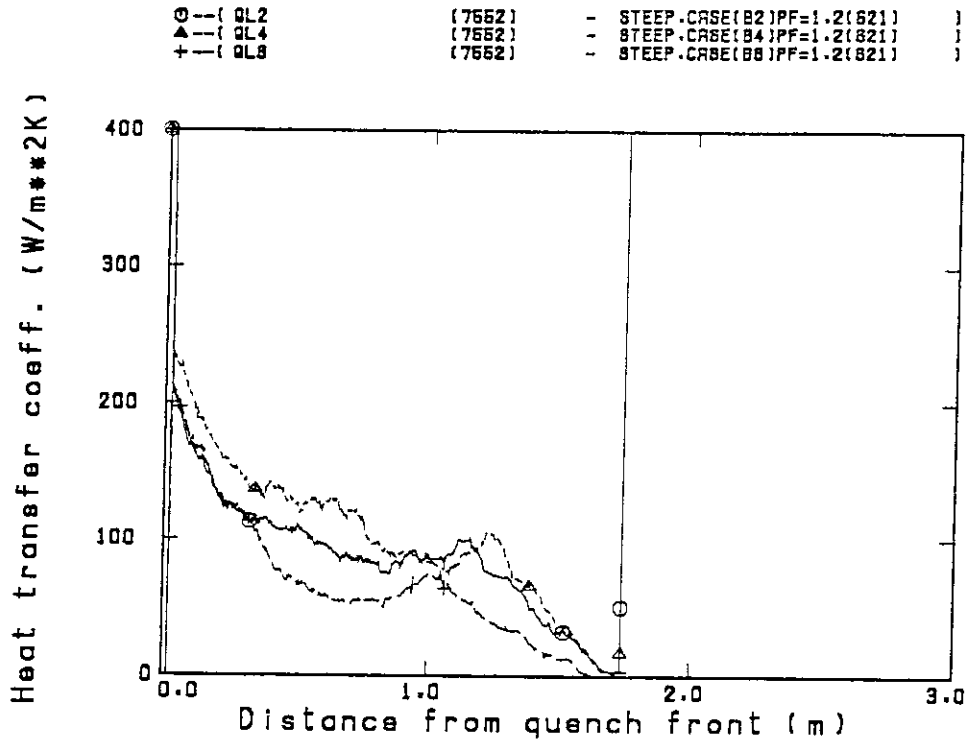

Fig.3.3.3(1) Radial comparison of heat transfer coefficient at 1.735m under peak power ratio of 1.2

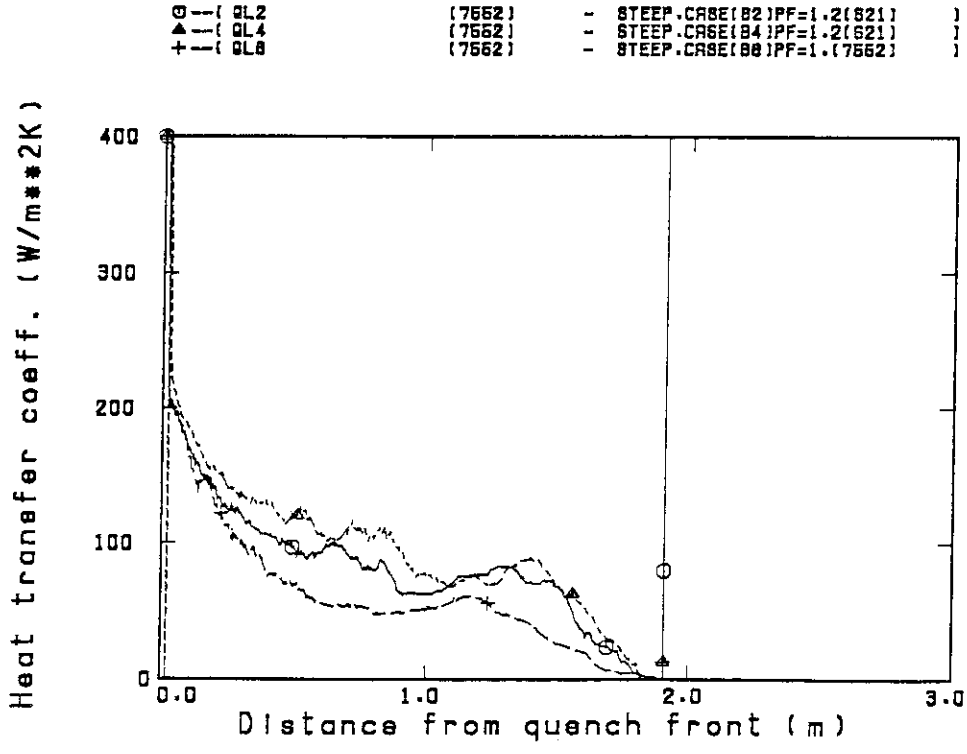

Fig.3.3.3(2) Radial comparison of heat transfer coefficient at 1.905m under peak power ratio of 1.2

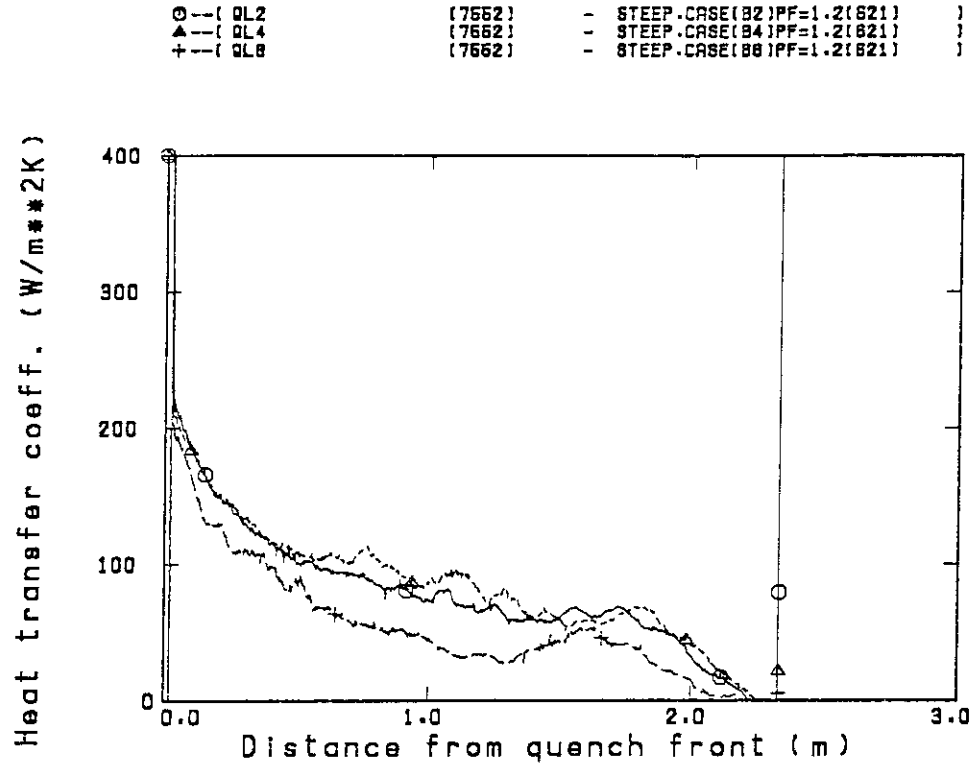

Fig.3.3.3(3) Radial comparison of heat transfer coefficient at 2.33m under peak power ratio of 1.2

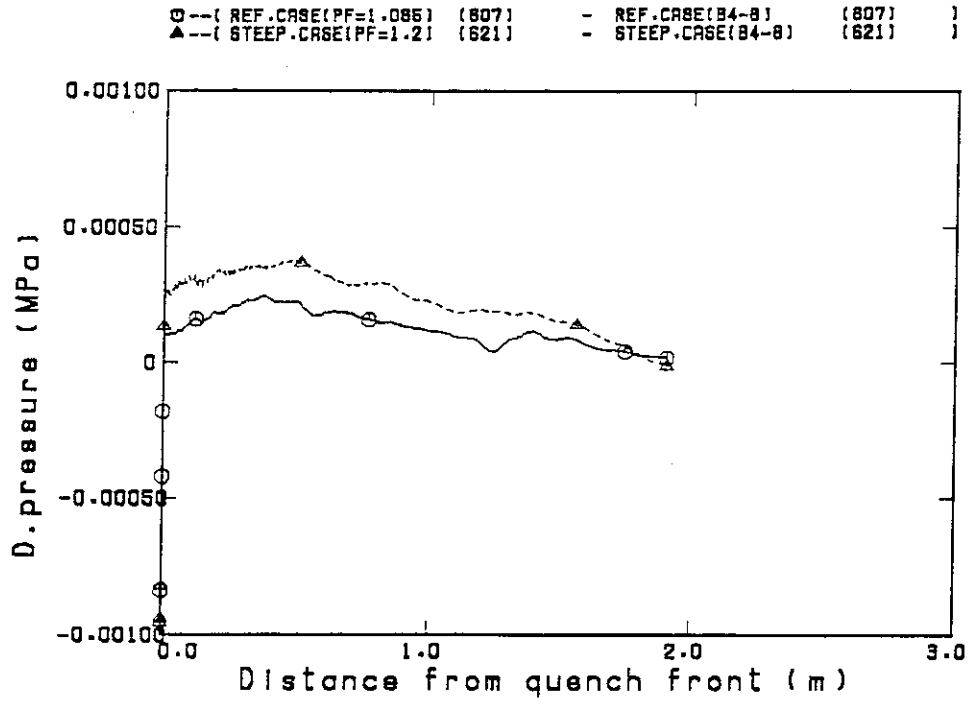

Fig.3.3.5 Comparison of horizontal differential pressure at 1.905m in tests with a radial power profile

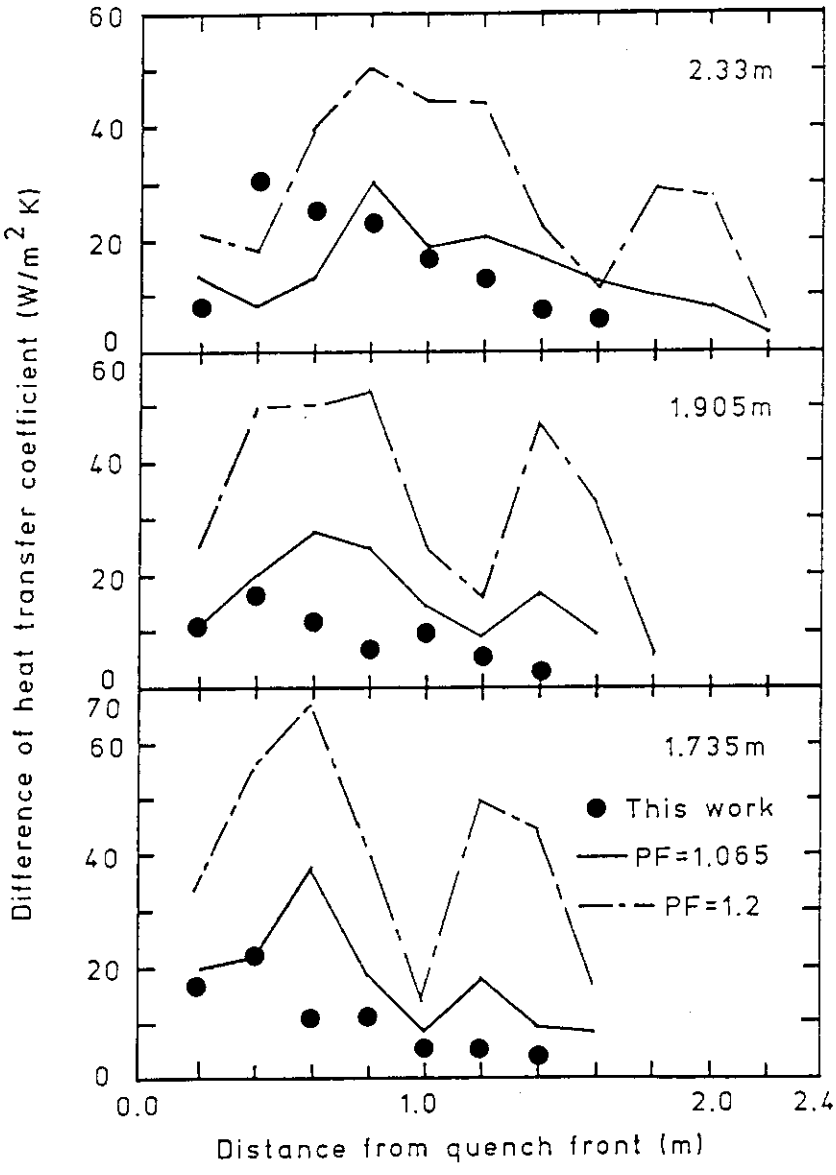

Fig.3.3.4 Comparison of difference of heat transfer coefficient

Appendix Selected Data of Test S2-19

Locations of selected data in this appendix
are shown in the following figures,

Fig. A-1 Thermocouple Locations of Heater Rod Surface Temperature Measurements

Fig. A-2 Thermocouple Locations of Fluid Temperature Measurement just above and below End Box Tie Plate

Fig. A-3 Thermocouple Locations of Fluid Temperature Measurements at Core Inlet

Fig. A-4 Locations of Differential Pressure Measurements across End Box Tie Plate and Liquid Level Measurements above UCSP and End Box Tie Plate,

Fig. A-5 Locations of Hot Leg Instruments

Fig. A-6 Locations of Vertical Differential Pressure Measurements in Core and

Fig. A-7 Measurement Locations of Horizontal Differential Pressures in Core and Differential Pressures in Upper Plenum.

List of figures for selected data

Figs. A-8∿A-15	Heater rod temperature
Figs. A-16 and A-17	Fluid temperature just above end box tie plate
Figs. A-18 and A-19	Fluid temperature at core inlet
Figs. A-20 and A-21	Liquid level above UCSP
Fig. A-22	Liquid level in hot leg
Figs. A-23 and A-24	Differential pressure of core full height
Figs. A-25∿A-27	Horizontal differential pressure in core

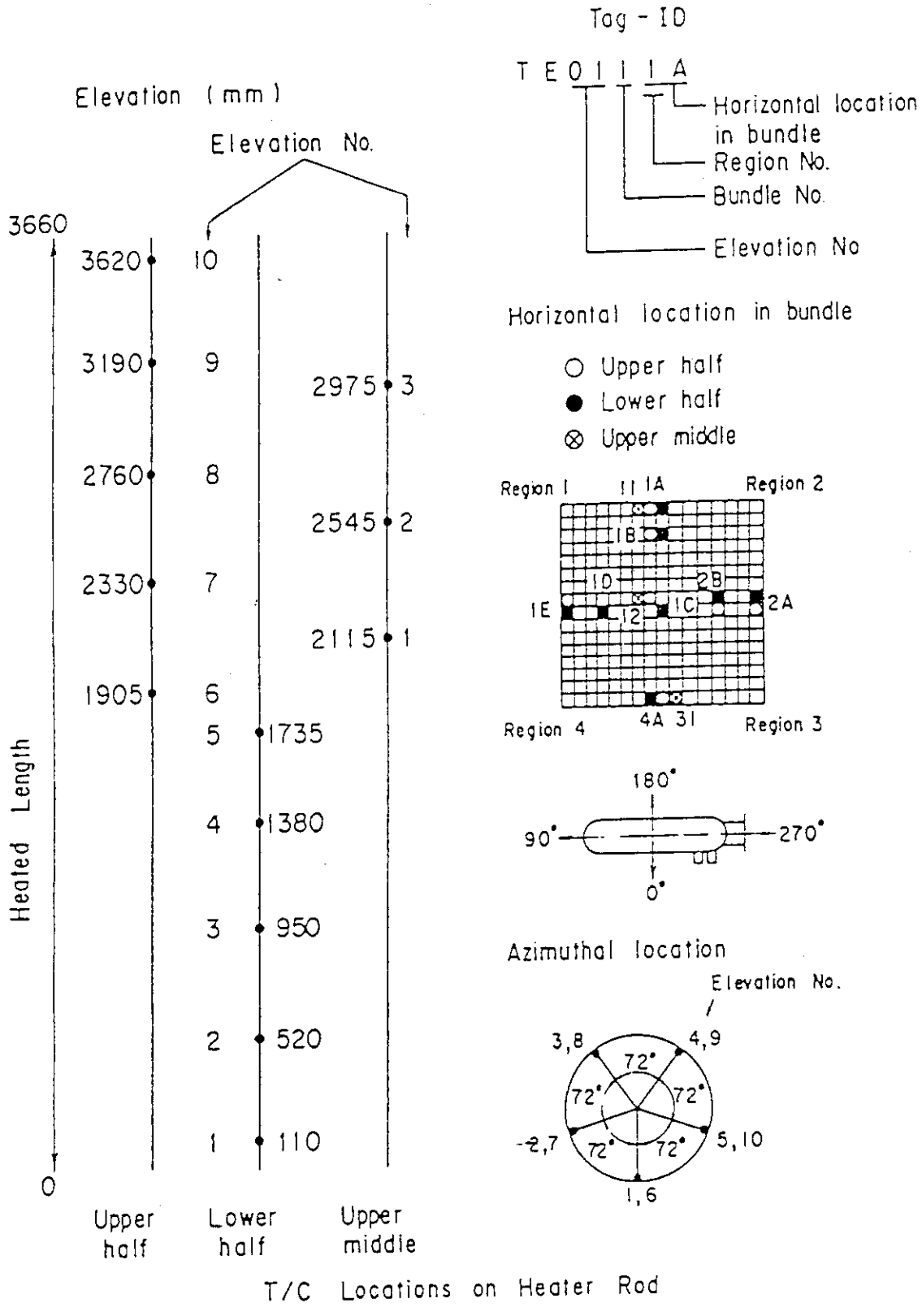

Fig. A-1 Thermocouple Locations of Heater Rod Surface Temperature Measurements

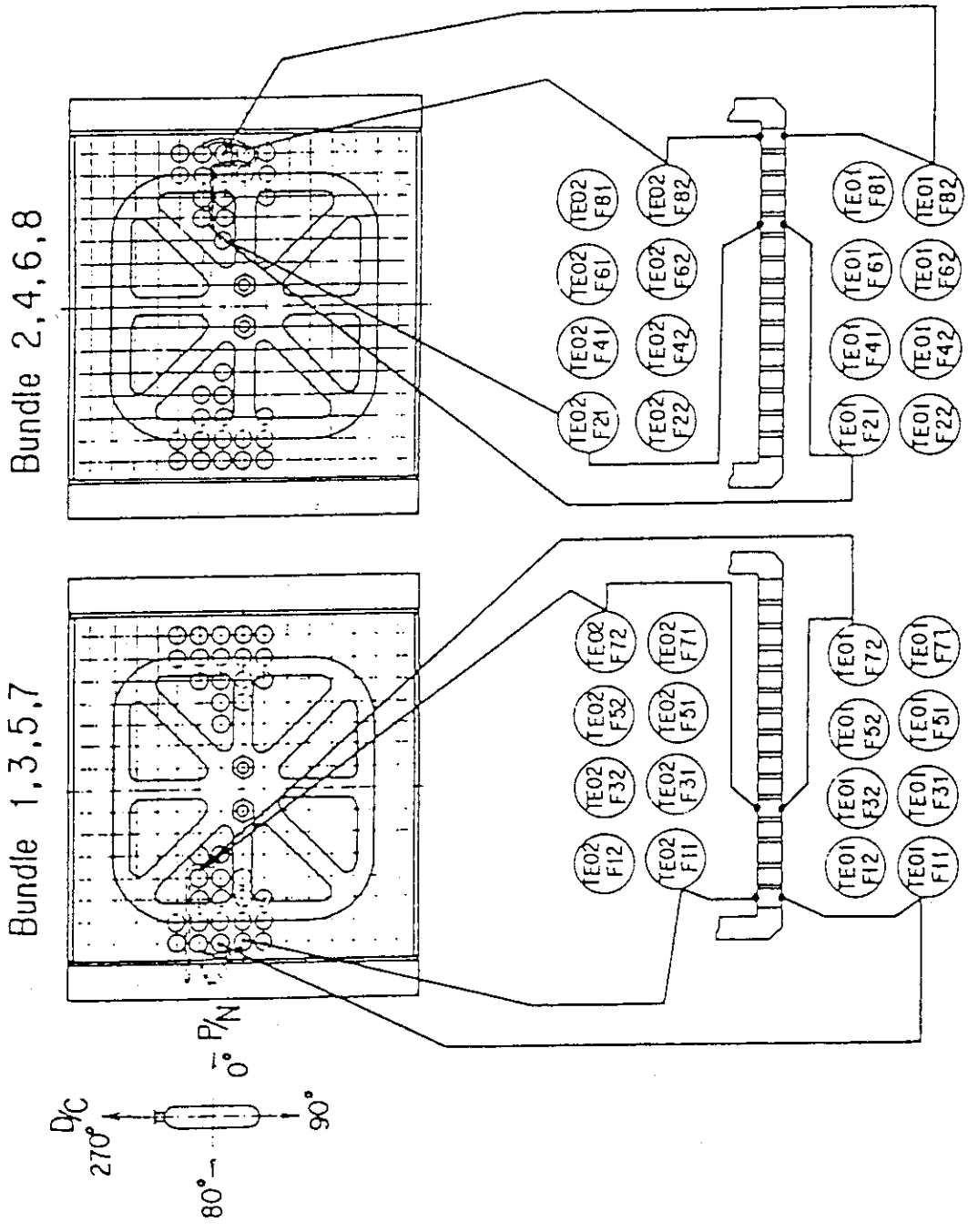

Fig. A-2 Thermocouple Locations of Fluid Temperature Measurement just above and below End Box Tie Plate

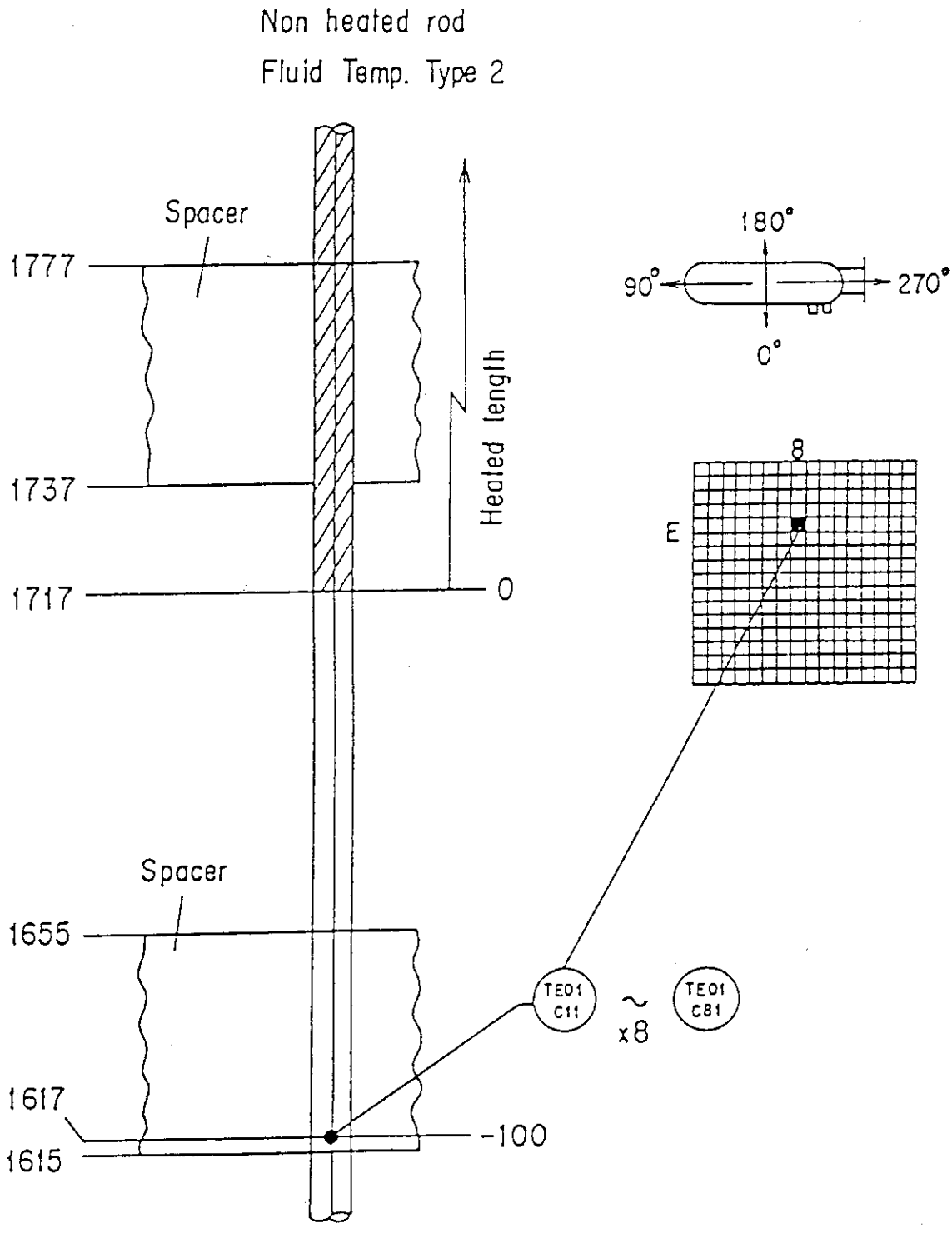

Fig. A-3 Thermocouple Locations of Fluid Temperature Measurements at Core Inlet

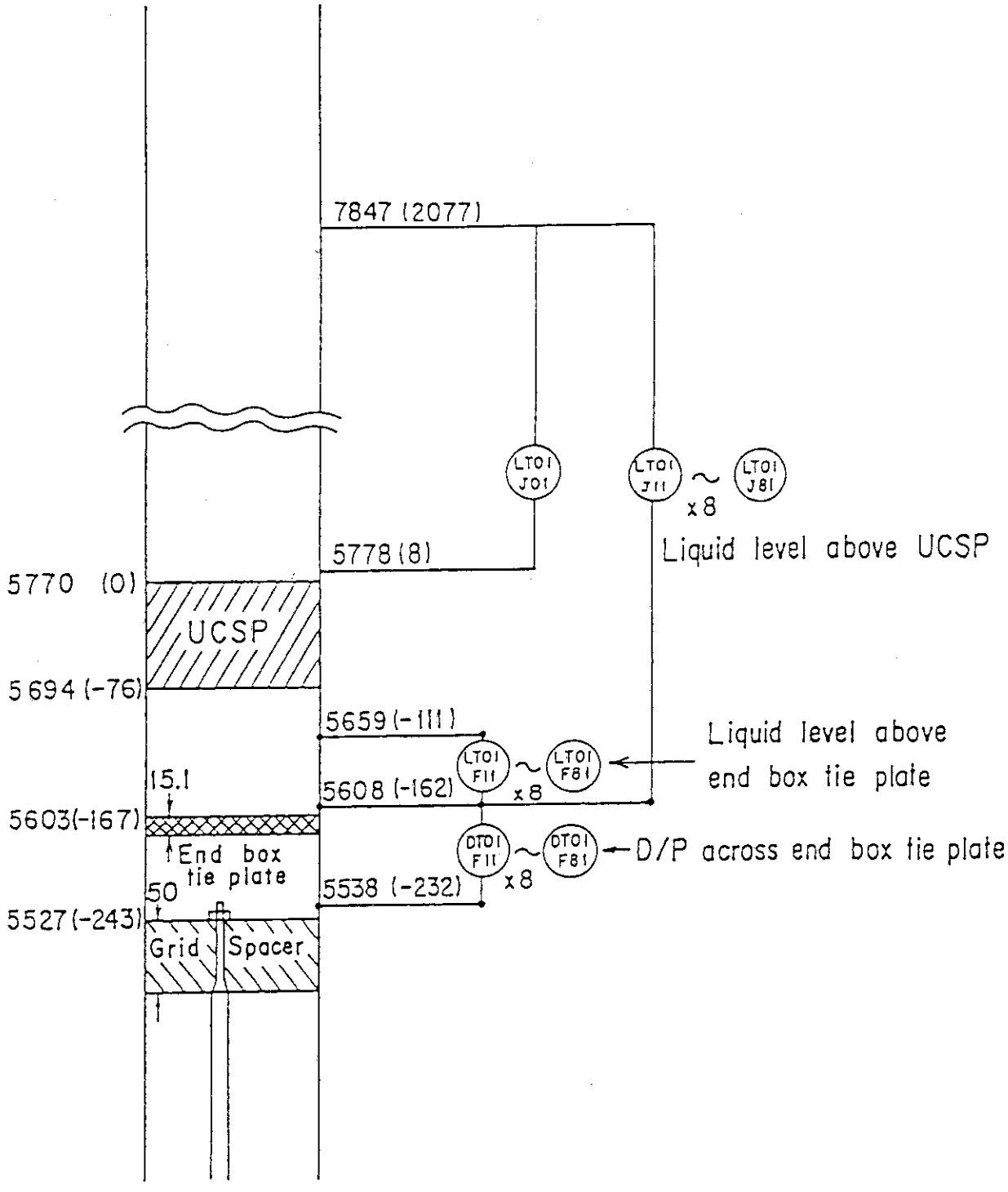

Fig. A-4 Locations of Differential Pressure Measurements across End Box Tie Plate and Liquid Level Measurements above UCSP and End Box Tie Plate,

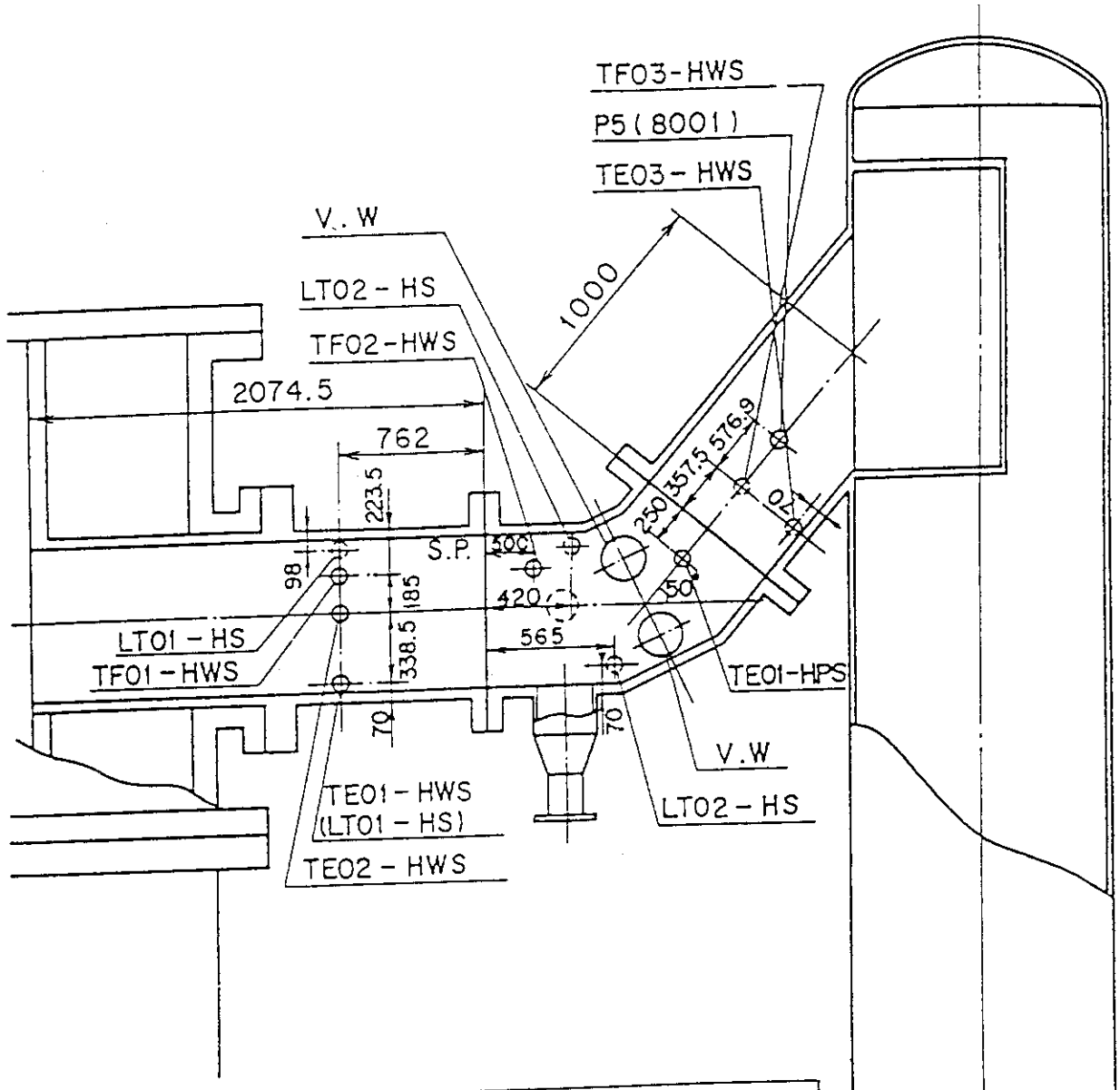

Tag no.	Location
DT01 HS	$P5^{L}$- Inlet of hot leg^{H}
DT01 GS	$P5^{L}$- Broken cold leg (S-W separator side)^{H}
DT02 GS	$P5^{H}$- S-W separator $tank^{L}$

Fig. A-5 Locations of Hot Leg Instruments

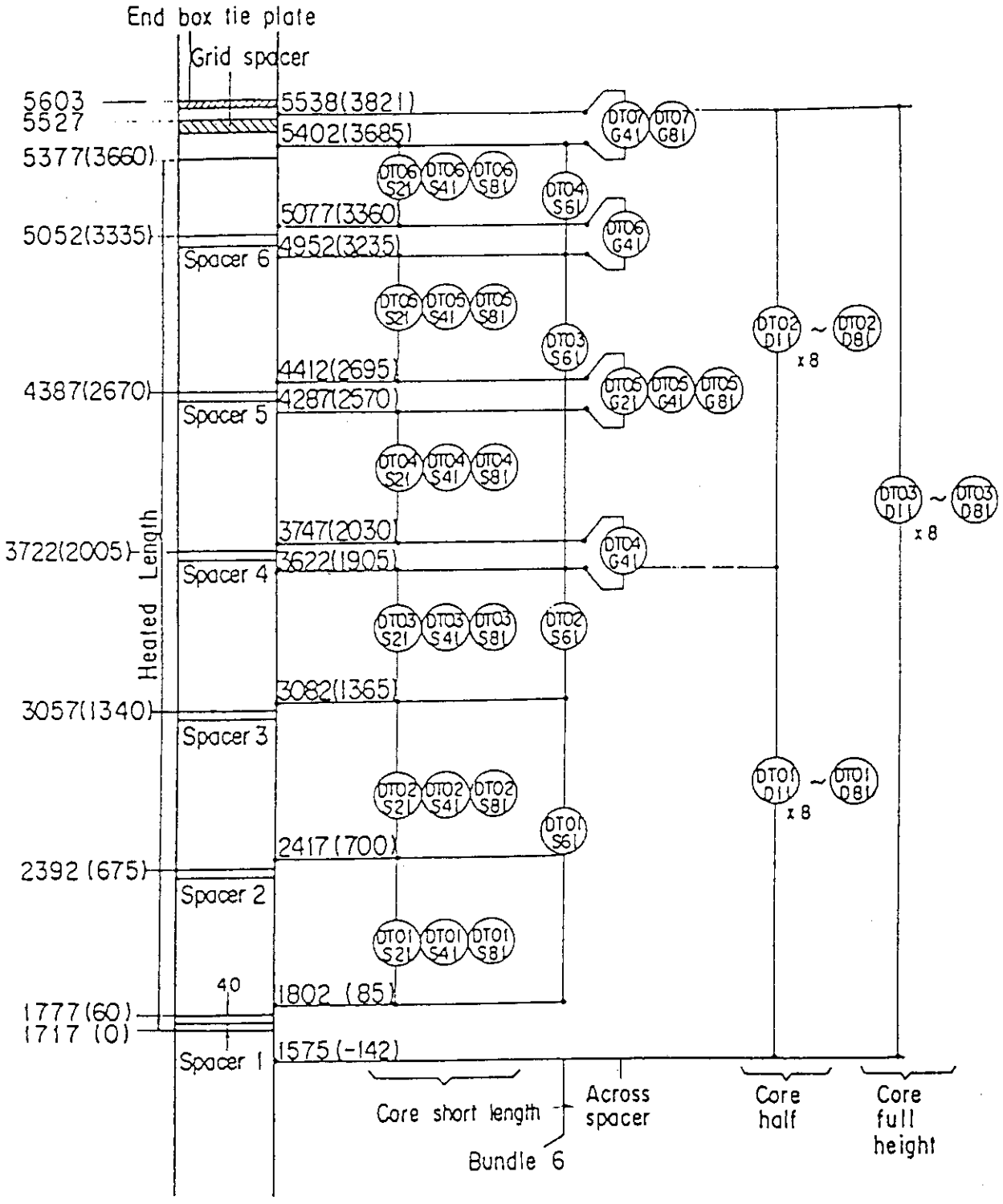

Fig. A-6 Locations of Vertical Differential Pressure Measurements in Core and

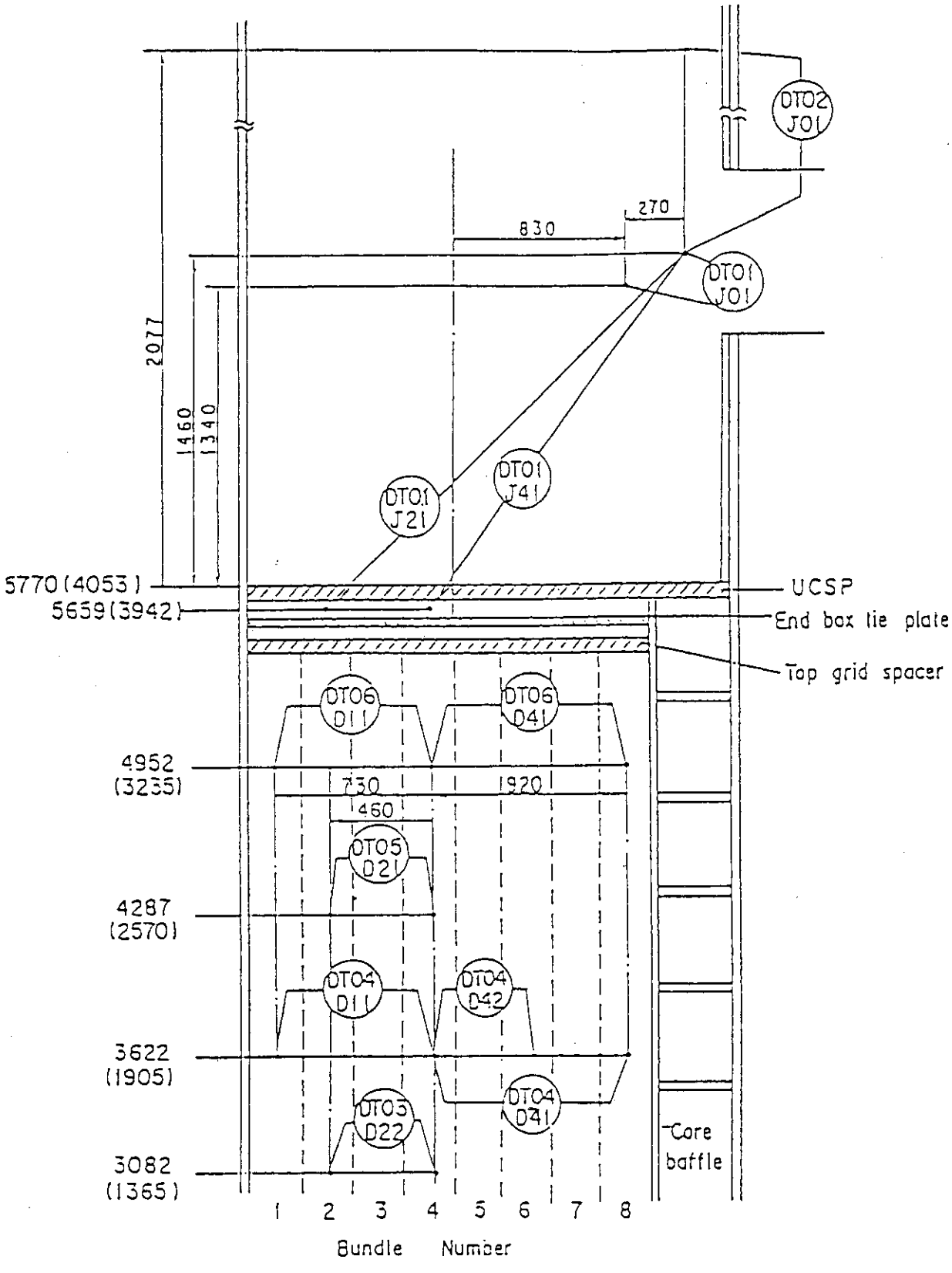

Fig. A-7 Measurement Locations of Horizontal Differential Pressures in Core and Differential Pressures in Vpper Plenum.

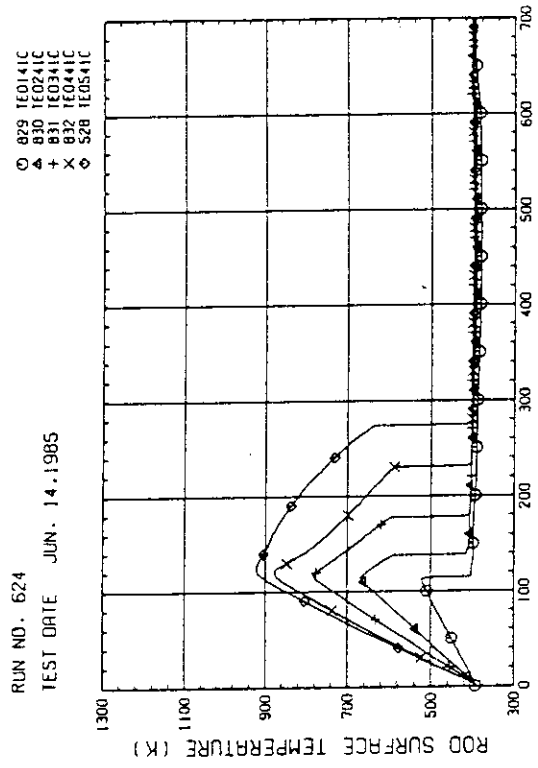

Fig. A-10 HEATER ROD TEMPERATURE (BUNDLE 4-1C, LOWER HALF)

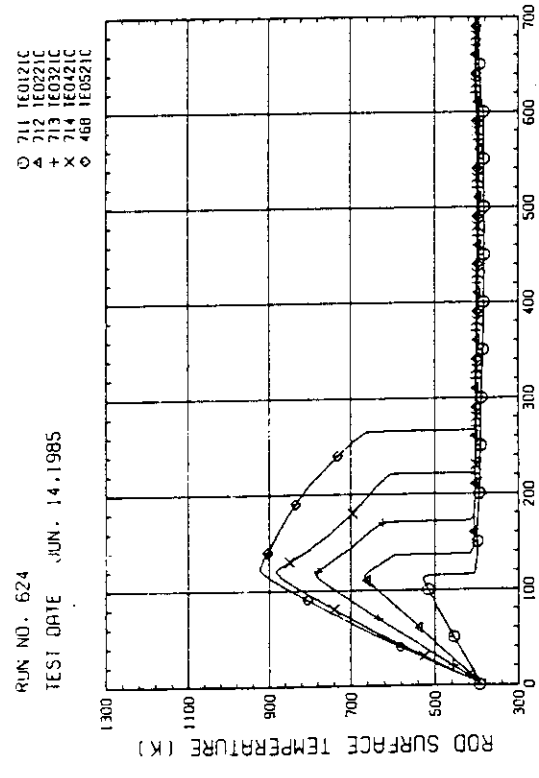

Fig. A-8 HEATER ROD TEMPERATURE (BUNDLE 2-1C, LOWER HALF)

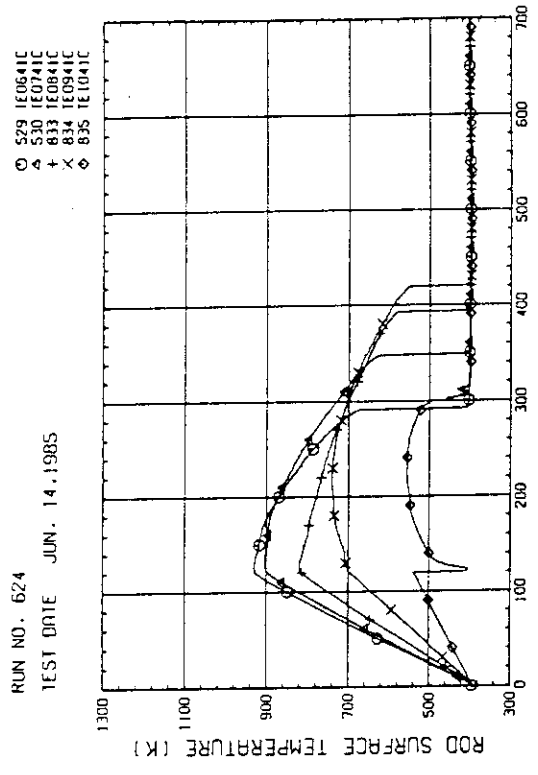

Fig. A-11 HEATER ROD TEMPERATURE (BUNDLE 4-1C, UPPER HALF)

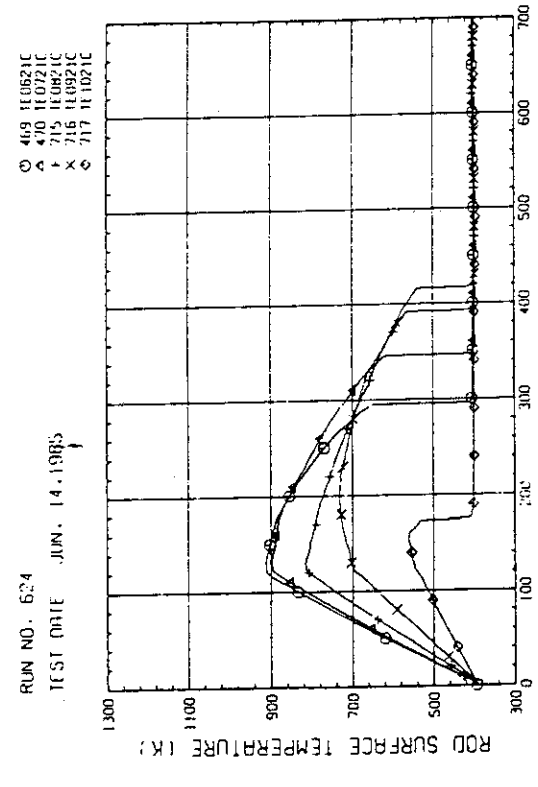

Fig. A-9 HEATER ROD TEMPERATURE (BUNDLE 2-1C, UPPER HALF)

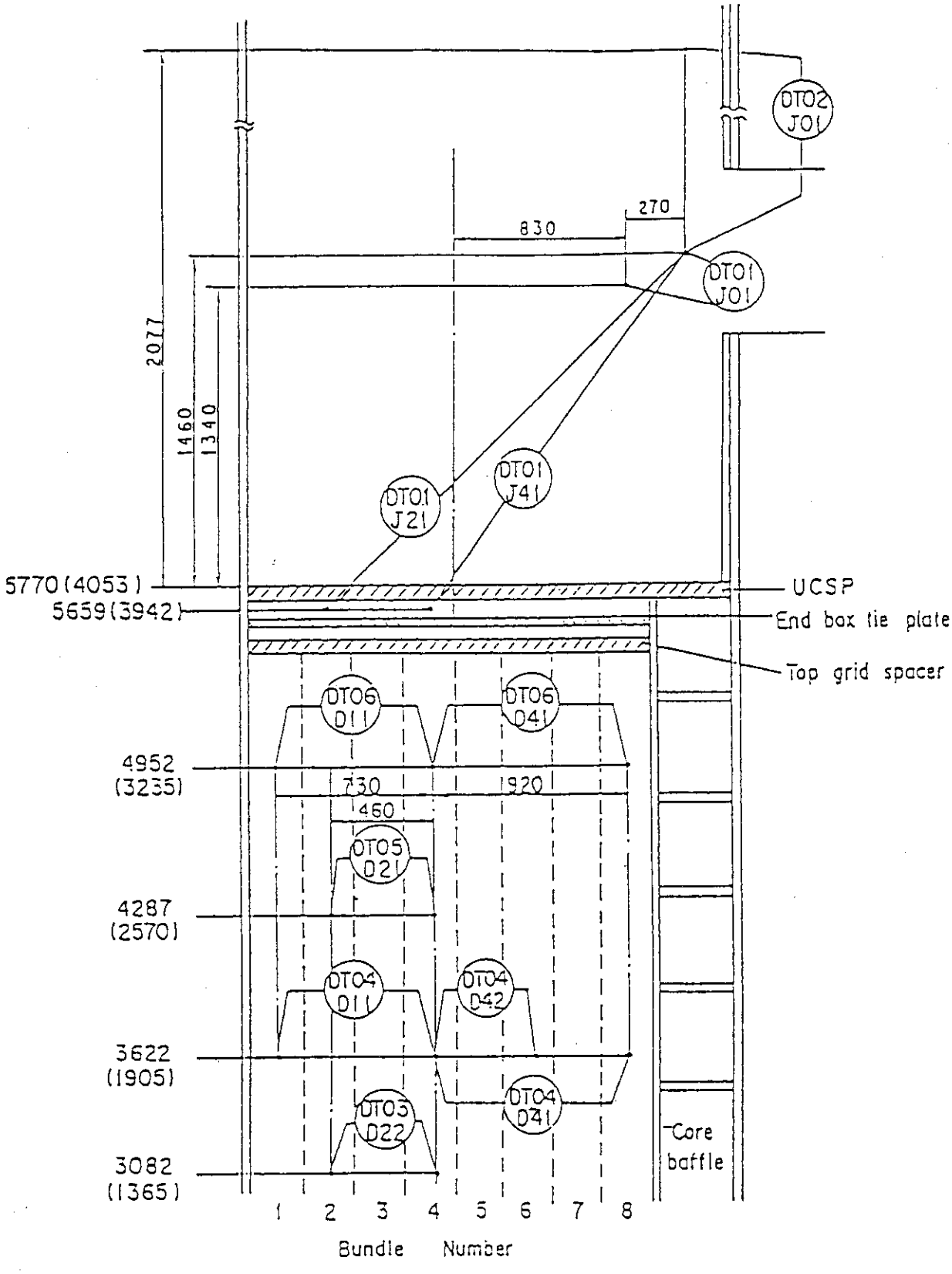

Fig. A-7 Measurement Locations of Horizontal Differential Pressures in Core and Differential Pressures in Vpper Plenum.

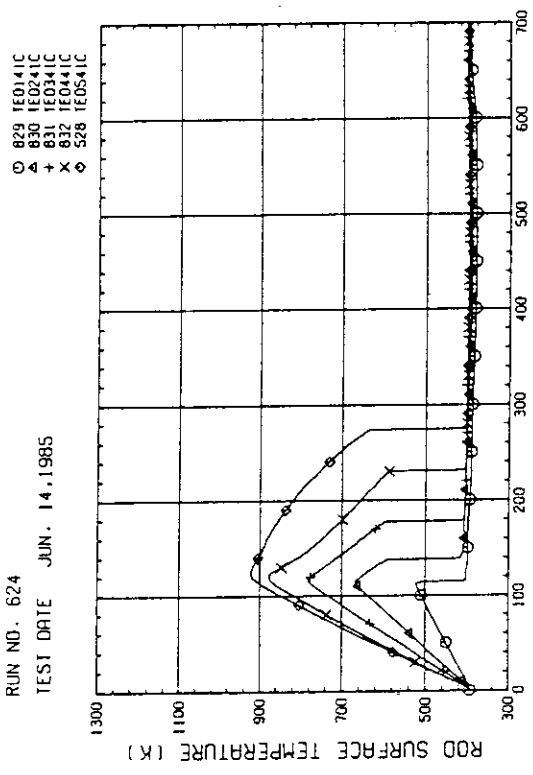

Fig. A-10 HEATER ROD TEMPERATURE (BUNDLE 4-1C, LOWER HALF)

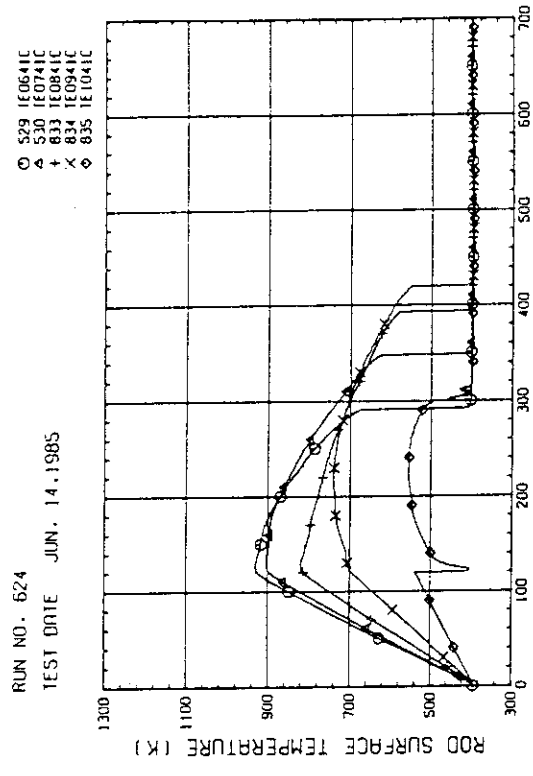

Fig. A-11 HEATER ROD TEMPERATURE (BUNDLE 4-1C, UPPER HALF)

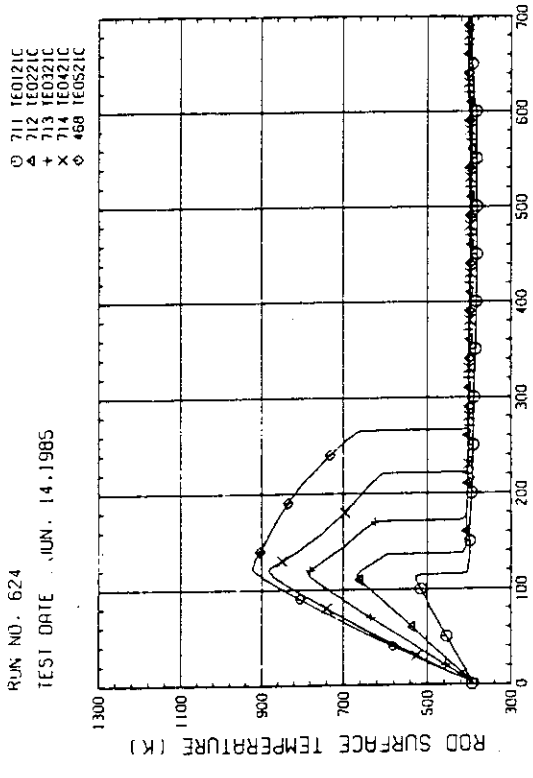

Fig. A-8 HEATER ROD TEMPERATURE (BUNDLE 2-1C, LOWER HALF)

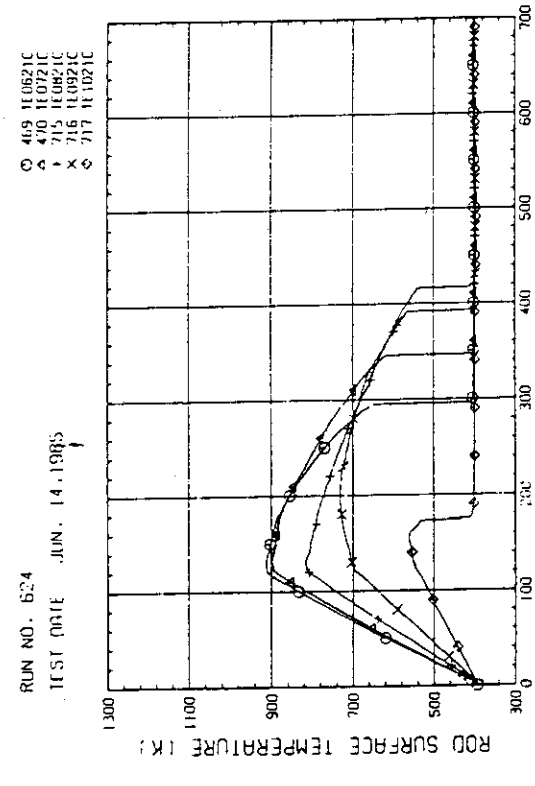

Fig. A-9 HEATER ROD TEMPERATURE (BUNDLE 2-1C, UPPER HALF)

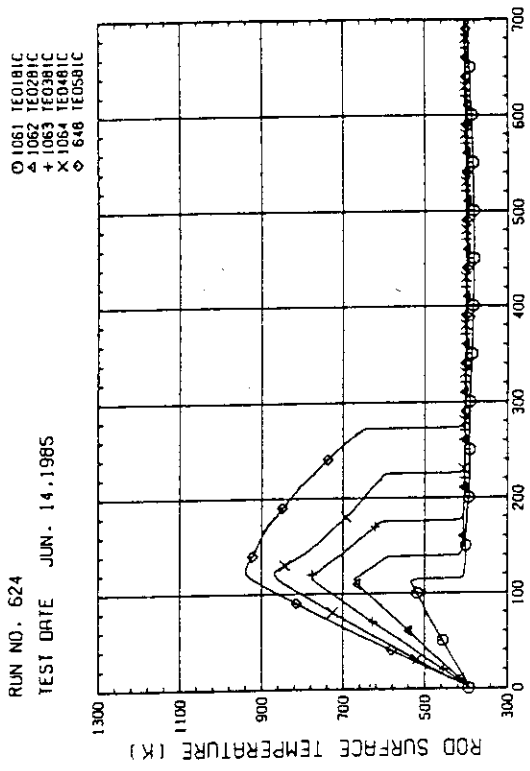

Fig. A-14 HEATER ROD TEMPERATURE (BUNDLE 8-1C, LOWER HALF)

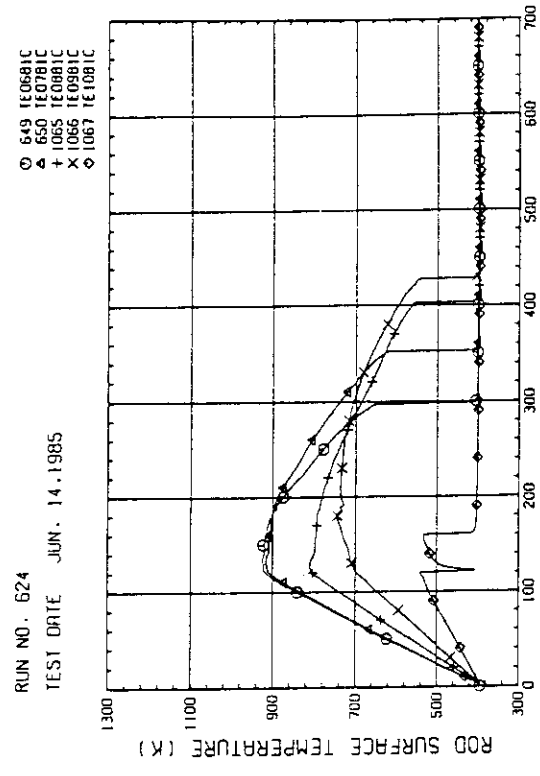

Fig. A-15 HEATER ROD TEMPERATURE (BUNDLE 8-1C, UPPER HALF)

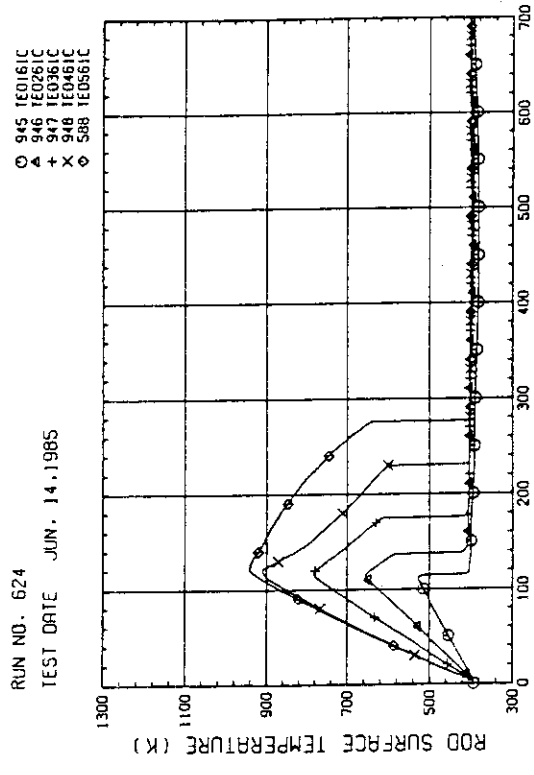

Fig. A-12 HEATER ROD TEMPERATURE (BUNDLE 6-1C, LOWER HALF)

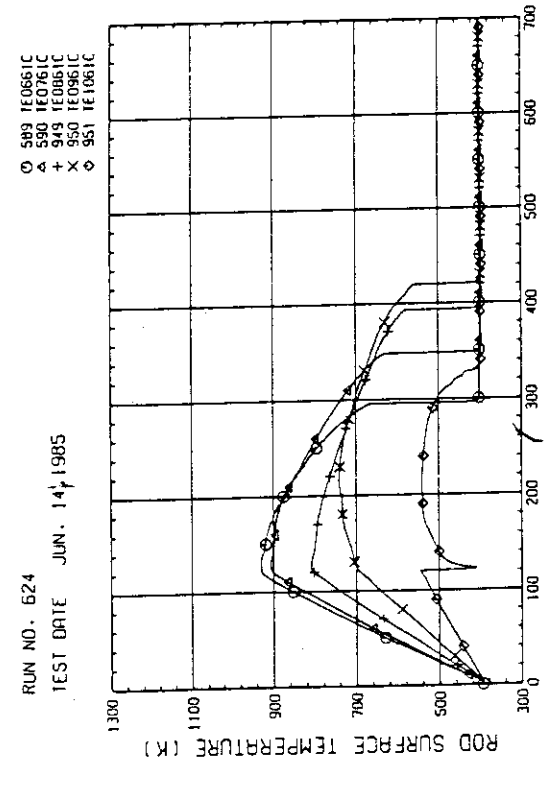

Fig. A-13 HEATER ROD TEMPERATURE (BUNDLE 6-1C, UPPER HALF)

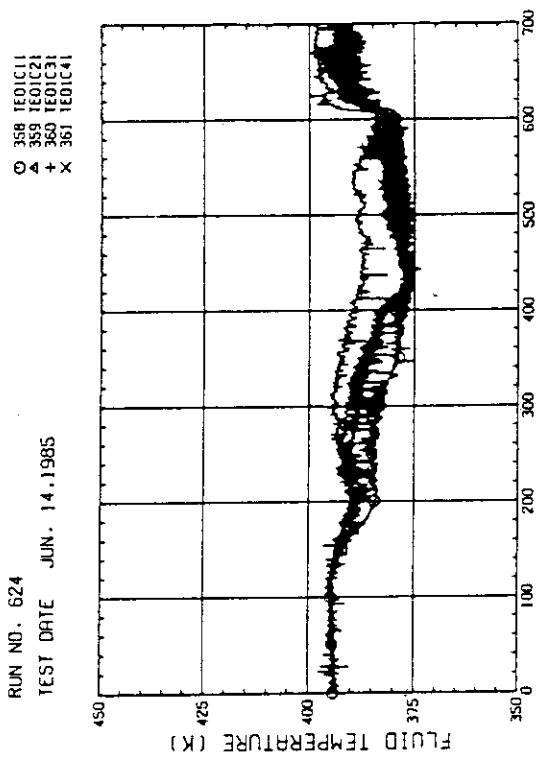

Fig. A-18 FLUID TEMPERATURE AT CORE INLET (BUNDLE 1.2.3.4. 100MM BELOW HEATED PART)

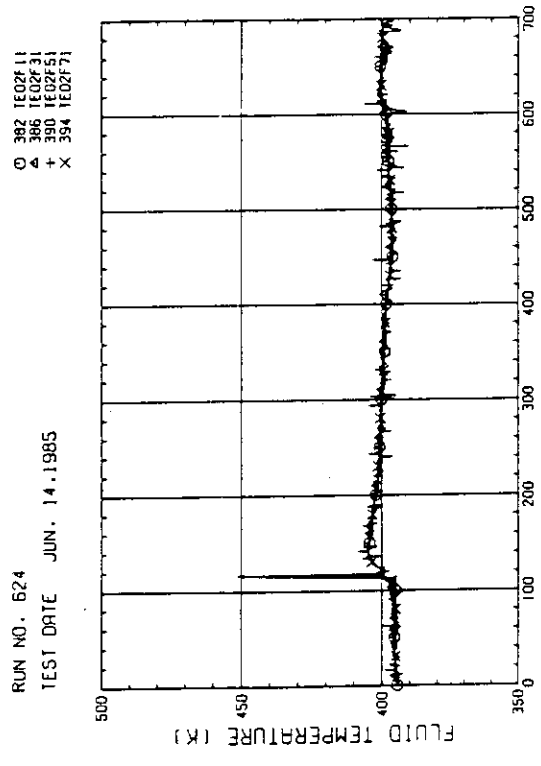

Fig. A-16 FLUID TEMPERATURE JUST ABOVE END BOX TIE PLATE (BUNDLE 1.3.5.7. OPPOSITE SIDE OF COLD LEG, OUTER)

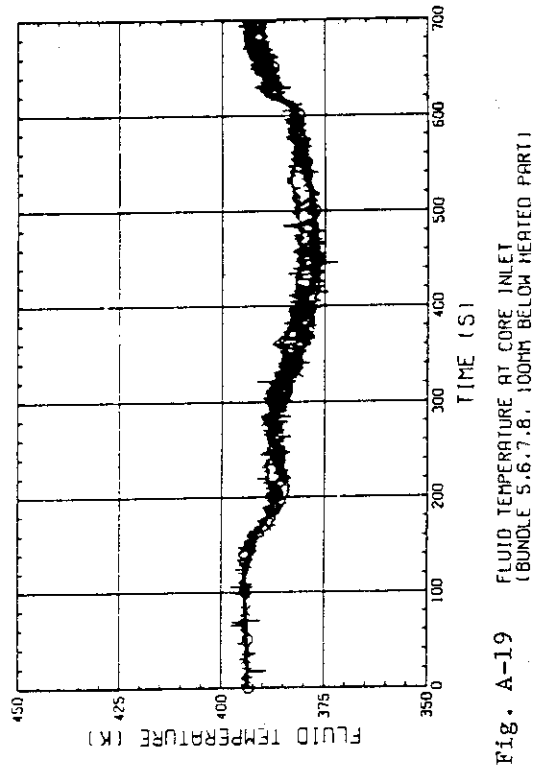

Fig. A-19 FLUID TEMPERATURE AT CORE INLET (BUNDLE 5.6.7.8. 100MM BELOW HEATED PART)

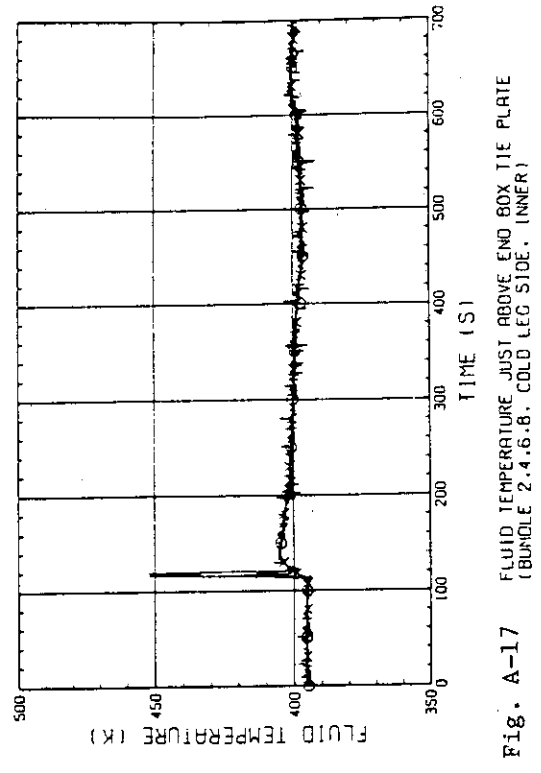

Fig. A-17 FLUID TEMPERATURE JUST ABOVE END BOX TIE PLATE (BUNDLE 2.4.6.8. COLD LEG SIDE, INNER)

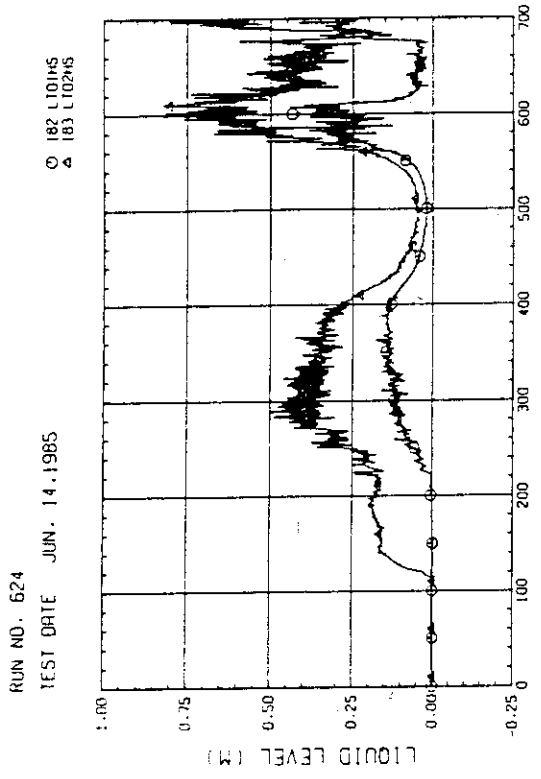

Fig. A-22 LIQUID LEVEL IN HOT LEG
(101HS - PV SIDE, 02HS - STEAM/WATER SEPARATOR SIDE)

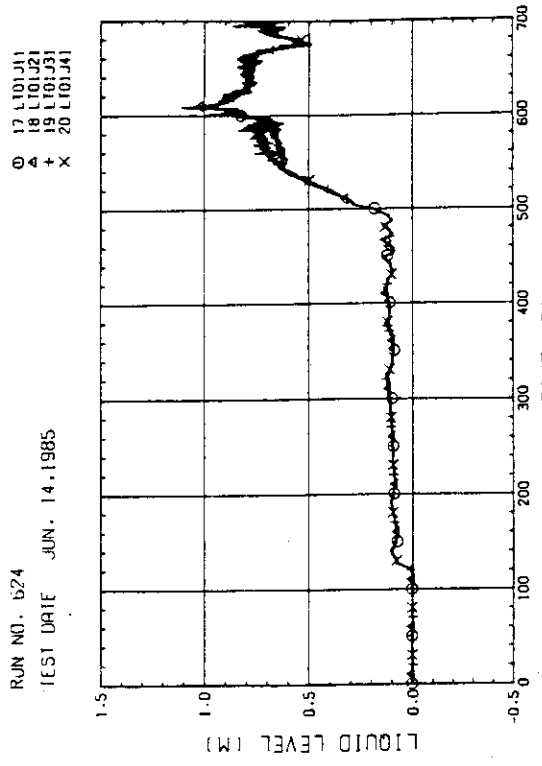

Fig. A-20 LIQUID LEVEL ABOVE UCSP
(BUNDLE 1.2.3.4)

Fig. A-21 LIQUID LEVEL ABOVE UCSP
(BUNDLE 5.6.7.8 AND CORE BAFFLE)

Fig. A-23 DIFFERENTIAL PRESSURE OF CORE FULL HEIGHT
(BUNDLE 1.2.3.4)

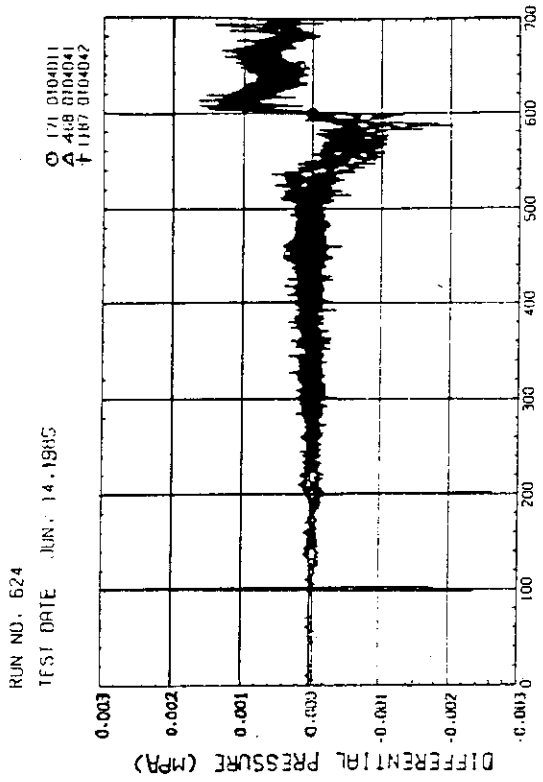

Fig. A-26 DIFFERENTIAL PRESSURE, HORIZONTAL AT 1905 MM (11-BUNDLE 1-4, 41-BUNDLE 4-8, 42-BUNDLE 4-6)

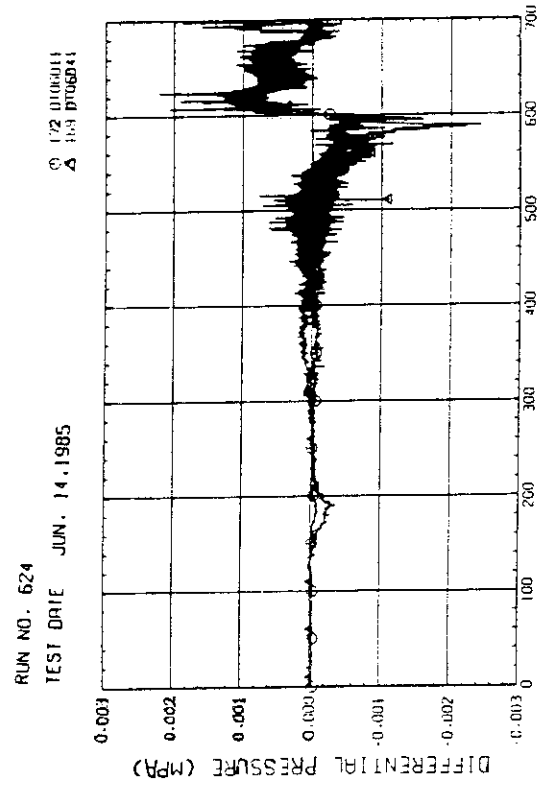

Fig. A-27 DIFFERENTIAL PRESSURE, HORIZONTAL AT 3235 MM (11-BUNDLE 1-4, 41-BUNDLE 4-8)

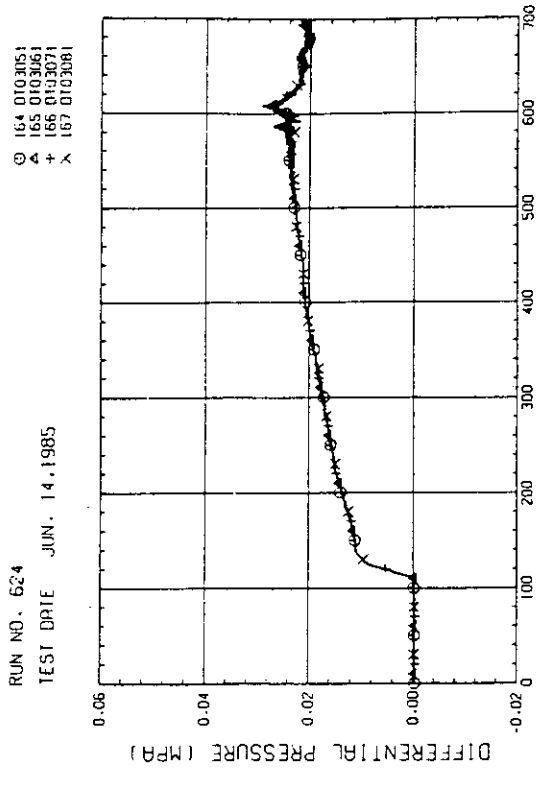

Fig. A-24 DIFFERENTIAL PRESSURE OF CORE FULL HEIGHT (BUNDLE 5.6.7.8)

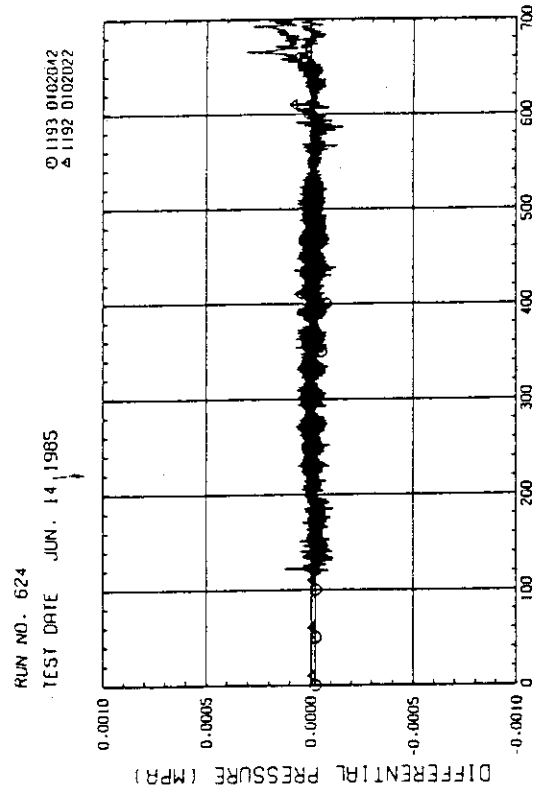

Fig. A-25 DIFFERENTIAL PRESSURE, HORIZONTAL AT 700 MM (42-BUNDLE 4-8, 22-BUNDLE 2-4)